UNIVERSITÉ DE GENÈVE FACULTÉ DES SCIENCES

Section de médecine fondamentale
Département de physiologie cellulaire et métabolisme Professeur Mirko Trajkovski
Département de Génétique et Évolution Professeur Evgeny M. Zdobnov

Computational Approaches for a Healthier Microbiome

THÈSE

présentée aux Facultés de médecine et des sciences de l'Université de Genève
pour obtenir le grade de Docteur ès sciences en sciences de la vie,
mention Sciences biomédicales

par

Silas Daniel Kieser

de

Lenzburg (Aargau)

Thèse N° 144

GENÈVE

2021

LIFE SCIENCES PhD SCHOOL GENEVA

DOCTORAT ÈS SCIENCES EN SCIENCES DE LA VIE DES FACULTÉS DE MÉDECINE ET DES SCIENCES MENTION SCIENCES BIOMEDICALES

Thèse de Mr SILAS KIESER

intitulée :

« Computational approaches for a healthier microbiome »

Les Facultés de médecine et des sciences, sur le préavis de Monsieur Mirko TRAJKOVSKI, Professeur ordinaire et directeur de thèse (Département de Physiologie Cellulaire et Métabolisme), Monsieur Evgeny ZDOBNOV, Professeur ordinaire et co-directeur de thèse, (Département de Médecine Génétique et Développement) Monsieur Mirco SCHMOLKE, Professeur associé et Président du Jury (Département de Microbiologie et Médecine Moléculaire), Monsieur Shinichi SUNAGAWA Professeur associé, (Département de Biologie, E.T.H Zürich, Suisse) autorisent l'impression de la présente thèse, sans exprimer d'opinion sur les propositions qui y sont énoncées.

Genève, le 31 août 2021

Thèse - 114 -

Le Doyen
Faculté de médecine

Le Doyen
Faculté des sciences

N.B. - La thèse doit porter la déclaration précédente et remplir les conditions énumérées dans les "Informations relatives aux thèses de doctorat à l'Université de Genève".

FACULTÉ DE MÉDECINE
FACULTÉ DES SCIENCES

UNIVERSITÉ DE GENÈVE

I would like to dedicate this thesis to my loving wife, Milena,
who supported me throughout my P.h.D.

Abstract

Our gut flora, the microbiome, plays an indispensable role in our health. Changes in the microbiome have been linked to an increasing list of diseases. *Metagenomics* is a technique that allows the sequencing of microbiomes directly from samples, giving valuable insight into the composition and functional potential of microbial populations. The analysis of metagenomic data is complex and depends on the availability of reference genomes. This work describes computational methods that allow the analysis of microbiomes with a lack of reference genomes by assembling genomes from the metagenomic data. We demonstrate how our methods can be used to infer the functional potential of a microbiome and how they allow us to link each function to the responsible species. We could predict changes in metabolites that were confirmed by targeted measurements. The mouse is the most used model for studying the impact of microbiota on its host. However, the species living in the mouse gut remain poorly characterized. By analyzing all publicly available metagenomes from the mouse gut, we created a comprehensive catalog of all bacterial species commonly living in the gut of laboratory mice. We assembled over 30'000 bacterial genomes, as well as the sequences from viruses and plasmids. Our catalog effectively answers the need for reference genomes for this microbiome. It allows efficient analysis of mouse gut metagenomes at the species and subspecies level. We discovered that mice and humans harbor a largely distinct set of species in their gastrointestinal tracts, an analysis which was hereto unfeasible.

Résumé

Notre flore intestinale, le microbiote, joue un rôle indispensable dans notre santé. Des changements dans le microbiote sont associés à une liste croissante de maladies. *La métagénomique* est une technique qui permet le séquençage de microbiotes directement à partir d'échantillons, donnant un aperçu utile de la composition et du potentiel fonctionnel des populations microbiennes. L'analyse des données métagénomiques est complexe et dépend de la disponibilité de génomes de référence. Ce travail décrit des méthodes de calcul qui permettent l'analyse de microbiotes lors d'un manque de génomes de référence en assemblant des génomes à partir des données métagénomiques. Nous démontrons comment nos méthodes peuvent être utilisées pour déduire le potentiel fonctionnel d'un microbiote et comment elles nous permettent de lier chaque fonction à l'espèce responsable. Nous avons pu prédire des changements dans les métabolites qui ont été confirmés par une analyse ciblée. La souris est le modèle le plus utilisé pour étudier l'impact du microbiote sur son hôte. Cependant, les espèces vivant dans l'intestin de la souris restent mal caractérisées. En analysant tous les métagénomes de l'intestin de la souris en libre accès, nous avons créé un catalogue complet de toutes les espèces bactériennes vivant couramment dans l'intestin des souris de laboratoire. Nous avons assemblé plus de 30'000 génomes bactériens, ainsi que les séquences de virus et de plasmides. Notre catalogue répond efficacement au besoin de génomes de référence pour ce microbiote. Il permet une analyse efficace des métagénomes intestinaux de souris au niveau des espèces et des sous-espèces. Nous avons découvert que les souris et les humains hébergent un ensemble d'espèces largement distinct dans leur système digestif, une analyse qui n'était jusqu'à présent pas réalisable.

Table of contents

Terms & Acronyms

Microbe	Microorganism. A tiny organism. Most microbes are prokaryotes, but also some small eukaryotes are counted as microbes[1].
Prokaryotes	Unicellular organisms that do not contain a nucleus. Bacteria and Archaea.
Eukaryotes	All organisms that contain a nucleus. All animals, plants, fungi, but also protists
Genome	Main genetic material of a cell.
Sequencing	The process of reading DNA, often in fractions
Read	A (short) DNA sequence, the output of a sequencer
Assembly	The process of putting small DNA fragments together to create longer ones
Contig	A continuous DNA sequence, often the result of an assembly of multiple reads
Amplicon sequencing	Sequencing of an amplified DNA region. I use it as synonym for 16S rDNA sequencing
16S rDNA sequencing	Sequencing (parts of) the 16S that allows the identification of microbes
16S rDNA	The DNA of the gene for the small ribosomal subunit in prokaryotes
Primers	Small DNA or used to initiate PCR amplification
PCR	Polymerase chain reaction. A laboratory method invented in 1983 that allows to amplify even small amounts of DNA fragments up to 10kbp in length.
Metagenome	Collection of all genomes from an environment. See Box.
Metagenomics	The study of metagenomes
MAG	Metagenome assembled genome
kbp	Killo base pairs = 1000 bp, unit for measurnign the lenght of DNA
CLR	Centered log ratio

[1]The definition is not very clear as discussed in "What Counts as a Microbe?" on asm.org

Introduction

> *What is the role, in the overall scheme of creation, of some of these little beings who are the agents of fermentation, the agents of putrefaction, of disorganization of everything that life has had on the surface of the globe? This role is immense, marvelous, really moving. Maybe one day, I will be given the opportunity to explain some of these results.*
>
> — Louis Pasteur[1]

Ex nihilo nihil fit (From nothing, nothing comes) is a fundamental philosophical principle. There might still be a debate in metaphysics about whether the universe could arise from nothing and what that *nothing* would be. In biology, the idea of spontaneous creation was eliminated from the discipline by Louis Pasteur in the middle of the 19th century. He not only showed that a closed, sterile system remains sterile but at the same time that microbes are all around us. He became one of the founders of Microbiology and postulated that germs are the cause of many diseases. The change in mentality led to the identification of many diseases' pathogens. Lives could be saved by simple measures such as hand sanitation, which was not a common practice for clinicians at that time.

Even if it was possible to see microbes since Antonie van Leeuwenhoek discovered the microscope, a large fraction of the microbial diversity was still hidden until 1950, when Robert. E. Hungate developed his technique to cultivate anaerobic microbes (Hungate, 1944). Even with the ability to culture anaerobic microorganisms, the vast majority of microbes went unnoticed. In 1985, it was estimated that less than 1% of the microorganisms found in an environmental sample could be cultured on plates. This fact came to be known as "*the great*

[1] René Vallery-Radot (1902). *The life of Pasteur*. New York: Phillips McClure, p. 142

plate count anomaly" (Staley & Konopka, 1985) and spurred the interest in sequencing microbes directly from the environment.

1.1 The history of microbiome sequencing

> *[Sequencing] ... has been at the center of all my research since 1943, both because of its intrinsic fascination and my conviction that a knowledge of sequences could contribute much to our understanding of living matter*
>
> — Frederick Sanger[2]

In 1977, Frederick Sanger started to develop his sequencing method (Sanger et al., 1977), which kicked off a revolution in sequencing. Even before that, researchers studied microorganisms by sequencing short fragments of ribonucleic acid (RNA) (Heather & Chain, 2016). So determined Carl. R. Woese & George. E. Fox 20 years before the first microbial genome was sequenced, that living organisms consist not only of Eukaryotes[3] and bacteria but that there is a third domain: the Archaea (Woese & Fox, 1977). The discovery of a whole new domain of life was revolutionary for its time and was met with a lot of criticism (Goldenfeld & Pace, 2013). It showed that life evolved not in a linear fashion from simple to more complex life, but that there are deep branches in the *tree of life* going all the way down to its root. "*The 1977 paper is one of the most influential in microbiology and arguably, all of biology. It ranks with the works of Watson and Crick and Darwin, providing an evolutionary framework for the incredible diversity of the microbial world*" (Nair, 2012).

More practically, Carl. R. Woese & George. E. Fox showed convincingly that (microbial) life could be analyzed by sequencing. They differentiated the organisms based on the small ribosomal unit, whose RNA is highly abundant in cells. The corresponding gene, also known as the 16S gene (18S in Eukaryotes), is present in all living organisms. The functional constraints on the ribosome keep the sequence of the rRNA-gene comparable between all domains of life. The publication from 1977 consists mainly of one table that shows how the 16S (18S) sequence from representatives of the three domains of life are more similar within the domain than between the domains.

[2] Frederick Sanger, Biographical, NobelPrize.org

[3] Organisms that have a nucleus: animals, plants, fungi, protists...

However, the sequencing of the small ribosomal unit still required the cultivation of the species under investigation, which was difficult, especially for the new domain of archaea. The solution to this problem came almost ten years later. During this time, the polymerase chain reaction (PCR) was invented, which allowed the amplification of small amounts of DNA, and the Sanger sequencing became widely available. In 1985, Norman R. Pace and co-workers developed a technique to rapidly sequence the 16S gene directly from the environment (Lane et al., 1985). They propose *universal primers* for amplification of the 16S gene. Norman Pece came to be named "The man who blew the door off the microbial world" (Young, 2017), as his technique allowed for the first time to see the full diversity of microbes in a sample. Again 10 years later, the first time the human gut microbiome was sequenced (Wilson & Blitchington, 1996), see also box.

1.1.1 16S amplicon sequencing

Today amplicon sequencing of the 16S gene is a routine experiment: First, DNA is extracted from a sample, then PCR is used to amplify a part of the 16S gene. Not all regions of the 16S genes are equally conserved between taxa. Conserved regions are interspaced by 9 variable regions (Fig. 1.1 on the following page). These variable regions belong to loops in the ribosome with little constraints and are therefore free to evolve. The *universal primers* target the flanking conserved regions around one or multiple variable regions, which then are sequenced.

As with almost everything in biology, there are no rules that apply without exception, and so not the *universal* primer sites of the 16S are not universal. Different versions of primer(-mixtures) are proposed for different target microbiomes (For example, Sim et al., 2012). Also, not all variable regions are suited to discriminating all taxa, and PCR bias can artificially increase specific species. Therefore, it is generally accepted that 16S amplicon sequencing, based on one or two variable regions, can classify organisms down to the genus level but is not suited to classify at species level robustly (See section 6.2.1 for an in-depth discussion). Despite all these drawbacks, 16S sequencing is the most used technique to analyze microbiomes at a low cost. Many of these limitations are addressed by long-read sequencing, which allows the sequencing of all nine variable regions (Karst et al., 2018).

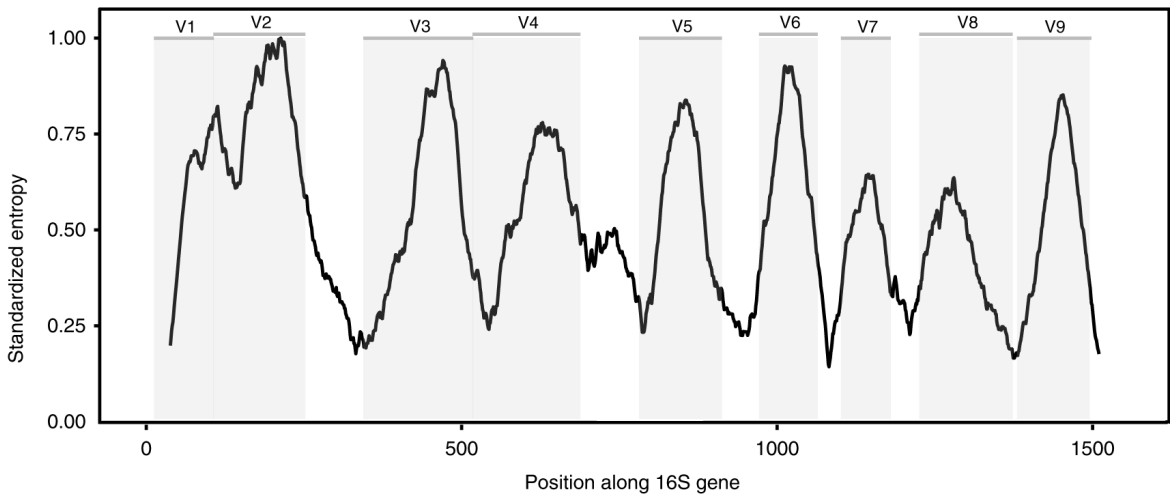

Fig. 1.1 Variability across the 16S gene based on the alignment of a single representative sequence for each known species present in the Greengenes database. Sequences were aligned against a single reference 16S gene for Escherichia coli K-12 MG1655. Gray panels depict variable regions defined by commonly used primer-binding sites.
Adapted from Johnson et al., 2019

The human microbiome

The ubiquity of microbial life was confirmed over and over again. It is difficult to imagine a place on earth that is not populated with microbial life, and it is even speculated that Mars is the home of microbes brought from earth (Mason, 2021). Interestingly, the human gut is among the most densely populated habitats for microorganisms in the world (Whitman et al., 1998). Also, the gut is densely covered with immune cells from within (Vijay-Kumar et al., 2014), indicating that the gut is an essential point in host-microbe interaction. Bacteria are the most numerous domain of life in the human gut microbiota (Guarner & Malagelada, 2003). Archaea, fungi, and protists belong to the microorganism living in the human gut. Not surprisingly, phages and other viruses outnumber the living organisms and play the critical role of predators in this environment (Fernández et al., 2018).

1.1.2 Metagenomics[4]

Even with the improved techniques, the 16S rDNA sequencing allows only to identify the taxonomy of a prokaryote. If the microbe is not present in a database, one can match the sequence to the closest relative, but no more information can be gained from the small ribosomal unit. What can one do if one wants to know more about an unknown species of prokaryote? Ideally, one wants to culture the microbe, but this might not be easy, especially as we do not know which medium we would need to cultivate the prokaryote.

Stein et al. faced the same challenge: They wanted to know more about an uncultured clade of marine Archaea. They knew from 16S marker surveys that this clade is abundant in the surface water of the Hawaiian ocean. Stein et al. were the first to use a metagenomic sequencing approach. They extracted DNA fragments from the ocean water and cloned them into a library of *E. coli*. Clones that contained the 16S signature of the clade of interest were selected for sequencing. Sequencing was labor-intensive and involved digesting the fragment of interest with restriction enzymes and cloning sub-fragments into plasmids before sequencing the sub-fragments in steps of less than 1kpb in length. Using a technique called primer-walking, Stein et al. were able to, in the best case, rebuild a 40kb-fragment around the 16S gene.[5] Even though this fragment did not contain any genes with novel functions, their study laid the groundwork for a new era of environmental sequencing of uncultured species.

Shotgun genomics

Primer walking is inherently slow as one has to finish sequencing one step to design a primer for the next. **Shotgun sequencing** was invented in order to circumvent this constraint (Staden, 1979; Anderson, 1981). DNA is shredded into random (overlapping) fragments that are assembled with the aid of a computer. Because of computational limitations, shotgun metagenomics was initially limited to DNA fragments of 50kb. It allowed the sequencing of viruses, but to sequence larger genomes, the genome must to be split into fragments of this size, amplified in bacteria or yeast, before being sequenced with the shotgun

[4]This section was inspired by the excellent blog post by Matthew Schechter, "The history of metagenomics: An incomplete summary," merenlab.org

[5]It is worth noting the progress in sequencing technology. DNA fragments of 40kpb and longer can be sequenced today as a single molecule using a long-read sequencer (Dijk et al., 2018)

Origin of the term metagenome

The term metagenome was first used by Handelsman et al. in their work about the soil metagenome (Handelsman et al., 1998). They did not use sequencing but rather extracted long DNA fragments from the soil and cloned them into *E. coli* cells. Testing this *E. coli* library for new natural products accelerated the search and identification of biosynthetic gene clusters. As the DNA fragments did not come from specific microbes, Handelsman et al. introduced the term *metagenome* to describe the ensemble of genomes and biosynthetic machinery of the soil microflora. The term is sometimes used as a synonym for *microbiome*, as both describe the collection of all microbes in an environment.

approach. This hierarchical shotgun strategy was used for most of the genomes sequenced in the context of the human genome project.

The team of Craig Venter leveraged shotgun metagenomics to assemble whole genomes. They sequenced the first bacterial genome in 1995 (*Haemophilus Influenzae*, 1.8 Mbp, Fleischmann et al., 1995). They proposed to use *whole-genome shotgun sequencing* for the human genome (J. Craig Venter, Smith, et al., 1996), but the proposition was not received. There was still doubt if the shotgun approach can scale to large genomes of eukaryotes with many repetitive sequences (J Craig Venter, 2006). The team of Craig venter sequenced the genome of *Drosophila* (Myers et al., 2000) and finally *Homo sapiens* (J. Craig Venter, Adams, et al., 2001) as part of a private initiative [6].

Shotgun meta-genomics

After having sequenced the human genome, Craig Venter went on to sequence the marine metagenome. The goal was to sequence samples from all the world's oceans, but already for the first samples, the Caldera assembler failed (J. Craig Venter, Remington, et al., 2004). Only a quarter of the reads could be assembled into well-covered contigs. The diversity of the microbes made it too difficult to assemble their genomes. If genomes cannot be assembled, it is still possible to

[6] To be precise, the efforts of the Human genome project and Celera Genomics achieved the assembly of about 90% of the whole human genome. Only now the remaining gaps were filled (Nurk, Koren, et al., 2021)

perform analyses about the functional and taxonomic composition of a metagenome based on genes predicted on the contigs or the reads themselves. In this way, J. Craig Venter, Remington, et al. estimated that they sequenced DNA from almost 2000 different species, including 148 types of bacteria never seen before.

Such gene-centric metagenome analyses became wildly popular at the beginning of large-scale metagenome studies (McMahon, 2015). Significant collaborative efforts were undertaken to construct reference gene-catalogs for specific microbiomes, for example, the mentioned *Global Ocean Sampling Expedition*, the Human microbiome project, and the MetaHIT (METAgenomics of the Human Intestinal Tract) project (Yooseph et al., 2007; Turnbaugh et al., 2007; Qin et al., 2010). These efforts uncovered millions of new genes for different metagenomes. Even if the fraction of annotatable genes is small, these catalogs enabled the comparative analysis of metagenomes based on function and even the inference of metabolic pathways (Tringe, 2005). Metagenomic tools developed during this time, e.g., HUMAnN2 (Abubucker et al., 2012) are still prevalent.

However, gene-centric annotations approaches have several limitations because they treat the whole microbiome as one entity: First, the quantification of functions is based on reads mapping to genes that are even more subject to variation than genomes, e.g., through ongoing genome duplication or gene multiplicity. Second, the taxonomic and functional annotation are not linked. It is not easy to see which species is responsible for which function. Therefore, it becomes difficult to relate taxonomic changes to changes in functional abundances. Third, metabolic pathways are reconstructed for the whole metagenome instead of individual genomes, obfuscating any metabolic mutualism or competition between different species by considering them as the same entity.

> *Genes are expressed within cells, not in a homogenized cytoplasmic soup. It matters a lot whether a complete metabolic pathway is found in a genome versus distributed across multiple distinct genomes.*
>
> — McMahon, 2015

A genome-centered approach to metagenomic data can overcome these limitations. In the following section, we will look at the technological and algorithmic advancements that made this change possible.

1.2 Genome-resolved metagenomics

1.2.1 Metagenome assembly

The assembly of metagenomes is still a challenge today. One of the significant advances in terms of algorithms was the introduction of graph-based assemblers. Before, assembly algorithms compared each read to each other, successively merging reads with the most significant overlap to creating a consensus sequence. Overlap-layout consensus (OLC) algorithms have difficulty finding a consensus if the reads have multiple overlaps due to repeated regions. Nor do they scale well to large sets of reads, as each read has to be compared to each other, making the computational burden increase exponentially with the number of reads.

> *Children like puzzles, and they usually assemble them by trying all possible pairs of pieces and putting together pieces that match. Biologists assemble genomes in a surprisingly similar way, the main difference being that the number of pieces is more significant.*
>
> — Pevzner et al., 2001

Myers, who helped assemble the *Drosophila* and the human genome, saw the limitations of their assembly algorithm and proposed a new idea. The idea is to use a (de Bruijn) graph to represent the sequenced reads and framed the assembly as a problem to find the optimal path in this graph. The sequenced reads are split into short sub-sequences of a fixed size, the so-called k-mers. These represent the graph's nodes. Two k-mers are connected in the chart if they are adjacent in at least one sequencing read. The reads represent short paths connecting this node. The assembly consists of applying several graph-simplification algorithms to find paths that are as long as possible. In theory, the optimal path can be found in linear-time (Pevzner et al., 2001), but because the coverage is never homogenous, it is rarely possible to find a complete genome. The choice of the k-mer-length is crucial: short k-mers create a well-connected graph, with the risk of having too many overlaps that make it challenging to resolve repeats. Long k-mers can better resolve repeats but decrease the chance of overlaps between the sequencing reads. Algorithms based on the de Bruijn graph reduce the computational costs drastically because the chart stores the sequencing data more efficiently. The graph's memory requirements can be

even more reduced by removing sequencing errors before or during the building of the graph. Sequencing errors introduce false k-mer-nodes and lead to spurious branches. Graph-based assembly algorithms became popular after the human genome was sequenced, and (**next-generation sequencing**) came available that allows much cheaper and parallelized sequencing albeit with a limitation of the read-length.

Even though prokaryote genomes are relatively simple to assemble, the assembly of a complex mixture thereof, a metagenome, is challenging. Overlaps within a genome and between different genomes are formed at regions that are similar, such as the conserved genes for the ribosome. Many bacterial species in a microbiome are represented by a mixture of strains with a conserved core genome and additional variable regions (Kashtan et al., 2014). The coverage over the different genomes is very uneven due to the overlaps, amplification bias, and the difference in the abundance of the organisms in the original sample. It can become challenging to distinguish low-abundant strain variation from sequencing errors.

Modern metagenome assemblers such as `Megahit` and `metaSPAdes` (D. Li et al., 2015; Nurk, Meleshko, et al., 2017) deal with these challenges by different modifications to a standard-genome assembly algorithm. Both use multiple graphs with different k-mer- lengths to benefit from the advantages of both small and large k-mers. Smal k-mers allow assembling better regions with low coverage, whereas longer k-mers allow disentangling repeats and inter-genome overlaps. The graph for one k-mer-length is used to build the next larger k-mer-graph. The tools fall on different sides of the tradeoff between correcting sequencing errors and overwriting strain variation. `Megahit` is sensitive to strain variation. There are no specific error-correction steps other than removing k-mers below a threshold from the graph. Discarded k-mers can be recovered if they fit in the assembly graph. `metaSPAdes`, on the other hand, corrects the sequencing reads before the graph generation. The tool uses stringent graph simplification algorithms that ignore strain-specific features of rare strains to reconstruct a consensus backbone of a strain mixture. Interestingly, the aglomerating approach of `metaSPAdes` gives the best results as an independent benchmark of metagenome assemblers from 2017 (Vollmers et al., 2017). The tool produces the longest scaffolds, even from highly complex metagenomes. `metaSPAdes` is often used for large-scale metagenome assembly projects unless the memory

requirements are too high (Pasolli et al., 2019; Almeida et al., 2019; Nayfach et al., 2019). In which case, often, `Megahit` is used instead. `Megahit` is the most efficient tool, according to the same benchmark, and often produces the largest assembly even if it is more fractionized (Vollmers et al., 2017). Both assemblers rarely produce complete genomes, and therefore, it is necessary to cluster the resulting contigs into bins that could be thought of as genomes, a process called *binning*.

1.2.2 Recovering genomes from metagenomes

The beginning of binning

Even before performant graph-based assemblers were available, researchers attempted to recover genomes from metagenomes. Tyson et al., were the first that succeeded. Their landmark paper (Tyson et al., 2004), focuses on a microbiome with relatively low diversity from an acid mine drainage. The microbes living in these harsh conditions (pH 0.83) oxidize iron and exacerbate the pollution of the mine outflows. The microbiome that consists mainly of different bacterial species grows as a biofilm. To understand the metabolic interaction between the different uncultured species, Tyson et al. attempted to reconstruct genomes directly from the metagenome sample.

To do so, they performed an unprecedentedly deep metagenomic sequencing (76.2 Mbp) that should cover the genomes up to 10 fold. The modified a overlap-based assembly algorithm prioritizes continuity of the assembly over the accuracy, which is in line with the modifications in modern algorithms as described above. The shift had its effect; over 85 % of the reads could be assembled into scaffolds longer than 2 kbp. Tyson et al. calculated the average GC-content (fraction of guanine + cytosine) and coverage for each contig. When they looked at their distribution, four peaks emerged (Fig. 1.2 on the next page). Could this be four different genomes? If so, are they complete? The contigs of two clusters showed similarity to an earlier sequenced genome of an archaeon, and the sum of the contig's length matched the genome size of the sequenced genome. The two other clusters contained a 16S gene corresponding to the dominant bacterial genus *Leptospirillum*, which had no sequenced genome for the entire phylum.

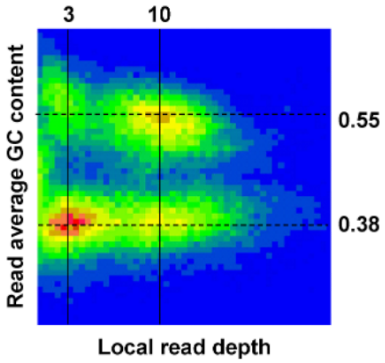

Fig. 1.2 Distribution of GC content versus local read depth (coverage) of a deeply sequenced metagenome from an acid mine drainage. Four peaks are visible at the intersections of the grid lines. Source: (Tyson et al., 2004)

How would one show the completeness of a genome without related reference genomes? Tyson et al. did so by verifying if all genes for the essential transfer RNA synthetases were present in the cluster. Based on this estimation, one *Leptospirillum* species was complete, and one nearly. Interestingly, the lower abundant species were the only species to fix nitrogen and supplied it to the community. This result could not be obtained other than culturing or genome-resolved metagenomics. Also, because they used such a deep sequencing, they could investigate the strain distribution. The *Leptospirillum* species existed as a unique strain, whereas the archaea species was a mosaic of free recombining cells originating from three ancestral strains. This initial success of recovering two nearly complete genomes laid the stepping stone for further studies (See also Fig. 6.2 on page 108).

Tyson et al. used simple thresholds to define *bins*, which they showed to be reasonable approximations of genomes. Even though today, much more sophisticated algorithms are used to segregate contigs into genomes, the term **binning** stuck. Most algorithms work under the paradigm that one contig belongs only to one bin.

How do we bin contigs into genomes?

Since the first genomes were recovered from metagenomes, a plethora of algorithms was developed for metagenomic binning. Some rely on visual inspection and manual curation (Zhu, Dupont, et al., 2018; Eren, Esen, et al., 2015), while

others are fully automated. The explosion of developed algorithms and the advancement of metagenome assembly made it difficult to compare the different tools on even ground. The *critical assessment of metagenome interpretation* (CAMI) challenge was initiated to benchmark various metagenomic tools on newly sequenced and real datasets, but the benchmark could not keep up with the development of new algorithms.

The binning algorithms become more and more sophisticated, but the idea stays the same: Grouping contigs into genomes based on two sets of features, **sequence features**, and **abundance features**: Many ways exist to extract features from the DNA sequence of a contig (or a read). It is possible to predict genes and map them or their translated protein to a database to find similarities with existing genes. Genes that are generally found only once in a genome can be used to constrain the clustering or estimate the number of genomes present in the sample (See more in sec. 1.2.3 and 6.4.1).

More directly, the raw **sequence composition**, measured as frequencies of k-mers, can be used as features. Even before sequencing was available, it was recognized that the frequencies of the four DNA bases (A, T, G, C) and their combination follows non-random patterns (Josse et al., 1961). It was shown that the sequence composition is more similar between genomes of the same taxon than from a different (Nussinov, 1980) and that it can be used to classify genomes or contigs into a taxonomy (Sandberg et al., 2001). The GC-content is the sum of guanine (G) and cytosine (C) frequencies ($k = 1$). While the specificity of the genome signature increases with the length, the number of possibilities increases exponentially with k. Today, most of the time, frequencies of **tetranucleotides**, k-mers of size 4, were used to measure the sequence composition. The tetra-nucleotide frequency captures more of the particularities of the contig sequences as they incorporate the GC-content and codon-bias.

The feature of the abundance is, most of the time, the average coverage of a contig. However, instead of using only the coverage information from one sample, contigs can be clustered by the abundance from different samples. An idea that was first developed by Albertsen et al., who used two different extraction protocols of the same microbiome sample to get two different abundance values of the same strains. Using this method, the researchers could recover 31 genomes from a bioreactor, including from low abundant species.

Binning based on differential abundance

Binning based on differential abundance requires one assembly with coverage information from different samples. To achieve this, usually, all samples are **co-assembled**, and the reads from all samples are mapped to the same assembly. Because co-assembly combines the data from multiple samples, it allows the assembly of contigs from more low-abundant genomes. However, co-assembly also cumulates the (strain-)diversity from numerous samples and multiplies the challenges associated with metagenome assembly. It is also possible to assemble samples separately and merge the assemblies, which reduces the computational burden for the co-assembly. However, it looses also the advantage of assembling low-abundant genomes, and it still contains inter-sample chimeras.
Alternatively, one can map the reads from each sample to all assemblies of a project. In this way, one keeps the advantages of both single-sample assembly and binning based on differential abundance. However, the downside of **cross-mapping** is that it requires $N^2_{samples}$ mappings and is therefore not scalable.
An interesting new approach, implemented by Nissen et al., is based on single-sample assembly but **co-binning**. Each sample is assembled separately, and the assemblies are concatenated. As in co-assembly, the reads from all samples are mapped to the same assembly. Because the combined assembly contains multiple times the same genome, the multiple mapping sites of reads must be considered. Binning is performed using a deep variational autoencoder, which autonomously learns how to weight the sequence and the abundance feature. After clustering, the contigs from each sample are separated to create sample-specific bins for each cluster. This method pays much attention to strain variation by assembling samples separately and splitting the clusters in sample-specific bins. It allows disentangling strains up to 99.5%, according to the authors.

This idea of using the **differential abundance** of contigs in multiple samples was leveraged by Nielsen et al. from the MetaHIT consortium to produce the first binning of a complex microbiome (Nielsen et al., 2014). As the metagenome assemblers were still not at their best, the researchers based their analysis on genes quantified in 396 human gut metagenome samples. The correlation

of these abundance values allowed them to segregate the genes into clusters. Some of these clusters had the size of bacterial genomes, whereas others could be associated with phages. As the method is based on genes, the resulting clusters do not contain the genome sequence, but the segregation of the genes can assist assembly. By re-assembling all the reads associated with a specific cluster, the authors could reconstruct 360 genomes.

The year after, Christopher T. Brown et al. published eight complete and 789 draft genomes from a group of tiny bacteria (< 0.2 µm). These bacteria, which were only known by environmental sequencing, have shrunken genomes and lack many genes and pathways, thought to be essential (Christopher T. Brown et al., 2015). Their 16S gene is different from known bacteria, making more than half of these organisms undetectable by 16S sequencing. They were first thought to represent multiple phyla and are called the candidate phylum radiation (CPR). However, subsequent phylogenetic analysis showed that they are part of the phylum *Patescibacteria* (Donovan H Parks et al., 2018). This example shows again how genome-resolved metagenomics allows the studying of previously undetected organisms.

1.2.3 What does it mean to be complete?

Metagenome-assembled genomes, short MAGs, are only a bunch of contigs clustered together. Do they correspond to real genomes? Are they as good as genome sequencing from isolates? Comparing a MAG to a close reference genome can help to validate the binning. If the MAG does not have a related reference genome, the MAG quality is commonly estimated based on marker genes. Like Tyson et al., one can search for genes found in practically all microbial genomes, such as t- and rRNA genes and their associated proteins. The **completeness** of a genome is estimated as the fraction of marker genes present divided by their expected number (See equation below). Similarly, marker genes present only once in practically all microbial genes are used to estimate **contamination** of MAGs.

$$\text{Completeness} = \frac{\text{present}}{\text{expected}} \text{ marker genes}$$

$$\text{Contamination} = \frac{\text{duplicated}}{\text{expected}} \text{ marker genes}$$

In practice, the same set of genes is used to estimate completeness and contamination, even if not required. The set of marker genes can be adapted to the novelty of a MAG. For example, a MAG is first assessed based on universal marker genes and then placed in a phylogenetic tree. This approximative taxonomy is used to identify the closest clade for which a marker gene set is available, and the MAGs quality is assessed with more detail. There are approximately 50 genes that are single-copy and present in all bacteria and archaea. Still, over 100 phylum-specific marker genes can be defined, and even more for lower taxonomic levels.

The tool `checkM` was proposed first to perform this phylogenetic-specific quality assessment of prokaryote genomes. But its database and phylogenetic tree were not updated since 2015. During my Ph.D., I contributed to adapt `BUSCO` (Manni et al., 2021) to perform such analyses on microbial genomes. `BUSCO` is a more scalable approach developed initially for animal genomes. It is based on the marker genes of the regularly updated OrthoDB (Zdobnov et al., 2021) and assesses the quality not only of prokaryotes but also eukaryotes.

Commonly the completeness and contamination estimates are combined in a single quality score with five times more weight on the contamination (See equation below). Genomes below a quality score of 50% are regarded as low-quality, and genomes with >90% are counted as high-quality genomes. The *Minimum Information about a metagenome-assembled genome* (MIMAG) criteria additional expect the rRNA genes and at least 18 tRNAs (Bowers et al., 2017). However, these genes are complicated to assemble from metagenomes and are usually not counted as a requirement for high quality or near-complete MAG (Almeida et al., 2019; Gruber-Vodicka et al., 2020).

$$\text{Quality score} = \text{Completeness} - 5 \times \text{Contamination}$$

Most genomes recovered from metagenomes do not reach the maximal quality score. There can be biological reasons for this, as it is the case for the tiny bacteria of the candidate phylum radiation (sec. 1.2.2). These bacteria systematically miss subsets of the marker genes present in 90% of all bacteria (Eren & Delmont,

2017). However, this group is only the exception that confirms the rule. Most MAGs are not complete. Even MAGs that are of high quality might contain assembly errors, strain chimeras and are often much more fractionized (measured by the $N50$-metric) than isolated genomes (Chen et al., 2020). The isolation of a species followed by sequencing its genome is the optimal approach, even if it does not guarantee a complete genome or genome without contamination. As described in chapter 4, we found low-quality isolated genomes that are part of official culture databases. Some had even contamination of 100 %, meaning they consist of an isolate of two strains.

1.2.4 Who is doing what?

Regardless if a genome is assembled from an isolate or recovered from a metagenome, the bare DNA sequence is only an intermediate step. It is more interesting to annotate a genome with its taxonomy and the functional potential of its genes. The proteins predicted from identified genes are mapped to a database of functions to annotate them. Proteins can have wildly divergent sequences and still exhibit the same function. To optimize speed and sensitivity, often *hidden Markov models* (HMMs) are used to annotate genes with functions. The HMMs are constructed from the alignment of proteins with the same function and encode all of the similarities and variabilities of the proteins in a simple numerical matrix.

An optional but beneficial step for functional annotation is integrating the protein annotations into a higher organization order. We often use the term **pathway** to describe a collection of functions that represent a well-characterized segment of the molecular machinery of a cell. For instance, a metabolic pathway describes a group of enzymes used to produce a metabolite or its degradation. Other pathways may be implicated in cell-to-cell communication (quorum sensing) or the adaptation to an environment, for example, sporulation or biofilm formation. Some pathways are encoded by physically clustered groups of genes, for example, **biosynthetic gene clusters** (BGCs), genes that together encode a biosynthetic pathway (Medema et al., 2015) or operons, commonly regulated adjacent genes. Nonetheless, in general, pathways are only human-made schematic representations without genetic correspondence.

The most used database for functional annotation is KEGG (Kyoto Encyclopedia of Genes and Genomes, Kanehisa & Goto, 2000). The organization of the KEGG

database is based on KEGG-orthologs (KOs), curated groups of genes that have the same function. Metabolic KOs correspond most of the time to an enzyme from the Enzyme Commission (EC number). KOs are organized into modules (segments of pathways) and large overarching pathway maps. Analogous pathways can also be found in the MetaCyc database (Caspi et al., 2016).

The crucial step of the pathway integration is deciding if a set of genes are sufficient to mark the presence of a pathway in a genome or not. The challenge arises because functions can be part of multiple pathways and that various versions of pathways often exist. Therefore the presence of one or two functions does not mean that a pathway is present. On the other hand, a missing annotation might be a false negative, especially in MAGs, which are rarely complete. To infer the presence of pathways, it is necessary to model them to a certain extent. It is even possible to create metabolic models for the whole organism. These can then be used for inferring metabolic symbiosis between members in a microbiome (Machado, Andrejev, et al., 2018; Belcour et al., 2020; Machado, Maistrenko, et al., 2021). Nevertheless, less than half of genes can be annotated for most species. Even less can be integrated into pathways (Richardson et al., 2019), which lets substantial room for identifying new gene functions through metagenomic studies.

Taxonomic annotation of Genomes

Taxonomic annotation is also based on genes. Usually, conserver marker genes are predicted and aligned to a reference taxonomy, allowing to place the genome into a phylogenetic tree. On the other hand, for species attribution, a more precise method is necessary. Traditionally bacterial species were defined based on phenotypic characterization, for example, shape or enzymatic potential, in addition to a marker gene analysis. Species delineation based on the whole genome were realized even before they could be sequenced (Brenner, 1973). The genomic DNA of two species was mixed and allowed to hybridize. The strength of association between the two genomes is used as a measure for their similarity. With the possibility to sequence whole genomes easily, the calculation of the **average nucleotide identity** (ANI) between genomes replaced the hybridization experiments. A threshold of 95% ANI was found to recapitulate the majority of existing species boundaries (Konstantinidis & Tiedje, 2005; Jain et al., 2018).

Calculation of the ANI requires pairwise alignment of genomes, which scales quadratically with the number of genomes. To solve this computational problem, efficient tools must be used to deal with the flood of genomes recovered from metagenomes. One essential advancement is the implementation of a MinHash algorithm for genome comparison. So, allows the tool `mash` and other implementations, the fast comparisons of millions of genomes in low memory (Ondov et al., 2016).

Still, the best algorithms for taxonomic annotation are useless without a robust taxonomy, which was a critical bottleneck until recently. "Development of a robust bacterial taxonomy has been hindered by an inability to obtain most bacteria in pure culture and, to a lesser extent, by the historical use of phenotypes to guide classification. " (Donovan H Parks et al., 2018). Philip Hugenholtz, which was already a forerunner in systematizing prokaryote taxonomy based on the 16S gene (McDonald et al., 2012), developed the **genome taxonomy database** (GTDB), that establishes a robust genome-based taxonomy (Donovan H Parks et al., 2018; Donovan H. Parks, Chuvochina, et al., 2020). It includes all cultured genomes but also many genomes recovered from metagenomes. Not very surprising, most species in GTDB come only from metagenome-assembled genomes[7].

1.3 Goal of the thesis

The goal of my P.h.D thesis is to enable the analysis of the mouse gut metagenome.

Mice are the most used model organism to study the impact of the microbiome on its host. Several factors make the mouse a good model: The availability of samples from different parts of the gastrointestinal tract, treatment options, controlled diet, and housing environment, defined genetic background, and ethical considerations. However, the mouse gut microbiota has been poorly characterized, and only a fraction of the diversity observed by 16S rDNA sequencing is represented by genomes in public databases (Lagkouvardos et al., 2016). The majority of mouse microbiome studies are performed by sequencing the variable regions of the 16S gene. While this technique has allowed a general overview of the microbiota down to the genus level, it is not suited for

[7] gtdb.ecogenomic.org – Stats

identifying species for most organisms (Johnson et al., 2019). Different species from the same genus and even subspecies from the same species can exert distinct functions (Costea et al., 2017), stressing the importance of annotating the microbiome content at the lowest taxonomic level.

Shotgun metagenomics allows studying the full microbiota diversity of an environment, including uncultured microorganisms, viruses, and plasmids. However, its interpretation is limited by the availability of reference genomes. There is a lack of reference genomes from the members of the mouse microbiome, as is apparent from the low mapping rate (Fig. 1.3 on the next page). We could classify less than 20% using commonly used workflows to analyze the (human) metagenome. Even with a mouse-specific gene-catalog (Xiao et al., 2015), we could annotate about half of the reads, which corresponds to what the authors of the gene catalog have stated. It is important to note that while the gene-catalog is an essential reference for genes and functions, it has only a limited taxonomic annotation and does not contain genomes, which hinders the linking of function to species.

To solve the lack of reference genomes for the mouse microbiome, I turned to algorithms that make it possible to reconstruct genomes from metagenomes. I implemented these algorithms in an efficient pipeline that allows users to go from the raw reads to reconstructed and annotated genomes. In chapter 2, I describe the development of this pipeline called `metagenome-atlas`. Using this pipeline, we were able to annotate the functional potential of the mouse gut microbiome and predict changes in metabolites, which were confirmed by targeted metabolomics and have the potential to improve osteoporosis (ch. 3).

Motivated by the success of analyzing our data with `metagenome-atlas`, we wondered if we could improve the collection of genomes for the mouse gut, both by recovering more and better MAGs. We, therefore, processed all publicly available metagenomes of the mouse gut with `metagenome-atlas`. The resulting MAGs form the *comprehensive mouse gut metagenome* catalog (CMGM), described in chapter 4. We demonstrated how reconstructed genomes could be used to analyze metagenomes of mice and relate them to the host's health in section 4.2.

Finally, I describe in chapter 5 what I have learned about the statistical analysis of metagenome data and why it is crucial to take the compositional nature of

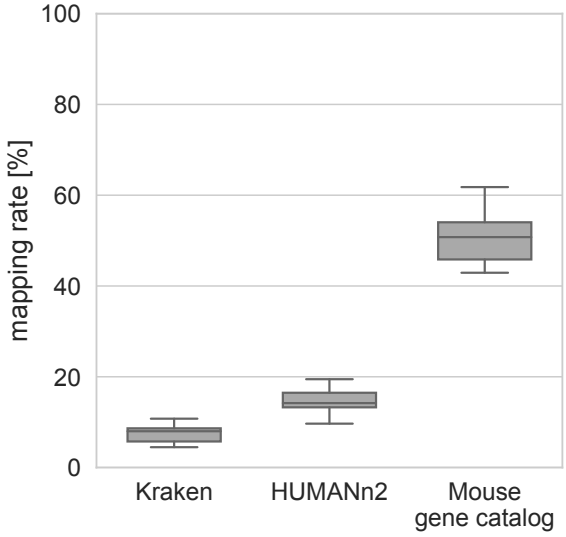

Fig. 1.3 Benchmark of metagenomics tools to classify reads from a mouse gut metagenome at the beginning of my Ph.D.: The faction of reads classified by HUMAnN2 (Franzosa et al., 2018), Kraken2 (Derrick E. Wood et al., 2019) with a database of all bacteria and virus genomes from RefSeq or the fraction or reds mapping to the mouse gene catalog (Xiao et al., 2015). Reads were mapped using bbmap, with a minimum identity of 0.9. To see the improvement achieved, see Ch. 4 Fig. 3B.

microbiome data into account, especially for microbiomes that have comprehensive catalogs available.

Recovering genomes made easy

Title: ATLAS: a Snakemake workflow for assembly, annotation, and genomic binning of metagenome sequence data

Authors: Silas Kieser, Joseph Brown, Evgeny M. Zdobnov, Mirko Trajkovski & Lee Ann McCue

Status: Published in *BMC Bioinformatics* 21, 2020

This manuscript describes the key method used in my P.h.D. It describes metagenome-atlas, a state-of-the-art pipeline for the analysis of metagenome data. Atlas enables *de novo* assembly of genomes from metagenomic reads. It quantifies the abundance of the recovered species and annotates them with taxonomy and the functional potential of their genes. The pipeline is easy to use and handles all steps from quality control, assembly, binning to annotation and quantification. It downloads all the required software tools and databases on the fly.

Contribution statement

The development of the pipeline was started by Joseph Brown at Pacific Northwest National Laboratory. In May 2018, I asked to contribute to the opensource pipeline and was accepted in the developer team. Since then, I became the main contributor and lead developer, as can be seen from the contributor statistics on the GitHub repository. I maintained the tool and helped to its popularization with tutorials, classes, and workshops. I wrote the manuscript together with the other co-authors.

Kieser et al. BMC Bioinformatics (2020) 21:257
https://doi.org/10.1186/s12859-020-03585-4

BMC Bioinformatics

SOFTWARE Open Access

ATLAS: a Snakemake workflow for assembly, annotation, and genomic binning of metagenome sequence data

Silas Kieser[1,2†], Joseph Brown[3,4†], Evgeny M. Zdobnov[2,5,6], Mirko Trajkovski[1,5,7] and Lee Ann McCue[3*]

* Correspondence: leeann.mccue@pnnl.gov
†Silas Kieser and Joseph Brown contributed equally to this work.
[3]Earth and Biological Sciences Directorate, Pacific Northwest National Laboratory, Richland, WA 99352, USA
Full list of author information is available at the end of the article

Abstract

Background: Metagenomics studies provide valuable insight into the composition and function of microbial populations from diverse environments; however, the data processing pipelines that rely on mapping reads to gene catalogs or genome databases for cultured strains yield results that underrepresent the genes and functional potential of uncultured microbes. Recent improvements in sequence assembly methods have eased the reliance on genome databases, thereby allowing the recovery of genomes from uncultured microbes. However, configuring these tools, linking them with advanced binning and annotation tools, and maintaining provenance of the processing continues to be challenging for researchers.

Results: Here we present ATLAS, a software package for customizable data processing from raw sequence reads to functional and taxonomic annotations using state-of-the-art tools to assemble, annotate, quantify, and bin metagenome data. Abundance estimates at genome resolution are provided for each sample in a dataset. ATLAS is written in Python and the workflow implemented in Snakemake; it operates in a Linux environment, and is compatible with Python 3.5+ and Anaconda 3+ versions. The source code for ATLAS is freely available, distributed under a BSD-3 license.

Conclusions: ATLAS provides a user-friendly, modular and customizable Snakemake workflow for metagenome data processing; it is easily installable with conda and maintained as open-source on GitHub at https://github.com/metagenome-atlas/atlas.

Keywords: Metagenomics, Analysis workflow, Annotation, Metagenome-assembled genomes

Background

Metagenomics has transformed microbial ecology studies with the ability to generate genome sequence information from environmental samples, yielding valuable insight into the composition and functional potential of natural microbial populations from diverse environments [1, 2]. Despite the prevalence of metagenome data, there are few broadly accepted standard methods, either for the generation of that data [3–5] or for its processing [6, 7]. In particular, processing metagenome data in an efficient and

reproducible manner is challenging because it requires implementation of several distinct tools, each designed for a specific task.

The most direct and frequently used way to analyze metagenome data is to map the sequence reads to reference genomes, when a suitable genome database from cultivated microbes is available (e.g. Humann2 [8]). However, these methods do not capture uncultivated species; studies using single-copy phylogenetic marker genes have improved estimates of species richness in metagenome data by expanding the representation of uncultivated species [9]. To truly characterize a natural microbial community and examine its functional potential, assembly-based metagenome analyses are needed. This has been demonstrated by recent studies that have recovered thousands of new genomes using co-abundance patterns among samples to bin contigs into clusters [10–13].

A number of assembly-based metagenome pipelines have been developed, each providing a subset of the required tools needed to carry out a complete analysis process from raw data to annotated genomes [14–17]. For example, MOCAT2 [16] relies on gene catalogs to evaluate the functional potential of the metagenome as a whole, but without directly relating functions to individual microbes. Metagenome processing pipelines commonly default to co-assembly of the samples rather than assembly of individual samples, resulting in more fragmented assemblies [18]. Only some applications (e.g., IMP [17]) permit the co-assembly of metagenomes and metatranscriptomes for individual samples. Furthermore, the configuration and technical constraints to user control often limit the adoption of these tools in the research community.

Here we present an entirely new version of ATLAS [19], an assembly-based pipeline for the recovery of genes and genomes from metagenomes, that produces annotated and quantified genomes from multiple samples in one run with as little as three commands. The pipeline integrates state-of-the art tools for quality control, assembly and binning. The installation of ATLAS is automated: it depends only on the availability of Anaconda and installs all dependencies and databases on the fly. The internal use of Snakemake [20] allows efficient and automated deployment on a computing cluster.

Implementation

The ATLAS framework organizes sequence data processing tools into four distinct analysis modules: [1] quality control, [2] assembly, [3] genome binning and [4] annotation (Fig. 1); each module can be run independently, or all four modules combined in a complete analysis workflow. ATLAS is implemented in Python and uses the Snakemake [20] workflow manager for extensive control of external tools, including versioning of configurations and environments, provenance capabilities, and scalability on high-performance computing clusters. ATLAS uses Anaconda [21] to simplify initial deployment and environment set-up, and dependencies are handled by Bioconda [22] at runtime. Complete usage and user options are outlined in the ATLAS documentation (https://metagenome-atlas.rtfd.io).

Quality control

Quality control of raw sequence data, in the form of single- or paired-end FASTQ files, is performed using utilities in the BBTools suite [23]. Specifically, *clumpify* is used remove PCR duplicates and compress the raw data files, followed by *BBduk* to remove

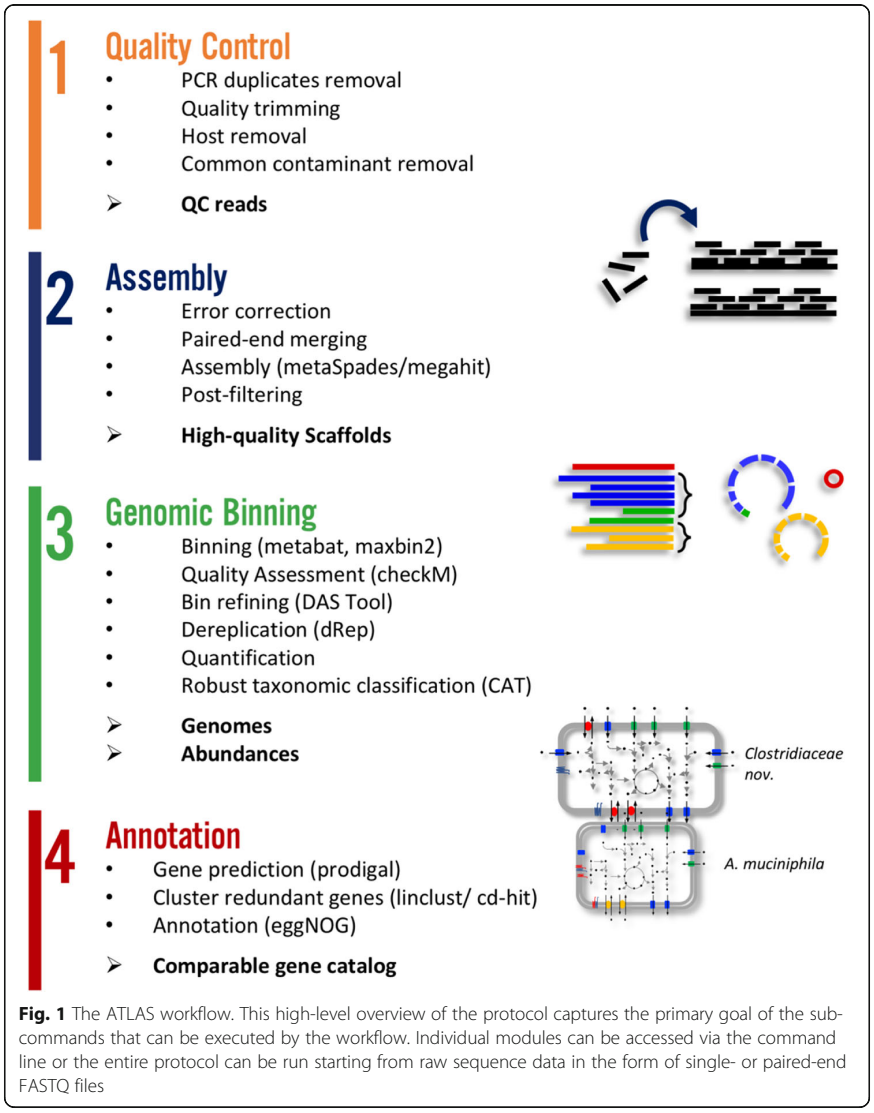

Fig. 1 The ATLAS workflow. This high-level overview of the protocol captures the primary goal of the sub-commands that can be executed by the workflow. Individual modules can be accessed via the command line or the entire protocol can be run starting from raw sequence data in the form of single- or paired-end FASTQ files

known adapters, trim and filter reads based on their quality and length (respectively), and error-correct overlapping paired-end reads where applicable. *BBSplit* is used to remove contaminating reads using reference sequences: PhiX is provided as a default or can be replaced by user-specified fasta-format sequences. To optimize data use, reads that lose their mate during these steps are seamlessly integrated into the later steps of the pipeline.

Assembly

Prior to metagenome assembly, ATLAS uses additional BBTools utilities [23] to perform an efficient error correction based on k-mer coverage (*Tadpole*) and paired-end read merging (*bbmerge*). If paired-end reads do not overlap, *bbmerge* can extend them using read-derived overlapping k-mers. ATLAS uses metaSPAdes [24] or MEGAHIT

[25, 26] for de novo assembly, with the ability to control parameters such as k-mer lengths and k-mer step size for each assembler, as well as hybrid-assembly of paired short- and long-read libraries. The quality-controlled reads are mapped to the assembled contigs, and bam files are generated to facilitate downstream calculations that may be of interest (e.g., calculating contig coverage). The assembled contigs shorter than a minimal length, or without mapped reads, are filtered out to yield high-quality contigs.

Genome binning

The prediction of metagenome-assembled genomes (MAGs) allows organism-specific analyses of metagenome datasets. In ATLAS, two binning methods are implemented (Fig. 1): metabat2 [27] and maxbin2 [28]. These methods use tetra-nucleotide frequencies, differential abundance, and/or the presence of marker genes as criteria. ATLAS supports assembly and binning for each sample individually, which produces more continuous genomes than co-assembly [29]. Definition of which samples are likely to contain the same bacterial species, via a group attribute in the Snakemake configuration file, supports binning based on co-abundance patterns across samples. Reads from all of the samples defined in a group are then aligned to the individual sample assemblies, to obtain the co-abundance patterns needed for efficient binning. The bins produced by the different binning tools can be combined using the dereplicate, aggregate and score tool (DAS Tool, [30]), to yield MAGs for each sample. Finally, the completeness and contamination of each MAG are assessed using CheckM [31].

Because the same genome may be identified in multiple samples, dRep [29] is used to obtain a non-redundant set of MAGs for the combined dataset by clustering genomes to a defined average nucleotide identity (ANI, default 0.95) and returning the representative with the highest dRep score in each cluster. dRep first filters genomes based on genome size (default > 5000 bp) and quality (default > 50% completeness, < 10% contamination), then clusters the genomes using Mash [32], followed by MUMmer [33], thereby benefitting from their combined speed (Mash) and accuracy (MUMmer). The abundance of each genome can then be quantified across samples by mapping the reads to the non-redundant MAGs and determining the median coverage across each the genome.

Taxonomic and functional annotation

For annotation, ATLAS supports the prediction of open reading frames (ORFs) using Prodigal [34]. The translated gene products are then clustered using linclust [35] or mmseqs [36] to generate non-redundant gene and protein catalogs, which are mapped to the eggNOG catalogue v5 [37, 38]. Robust taxonomic annotation is performed using the genome taxonomy database tool kit (GTDB-tk, [39]). In addition, phylogenetic trees are built based on the markers from GTDB and CheckM.

Output

The ATLAS output for each sample includes the quality-controlled reads, assembled contigs, bam files (reads mapped to contigs), and predicted genome bins, together with summary statistics in an HTML report. The final output includes results from all samples, including the raw and normalized counts for the set of non-redundant, high-quality MAGs, with a quality report and their inferred

taxonomy. From the annotation stage, two fasta files are produced containing the nucleotide and amino acid sequences of the representative genes in the non-redundant gene catalog, together with a table containing the gene annotations summarized at the genome level.

Figure 2 shows examples of ATLAS output in which we analyzed the metagenome data from paired feces and cecum samples of 8 mice fed ad libitum (PRJNA480387 [40];). On average, the sample data contained 3.5 Gbp, and produced assemblies of 108 Mbp per sample. There were 374 MAGS predicted (completeness > 50% and contamination < 10%), that formed 69 non-redundant clusters (ANI > 99%; Fig. 2A). These genomes account for 75% of the reads (Fig. 2B). In general, *Bacteroides* were more abundant than *Firmicutes*, in both cecum and feces (Fig. 2C,D). A principal coordinates analysis based on the functional annotation revealed two functionally distinct clusters of Firmicutes (Fig. 2E). Details of these results are provided on GitHub (https://github.com/metagenome-atlas/supp_data_atlas).

Conclusions

ATLAS is easy to install and provides documented and modular workflows for the analysis of metagenome data. The internal codes utilized by the workflow are highly

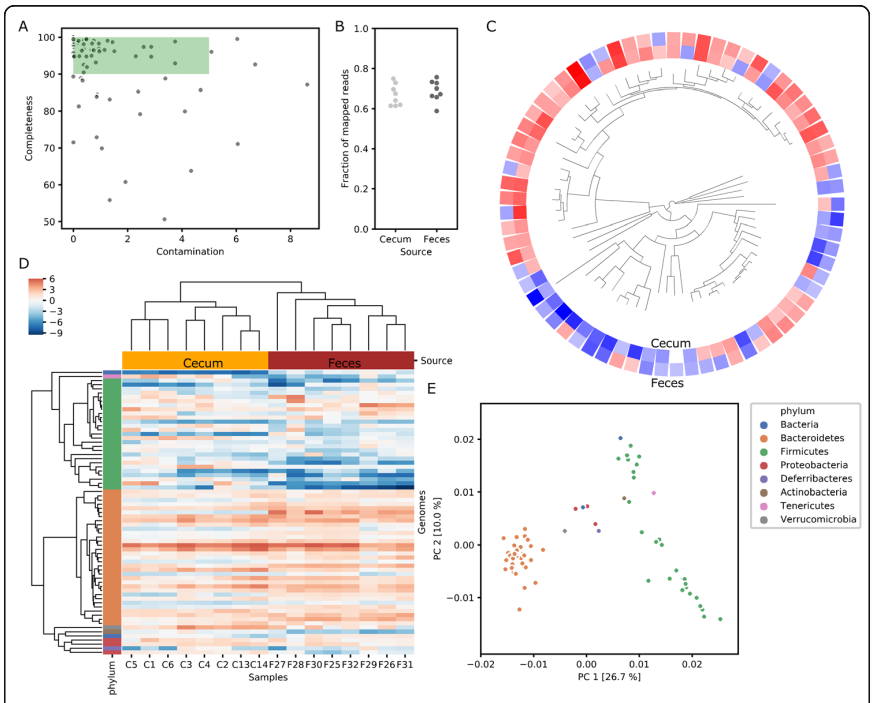

Fig. 2 Example output from the ATLAS workflow. Fecal microbiome data (PRJNA480387 [40];) processed by ATLAS show: A) the completeness and contamination of dereplicated MAGs, with high-quality genomes highlighted; B) the fraction of reads mapped to genomes; C) a phylogenetic tree of MAGs with average abundance in feces and cecum on a centered $\log_2$ scale; D) a heatmap of abundance on a centered $\log_2$ scale in which MAGs were clustered by phylogenetic distance and samples by Euclidian distance; E) a principle components analysis of the MAGs based on functional annotation

configurable using either a configuration file or via the command line. ATLAS provides a robust bioinformatics framework for high-throughput sequence data, where raw FASTQ files can be fully processed into annotated tabular files for downstream analysis and visualization. ATLAS fills a major analysis gap, namely the integration of tools for quality control, assembly, binning and annotation, in a manner that supports robust and reproducible analyses. ATLAS provides these analysis tools in a command-line interface amenable to high-performance computing clusters.

The source code for ATLAS is distributed under a BSD-3 license and is freely available at https://github.com/metagenome-atlas/atlas, with example data provided for testing. Software documentation is available at https://metagenome-atlas.rtfd.io, which describes the installation and use of ATLAS including a Docker container (https://hub.docker.com/r/metagenomeatlas/atlas).

Availability Project name: ATLAS.

Project home page: https://github.com/metagenome-atlas/atlas

Archived version: https://doi.org/10.1101/737528

Operating system(s): Linux.

Programming language: Snakemake/Python.

Other requirements: Miniconda.

License: BSD-3.

Any restrictions to use by non-academics: None.

Acknowledgements
A portion of the ATLAS framework was developed using PNNL Research Computing resources.

Authors' contributions
JB and SK developed the software and documentation; EZ, MT and LAM supervised the project; and JB, SK and LAM wrote the manuscript. All authors read and approved the final manuscript.

Funding
This work was supported by the Microbiomes in Transition Initiative at Pacific Northwest National Laboratory (PNNL) and conducted under the Laboratory Directed Research and Development Program at PNNL, a multi-program national laboratory operated by Battelle for the U.S. Department of Energy under Contract DE-AC05-76RL01830. This work was also supported by funding from the European Research Council (ERC) under the European Union's Horizon 2020 research and innovation programme (ERC-COG-2018), and the Swiss National Science Foundation Professorship to MT.

Availability of data and materials
Not applicable.

Ethics approval and consent to participate
Not applicable.

Consent for publication
Not applicable.

Competing interests
The authors declare that they have no competing interests.

Author details
[1]Department of Cell Physiology and Metabolism, Faculty of Medicine, Centre Medical Universitaire, 1206 Geneva, Switzerland. [2]Swiss Institute of Bioinformatics, Geneva, Switzerland. [3]Earth and Biological Sciences Directorate, Pacific Northwest National Laboratory, Richland, WA 99352, USA. [4]Current address: Department of Human Genetics, University of Utah, 15 S 2030 E, Salt Lake City, UT 84112, USA. [5]Institute of Genetics and Genomics in Geneva (iGE3), University of Geneva, 1206 Geneva, Switzerland. [6]Department of Genetic Medicine and Development, University of Geneva, 1206 Geneva, Switzerland. [7]Diabetes Center, Faculty of Medicine, Centre Medical Universitaire, 1206 Geneva, Switzerland.

Received: 23 May 2019 Accepted: 8 June 2020
Published online: 22 June 2020

References

1. Nayfach S, Pollard KS. Toward accurate and quantitative comparative metagenomics. Cell. 2016;166(5):1103–16.

2. Prosser JI. Dispersing misconceptions and identifying opportunities for the use of 'omics' in soil microbial ecology. Nat Rev Microbiol. 2015;13(7):439–46.
3. Costea PI, Zeller G, Sunagawa S, Pelletier E, Alberti A, Levenez F, et al. Towards standards for human fecal sample processing in metagenomic studies. Nat Biotechnol. 2017;35(11):1069–76.
4. Song SJ, Amir A, Metcalf JL, Amato KR, Xu ZZ, Humphrey G, et al. Preservation methods differ in fecal microbiome stability, affecting suitability for field studies. mSystems. 2016;1(3).
5. Wu WK, Chen CC, Panyod S, Chen RA, Wu MS, Sheen LY, et al. Optimization of fecal sample processing for microbiome study - the journey from bathroom to bench. J Formos Med Assoc. 2019;118(2):545–55.
6. Sczyrba A, Hofmann P, Belmann P, Koslicki D, Janssen S, Droge J, et al. Critical assessment of Metagenome interpretation-a benchmark of metagenomics software. Nat Methods. 2017;14(11):1063–71.
7. CAMI 2019 [Available from: https://data.cami-challenge.org/].
8. Franzosa EA, McIver LJ, Rahnavard G, Thompson LR, Schirmer M, Weingart G, et al. Species-level functional profiling of metagenomes and metatranscriptomes. Nat Methods. 2018;15(11):962–8.
9. Sunagawa S, Mende DR, Zeller G, Izquierdo-Carrasco F, Berger SA, Kultima JR, et al. Metagenomic species profiling using universal phylogenetic marker genes. Nat Methods. 2013;10(12):1196–9.
10. Almeida A, Mitchell AL, Boland M, Forster SC, Gloor GB, Tarkowska A, et al. A new genomic blueprint of the human gut microbiota. Nature. 2019;568(7753):499–504.
11. Nissen JN, Sonderby CK, Armenteros JJA, Groenbech CH, Nielsen HB, Petersen TN, et al. Binning microbial genomes using deep learning. bioRxiv. 2018:490078.
12. Parks DH, Rinke C, Chuvochina M, Chaumeil PA, Woodcroft BJ, Evans PN, et al. Recovery of nearly 8,000 metagenome-assembled genomes substantially expands the tree of life. Nat Microbiol. 2017;2(11):1533–42.
13. Stewart RD, Auffret MD, Warr A, Wiser AH, Press MO, Langford KW, et al. Assembly of 913 microbial genomes from metagenomic sequencing of the cow rumen. Nat Commun. 2018;9(1):870.
14. Chen IA, Markowitz VM, Chu K, Palaniappan K, Szeto E, Pillay M, et al. IMG/M: integrated genome and metagenome comparative data analysis system. Nucleic Acids Res. 2017;45(D1):D507–D16.
15. Eren AM, Esen OC, Quince C, Vineis JH, Morrison HG, Sogin ML, et al. Anvi'o: an advanced analysis and visualization platform for 'omics data. PeerJ. 2015;3:e1319.
16. Kultima JR, Coelho LP, Forslund K, Huerta-Cepas J, Li SS, Driessen M, et al. MOCAT2: a metagenomic assembly, annotation and profiling framework. Bioinformatics. 2016;32(16):2520–3.
17. Narayanasamy S, Jarosz Y, Muller EE, Heintz-Buschart A, Herold M, Kaysen A, et al. IMP: a pipeline for reproducible reference-independent integrated metagenomic and metatranscriptomic analyses. Genome Biol. 2016;17(1):260.
18. Mirebrahim H, Close TJ, Lonardi S. De novo meta-assembly of ultra-deep sequencing data. Bioinformatics. 2015; 31(12):i9–16.
19. White RA, Brown J, Colby S, Overall CC, Lee J-Y, Zucker J, et al. ATLAS (Automatic Tool for Local Assembly Structures) - a comprehensive infrastructure for assembly, annotation, and genomic bining of metagenomic and metatranscriptomic data. PeerJ. 2017;5:e2843v1.
20. Koster J, Rahmann S. Snakemake--a scalable bioinformatics workflow engine. Bioinformatics. 2012;28(19):2520–2.
21. Anaconda 2019 [Available from: https://www.continuum.io/].
22. Gruning B, Dale R, Sjodin A, Chapman BA, Rowe J, Tomkins-Tinch CH, et al. Bioconda: sustainable and comprehensive software distribution for the life sciences. Nat Methods. 2018;15(7):475–6.
23. Bushnell B. BBTools 2019 [Available from: https://sourceforge.net/projects/bbmap/].
24. Nurk S, Meleshko D, Korobeynikov A, Pevzner PA. metaSPAdes: a new versatile metagenomic assembler. Genome Res. 2017;27(5):824–34.
25. Li D, Liu CM, Luo R, Sadakane K, Lam TW. MEGAHIT: an ultra-fast single-node solution for large and complex metagenomics assembly via succinct de Bruijn graph. Bioinformatics. 2015;31(10):1674–6.
26. Li D, Luo R, Liu CM, Leung CM, Ting HF, Sadakane K, et al. MEGAHIT v1.0: A fast and scalable metagenome assembler driven by advanced methodologies and community practices. Methods. 2016;102:3–11.
27. Kang DD, Li F, Kirton E, Thomas A, Egan R, An H, et al. MetaBAT 2: an adaptive binning algorithm for robust and efficient genome reconstruction from metagenome assemblies. PeerJ. 2019;7:e7359.
28. Wu YW, Simmons BA, Singer SW. MaxBin 2.0: an automated binning algorithm to recover genomes from multiple metagenomic datasets. Bioinformatics. 2016;32(4):605–7.
29. Olm MR, Brown CT, Brooks B, Banfield JF. dRep: a tool for fast and accurate genomic comparisons that enables improved genome recovery from metagenomes through de-replication. ISME J. 2017;11(12):2864–8.
30. Sieber CMK, Probst AJ, Sharrar A, Thomas BC, Hess M, Tringe SG, et al. Recovery of genomes from metagenomes via a dereplication, aggregation and scoring strategy. Nat Microbiol. 2018;3(7):836–43.
31. Parks DH, Imelfort M, Skennerton CT, Hugenholtz P, Tyson GW. CheckM: assessing the quality of microbial genomes recovered from isolates, single cells, and metagenomes. Genome Res. 2015;25(7):1043–55.
32. Ondov BD, Treangen TJ, Melsted P, Mallonee AB, Bergman NH, Koren S, et al. Mash: fast genome and metagenome distance estimation using MinHash. Genome Biol. 2016;17(1):132.
33. Kurtz S, Phillippy A, Delcher AL, Smoot M, Shumway M, Antonescu C, et al. Versatile and open software for comparing large genomes. Genome Biol. 2004;5(2):R12.
34. Hyatt D, Chen GL, Locascio PF, Land ML, Larimer FW, Hauser LJ. Prodigal: prokaryotic gene recognition and translation initiation site identification. BMC Bioinformatics. 2010;11:119.
35. Steinegger M, Soding J. Clustering huge protein sequence sets in linear time. Nat Commun. 2018;9(1):2542.
36. Steinegger M, Soding J. MMseqs2 enables sensitive protein sequence searching for the analysis of massive data sets. Nat Biotechnol. 2017;35(11):1026–8.
37. Huerta-Cepas J, Forslund K, Coelho LP, Szklarczyk D, Jensen LJ, von Mering C, et al. Fast genome-wide functional annotation through Orthology assignment by eggNOG-mapper. Mol Biol Evol. 2017;34(8):2115–22.
38. Huerta-Cepas J, Szklarczyk D, Heller D, Hernandez-Plaza A, Forslund SK, Cook H, et al. eggNOG 5.0: a hierarchical, functionally and phylogenetically annotated orthology resource based on 5090 organisms and 2502 viruses. Nucleic Acids Res. 2019;47(D1):D309–D14.

39. Parks DH, Chuvochina M, Waite DW, Rinke C, Skarshewski A, Chaumeil PA, et al. A standardized bacterial taxonomy based on genome phylogeny substantially revises the tree of life. Nat Biotechnol. 2018;36(10):996–1004.
40. Fabbiano S, Suarez-Zamorano N, Chevalier C, Lazarevic V, Kieser S, Rigo D, et al. Functional gut microbiota remodeling contributes to the caloric restriction-induced metabolic improvements. Cell Metab. 2018;28(6):907–21 e7.

Publisher's Note

Relating functional changes in the microbiome to host health

Title: Warmth Prevents Bone Loss Through the Gut Microbiota

Authors: Claire Chevalier, Silas Kieser, Melis Çolakoğlu, Noushin Hadadi, Julia Brun, Dorothée Rigo, Nicolas Suárez-Zamorano, Martina Spiljar, Salvatore Fabbiano, Björn Busse, Julijana Ivanišević, Andrew Macpherson, Nicolas Bonnet & Mirko Trajkovski

Status: Published in *Cell Metabolism* 32, 2020

This study is the prime example of how metagenome-atlas can be used to analyze the mouse metagenome. My colleague, Claire Chevalier, analyzed the effect of ambient temperature on the metabolism of mice and the changes in their gut microbiome. When mice are exposed to warm ambient temperature for a prolonged time (34°C, 8weeks), they enlarge the tail and ears, which creates more surface for heat dissipation. The warm temperature not only has a remodeling effect on the bone but also on the gut microbiome. The transplantation of the gut microbiota of warm exposed mice induces similar changes on the bone of the recipient mice and can prevent osteoporosis. Epidemiological analysis shows a significant correlation between the incidence of hip fracture and the average temperature in 60 countries.

In order to identify the mechanism of how the gut microbiome influences the bone strength of the host, we used metagenomics and predicted the functional potential of the gut microbiome. Polyamine-synthesis was one of the most significant increased pathways in the gut microbiome upon warm exposure (Fig. 7). This prediction was confirmed by targeted metabolomics, and the effect of polyamine on the host was further corroborated by *in vivo* supplementation and

inhibition of their synthesis. The genome-resolved metagenomics not only allowed to identify an important pathway how the gut microbiome influences the host health, but also to identify the driver species (Fig. 6.1, which corresponds to Fig S6 in the publication).

Contribution statement

This project was led by my colleague Claire Chevalier. Like most other lab members, I helped at the end of the mouse experiment with the sacrifice of the mice. Together with her, we extracted the DNA and prepared the library for the 16S amplicon sequencing and shotgun metagenomics. I analyzed the metagenome data and implemented a functional prediction specific to this project. Together with her, we interpreted this data. I also (re-) analyzed the 16S data and made the corresponding figures. I performed the correlation analysis of the human epidemiological data.

Cell Metabolism

Article

Warmth Prevents Bone Loss Through the Gut Microbiota

Graphical Abstract

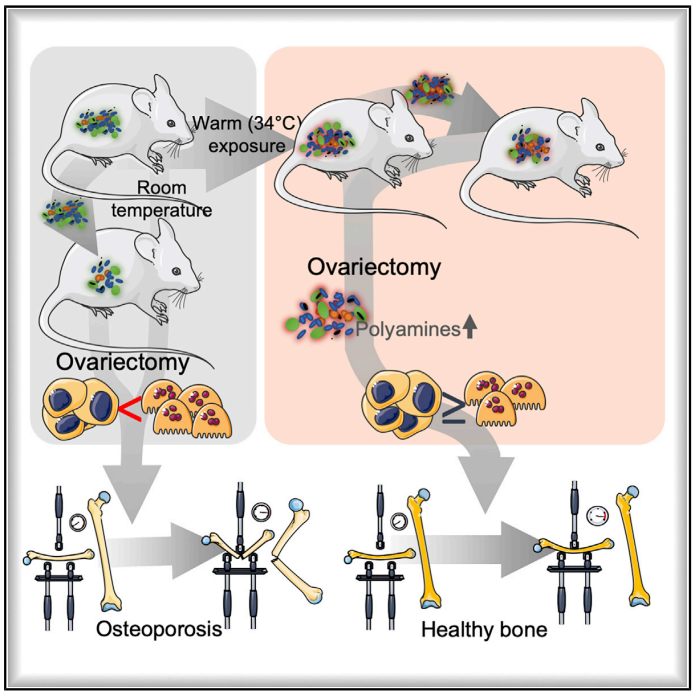

Highlights

- Warm exposure improves bone strength in adulthood and prevents osteoporosis in mice
- Human meta-analyses show inverse correlation between hip fractures and temperature
- Transplantation of warm-adapted microbiota prevents bone loss
- Warmth enhances production of polyamines that increase bone strength

Authors

Claire Chevalier, Silas Kieser, Melis Çolakoğlu, ..., Andrew Macpherson, Nicolas Bonnet, Mirko Trajkovski

Correspondence

mirko.trajkovski@unige.ch

In Brief

Osteoporosis is a disease manifested by bone loss and increased fracture risk. Chevalier et al. observe an inverse correlation between average environmental temperature and incidence of hip fractures in humans, and they demonstrate that warmth exposure prevents osteoporosis in mice, partially through changes in the gut microbiota and an increase in polyamine biosynthesis.

Chevalier et al., 2020, Cell Metabolism *32*, 575–590
October 6, 2020
https://doi.org/10.1016/j.cmet.2020.08.012

CellPress

Cell Metabolism

CellPress

Article

Warmth Prevents Bone Loss Through the Gut Microbiota

Claire Chevalier,[1,2] Silas Kieser,[1,2] Melis Çolakoğlu,[1,2] Noushin Hadadi,[1,2] Julia Brun,[3] Dorothée Rigo,[1,2] Nicolas Suárez-Zamorano,[1,2] Martina Spiljar,[1,2] Salvatore Fabbiano,[1,2] Björn Busse,[4] Julijana Ivanišević,[5] Andrew Macpherson,[6] Nicolas Bonnet,[2,7,8] and Mirko Trajkovski[1,2,9,*]

[1]Department of Cell Physiology and Metabolism, Centre Médical Universitaire (CMU), Faculty of Medicine, University of Geneva, 1211 Geneva, Switzerland
[2]Diabetes Center, Faculty of Medicine, University of Geneva, 1211 Geneva, Switzerland
[3]Division of Bone Diseases, Geneva University Hospitals, 1211 Geneva, Switzerland
[4]Institute for Osteology and Biomechanics, University Clinics Hamburg, 22529 Hamburg, Germany
[5]Metabolomics Unit, Faculty of Biology and Medicine, University of Lausanne, 1005 Lausanne, Switzerland
[6]Department for Biomedical Research, University of Bern, University Clinics for Visceral Surgery and Medicine, Inselspital, Bern University Hospitals, 3008 Bern, Switzerland
[7]Division of Bone Diseases, Geneva University Hospitals, 1211 Geneva, Switzerland
[8]Present address: Nestlé Research, Innovation EPFL Park, 1015 Lausanne, Switzerland
[9]Lead Contact
*Correspondence: mirko.trajkovski@unige.ch
https://doi.org/10.1016/j.cmet.2020.08.012

SUMMARY

Osteoporosis is the most prevalent metabolic bone disease, characterized by low bone mass and microarchitectural deterioration. Here, we show that warmth exposure (34°C) protects against ovariectomy-induced bone loss by increasing trabecular bone volume, connectivity density, and thickness, leading to improved biomechanical bone strength in adult female, as well as in young male mice. Transplantation of the warm-adapted microbiota phenocopies the warmth-induced bone effects. Both warmth and warm microbiota transplantation revert the ovariectomy-induced transcriptomics changes of the tibia and increase periosteal bone formation. Combinatorial metagenomics/metabolomics analysis shows that warmth enhances bacterial polyamine biosynthesis, resulting in higher total polyamine levels *in vivo*. Spermine and spermidine supplementation increases bone strength, while inhibiting polyamine biosynthesis *in vivo* limits the beneficial warmth effects on the bone. Our data suggest warmth exposure as a potential treatment option for osteoporosis while providing a mechanistic framework for its benefits in bone disease.

INTRODUCTION

External temperature is an environmental parameter that affects various aspects of physiology and requires constant adaptation by living organisms to its fluctuations. To dissipate heat, rodents increase skin vasodilation at specific locations where the surface-to-body ratio is high. They also adapt to increased temperatures partly by enlarging the tail and ear length/surface (Meyer et al., 2017; Alhilli and Wright, 1983; Ashoub, 1958; Harland, 1960), allowing further heat dissipation. Warmth exposure also has effects on development, for example, promoting femur growth (Romsos et al., 1985; Serrat et al., 2008) and favoring denser trabecular and cortical microarchitecture (Iwaniec et al., 2016). Unilateral heating of the limb from weaning is associated with elongation of the extremities on the heat-exposed side only (Serrat et al., 2015), and chondrocyte proliferation *in vitro* is higher at warmer incubation temperatures (Serrat et al., 2008; Serrat, 2014).

Osteoporosis is the most prevalent metabolic bone disease, characterized by low bone mass and microarchitectural deterioration (Sözen et al., 2017), leading to weaker bones and increased fracture risk. Bone remodeling is enabled by the coordinated action of the two major type of cells present in the bone: osteoblasts, which are responsible for bone formation and osteoclasts, which are involved in bone resorption. The most common type of primary osteoporosis occurs as a result of post-menopausal estrogen deficiency (Reginster and Burlet, 2006), and as such, it is exceedingly common in aging females but can also occur in men. Whether heat administration post-development and during late adulthood in healthy, or during osteoporotic states, can affect bone health, remodeling, and physiology is unknown.

The intestinal flora has emerged as an important regulator of host physiology, including the bone (Li et al., 2019; Hsu and Pacifici, 2018; Jones et al., 2017; Ohlsson and Sjögren, 2015, 2018; Parvaneh et al., 2014; Sjögren et al., 2012). We (Chevalier et al., 2015) and others (Ziętak et al., 2016) have previously shown that the host adaptation to cold is in part mediated by alterations of the gut microbiota composition. However, it is not clear whether

CellPress

Cell Metabolism
Article

elevated environmental temperature can affect the microbiota composition. It is also not known whether such alterations would have any effect on bone morphology and strength.

In this study, we show that warmth exposure applied at later stages of development improves bone microarchitecture and strength during healthy conditions. We further demonstrate that this phenomenon can be used in pathological conditions, where it prevents the deleterious effect of estrogen depletion in a mouse model of osteoporosis. These osteological improvements are mediated by warm temperature-induced alterations of the gut microbiota composition and are sufficient to prevent bone loss, indicating an existence of a signaling axis between warmth exposure and the bone that is mediated by the microbiota. In terms of possible translation, we performed human metadata analysis and found an inverse correlation between the incidence of osteoporotic hip fractures and external temperature that is independent of vitamin D and calcium levels. Mechanistically, through a combinatorial metagenomic, targeted metabolomic, and functional approach, we show that the warm-adapted microbiota has a higher potency to produce polyamines; in particular, acetylated spermidine and putrescine. Polyamine biosynthesis inhibition limits the benefits of warmth exposure, while polyamine supplementation mimics the effects of warmth *in vivo* in the mouse osteoporosis model. Our data suggest warmth exposure as a potential treatment option for the prevention of osteoporosis, while providing a mechanistic understanding of the role of a microbiota-host interaction during warmth exposure and bone disease.

RESULTS

Warmth Exposure Improves Bone Strength in Adulthood

Aging leads to a decrease in bone strength and mass and alterations in the microarchitecture (Boskey and Coleman, 2010; Demontiero et al., 2012; Mosekilde, 2000), which can increase the incidence of fracture. We, therefore, evaluated the effects of warm temperature exposure on mice after their development, using females exposed for 8 weeks to 34°C starting at 16 weeks of age. This treatment led to an increase in the tail length in the older female mice (Figure S1A), and the increase was even more pronounced following 34°C exposure for 1 month when started in 8-week-old male mice (Figure S1B). This was coupled to higher tail temperature as expected, without changing the overall body temperature (Figures S1C and S1D). Exposure to 34°C of the older females led to an increase in the trabecular bone volume (BV) versus total tibia volume ratio (BV/total volume [TV]), the connectivity density of the tibias (Figures 1A–1F), and in the BV/TV of the caudal vertebra (Figure 1G), without affecting the cortical bone of the tibias (Figures 1H–1J), indicating a positive effect of warmth exposure on the trabecular bone.

These structural changes were also reflected at a biomechanical level. A three-point bending test in the femur highlighted the improvements in the yield point (Figure 1K) above which mechanical force causes permanent damage to the bone structure and in the ultimate force (Figure 1L) that reflects the general integrity of the bone. No differences were detected in the elastic energy, energy to fracture, or the Young's modulus (Figures 1M–1O). Exposure to 34°C reduced the food intake by 25% (Figure S1E), consistent with slowing of the overall metabolism and reduced activity at elevated temperatures (Kaiyala et al., 2012) (Figures S1E and S1F). As lowered food intake affects the bone mass (Devlin et al., 2010; Hamrick et al., 2008) and reduces body weight at room temperature (RT) (Fabbiano et al., 2016), but not during warmth exposure (Figure S1F), we compared the effects of warmth exposure to a pair-fed set of animals kept at RT. Warmth exposure led to elevated trabecular BV/TV (Figure S1G) and higher cortical BV and width (Figures S1H–S1J) compared with the pair-fed controls. This was coupled to a marked improvement of the biomechanical resistance that was independent of the food intake (Figures S1K–S1O). In addition, the warmth exposure also led to elongated femurs in comparison to the pair-fed RT-housed controls (Figure S1P). These data show that warmth exposure exerts beneficial effects on the biomechanical bone parameters in mice during adulthood and that these effects are unrelated to the decreased food intake.

Warmth Exposure Correlates with Reduced Fracture Incidence in Humans and Prevents Experimentally Induced Bone Loss in Mice

We next investigated if the warmth exposure could have protective effects on bone loss. To address the potential relevance of the temperature on the osteoporosis-related fractures in humans, we performed human metadata analysis on the incidence of hip fractures per capita and country worldwide (Cauley et al., 2014; Wahl et al., 2012; Balk et al., 2017) and found a positive correlation between the fractures and the latitude (Figures 2A and S2A). Conversely, there was a negative correlation between the average temperature and hip fracture incidence both in women and in the total population (Figures 2B and S2B). Partial correlation analysis (with the effect of the vitamin D removed) showed that the temperature and latitude effect on the hip fracture incidence are independent of vitamin D (Figures S2C–S2G). Similarly, correcting for the calcium intake did not influence the effect of the temperature and latitude on the hip fracture incidences (Figures S2H and S2I). Instead, when correcting for temperature, the association between latitude and the hip fracture was largely eliminated (Figure S2J).

To directly test if warmer temperatures may exert protective effect on bone loss, we surgically ovariectomized 16-week-old mice, which is the most commonly used model for primary osteoporosis, and exposed them to 34°C or RT for 8 weeks (Ova34°C or OvaRT, respectively), using sham-operated mice as controls (Sham34°C or ShamRT). Warmth exposure lowered the food intake as expected, and this was unaffected by the oophorectomy (Figure S2K). Strikingly, warmth exposure prevented the trabecular BV/TV loss caused by ovariectomy (Figure 2C), as assessed by computed tomography (CT) and normalized to body weight (Figure S2L). This was consistent with the increase in the trabeculae number, the trabecular thickness, and the connectivity density (Figures 2D–2H) in the Ova34°C mice, compared with the OvaRT controls. No differences were detected in the trabecular spacing and femur length (Figures 2G and S2M). The ovariectomy-induced decrease in the cortical BV and width of tibias was prevented in the Ova34°C mice to similar levels as the ShamRT controls (Figures 2I–2K). This phenomenon was not restricted to long bones as we found that the decrease in the BV/TV of the caudal vertebra in the Ova34°C

Cell Metabolism
Article

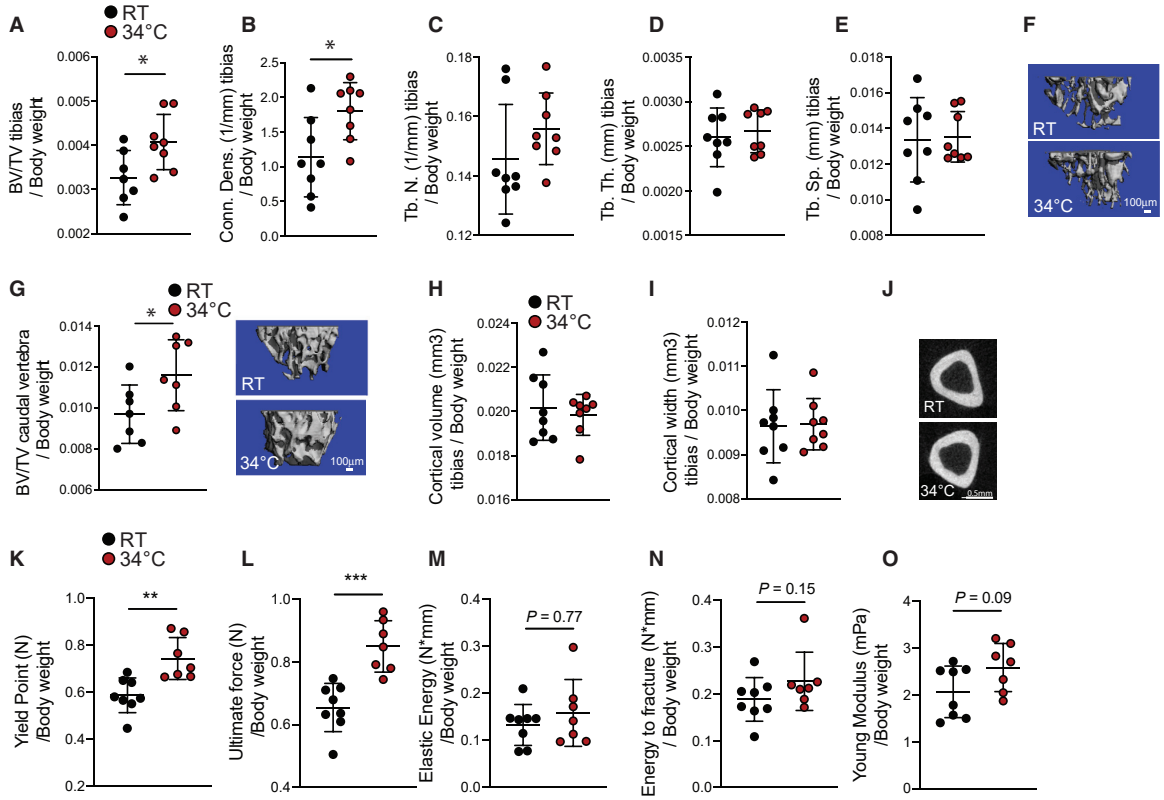

Figure 1. Warmth Exposure Improves Bone Strength during Adulthood

(A–E) Trabecular bone microarchitecture of tibias showing BV/TV (A), connectivity density (Conn. Dens) (B), number of trabeculae (Tb. N) (C), trabecular thickness (Tb.Th.) (D), and trabecular separation (Tb.Sp) (E) of 24-week-old female mice exposed to 34°C for 2 months prior to sacrifice and their RT controls (n = 8 per group), all normalized to body weight.

(F) Representative reconstruction of trabecular bone used for the calculations in (A)–(F). Scale bar, 100 µm. Each trabecular reconstruction was done by scanning and compiling 262 sections from the beginning of the growth plate to the midshaft in each mouse using n = 8 per group.

(G and H) Cortical BV (G) and width (H) of mice as in (A), measured in midshaft of the tibias and normalized to body weight. (G) Right: representative reconstruction (each consisting of 262 sections, n = 8 per group) of trabecular bone used for calculation. Scale bar, 100 µm.

(I) Representative cortical section (from 62 sections per bone of each mouse of n = 8 per group). Scale bar, 0.5 mm.

(J) BV/TV (left), measured in the caudal vertebra (CA2) (normalized to body weight) of mice as in (A).

(K–O) Biomechanical analysis of femur from mice as in (A) using a three-point bending test. The parameters measured include the yield point (K), the ultimate force (L), the elastic energy (M), the energy to fracture (N), and the Young's modulus (O) and normalized to their respective body weight.

Data are shown as mean ± SD (n = 8 per group). Significance (p value) is calculated using Mann-Whitney t test, *p < 0.05; **p < 0.01; ***p < 0.001.

mice was ameliorated to the levels seen in the ShamRT controls (Figure 2L). These structural improvements were accompanied by a reduced fragility of the bones in the Ova34°C mice, as shown by the biomechanical measurements during the three-point bending test (Figures 2M–2Q), as they showed similar reads for all the mechanical properties as the ShamRT controls, except for the elastic energy.

Warmth Exposure Alters the Microbiota Composition

Recent evidence suggest an interaction between the gut microbiota and bone metabolism (Li et al., 2019; Ohlsson and Sjögren, 2015; Hsu and Pacifici, 2018). To investigate whether warmth exposure can alter the microbiota composition, we performed 16S ribosomal DNA analysis of microbiota in cecum and feces from 24-week-old female mice that have been exposed to 34°C for 8 weeks. Among the 892 identified operational taxonomic units (OTUs), 81 were differently abundant ($p \leq 0.05$) in warmth- versus RT-treated animals. Principal component analysis (PCA) of all the microbiomes showed segregation between the two groups (Figure 3A). Despite the reduced richness of the gut flora after warmth exposure, the Shannon diversity was higher (Figures 3B and 3C), indicating a more even distribution in abundance of the bacterial species after warmth exposure. This observation was further supported by the family relative abundance (Figure 3D), where the predominance of the *Muribaculaceae* family was dampened in the warm-adapted microbiota. The hierarchical clustering of the samples associated with a heatmap confirmed the clustering of the microbiota

CellPress

Cell Metabolism
Article

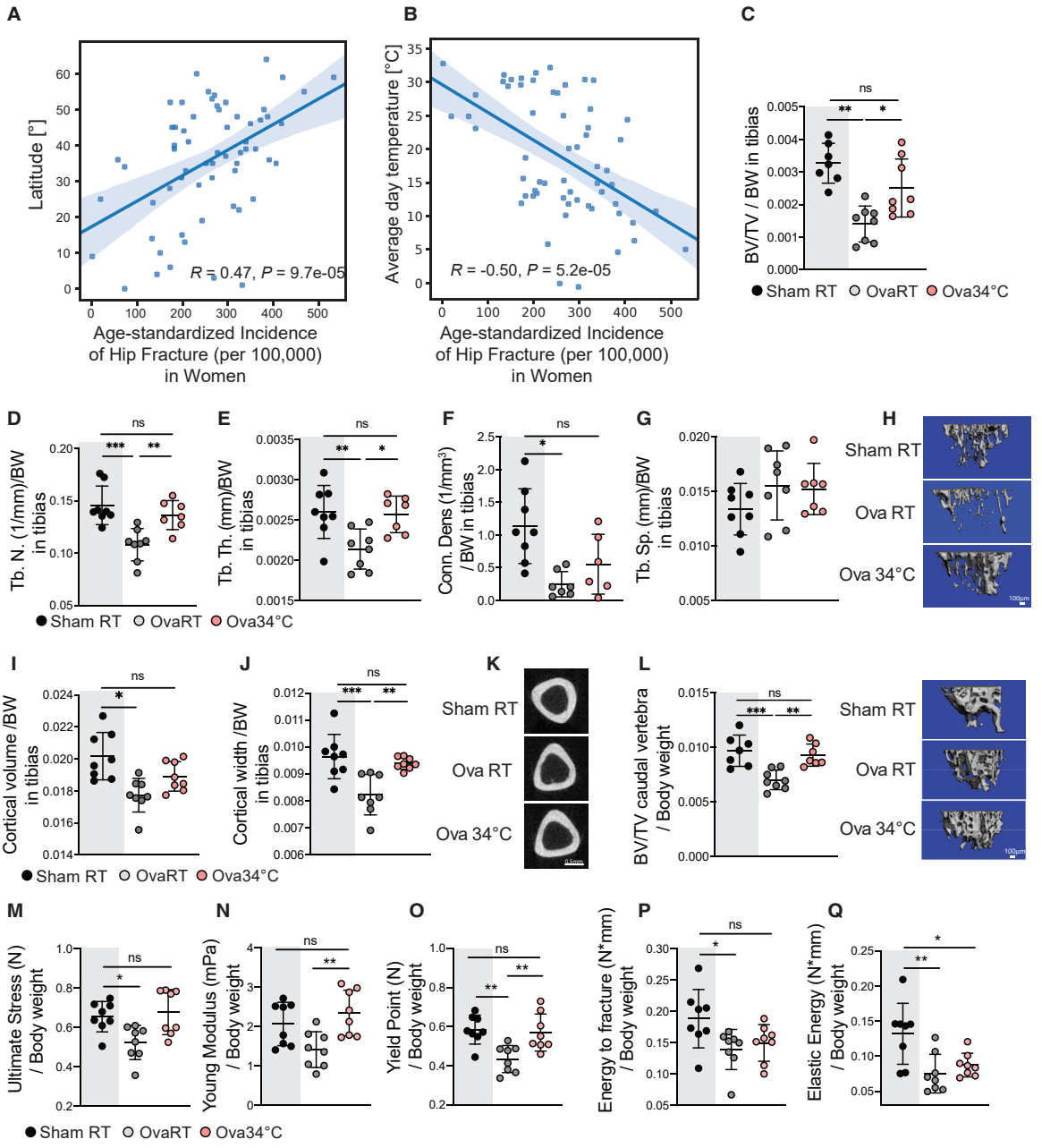

Figure 2. Warmth Exposure Protects against Osteoporosis

(A and B) Metadata analysis showing age-standardized correlation between hip fracture incidence (per 100,000 inhabitants) in women per country versus the latitude of the country's capitals (A) or versus the country's average day temperature (B).

(C–H) Trabecular bone microarchitecture of tibias in female mice that were ovariectomized, or sham-operated at 16 weeks of age, and then exposed to 34°C for 2 months (Ova34°C or Sham34°C, respectively), or kept at RT (OvaRT or ShamRT). BV/TV (C), the number of trabeculae (Tb. N) (D), the trabecular thickness (Tb.Th.) (E), the connectivity density (Conn. Dens) (F), and the trabecular separation (Tb.Sp) (G) from the mice as in (C) at the end of the warm exposure, normalized to their respective body weight. (H) Representative reconstruction (each consisting of 262 sections, n = 8 per group) of trabecular bone used for calculations. Scale bar, 100 μm.

(I and J) Cortical BV (I) and width (J) of mice as in (C) measured in the midshaft of the tibias and normalized to the body weight.

(legend continued on next page)

Cell Metabolism
Article

following warmth exposure, as well as the broad change in the microbial composition (Figure 3E). At a genus level, we observed a warm microbiota signature associated with an increase of the genera *Turicibacter*, *Ruminiclostridium_6*, *Akkermansia*, *Rhodospirillales*, *Clostridium_sensus_stricto_1*, and *Parabacteroides*, and a reduction of *GCA.900066575*, *Butyricicoccus*, *Peptococcaceae*, *or Ruminiclostridium* (Figures 3F and S3A). Curiously, despite the reduction of *Muribaculum* at the genus level, several of its OTUs were among the most elevated following warmth exposure, pointing to an extreme variability of the growth behavior within this genus (Figures 3G and S3B). *Akkermansia muciniphila* showed a strong increase in abundance after warmth exposure. Interestingly, this same species was strongly suppressed after cold exposure (Chevalier et al., 2015; Ziętak et al., 2016), suggesting that *Akkermansia muciniphila* is consistently affected by the environmental temperature.

To confirm the effect of the warm housing temperature in shaping the microbiota, we performed similar analysis in mice of different age and sex. Similar to the effect in the older females, 12-week-old male mice that were exposed to 34°C for 4 weeks showed altered microbiota composition as shown by PCA (Figure S3C), but without showing differences in the Shannon diversity or Richness (Figure S3D). The family abundance bar chart analysis revealed similar changes between the older females and the younger males despite the difference in the treatment length, with overall increase in the *Akkermansiaceae* and reduction of the *Muribaculaceae* family (Figure S3E). Similar to the most altered OTUs in the older females, *Muribaculaceae OTU2594*, *Clostridium_stricto_sensus_1_OTU2703*, and *Lactobacillus_otu2644* were more abundant (Figure S3F) in the microbiota of the warmth-exposed male mice than that of the RT controls. While the estrogen depletion caused changes in gut microbiota population (Figures S3G–S3H) (Markle et al., 2013; Cox-York et al., 2015; Kaliannan et al., 2018), the effects of warmth exposure on the microbiota composition were maintained after ovariectomy, with an increase in the *Akkermansiaceae* and reduction in the *Muribaculaceae* family. To further investigate the particular signature of the warmth exposure in changing the microbiota, we directly compared the warm-induced changes in the above three conditions: older female, young male, and ovariectomized mice. By plotting the PCAs, we observed a consistent shift in the microbiota composition selected by the PC2 (Figure S3H). Additional comparison of the 3 groups selected for consistent changes and a p value < 0.05, further supported these observations, and provided a signature of the warmth exposure on the microbiota composition with increase of *Muribaculaceae otu2594*, *Muribaculaceae otu2618*, *Lactobacillus otu2644*, *Clotridium_stricto_sensu_1_otu2703*, and *Lachnospiraceae otu2806* (Figure S3I). Accordingly, warmth exposure leads to robust and consistent changes in the gut microbiota composition that is independent of age, sex, or hormonal status.

Transplantation of Warm-Adapted Microbiota Prevents Bone Loss

To uncover whether the microbiota impacts the bone parameters during warmth exposure, we first eliminated the microbiota using antibiotics. Microbiota depletion abolished the warmth-induced increase in femur strength in 23-week-old female mice (Figures S3J–S3N) and limited the warmth-mediated increase in trabecular BV and connectivity density of the tibia (Figures S3O–S3S). Similarly, warmth exposure did not alter the cortical bone in the microbiota-depleted mice (Figures S3T–S3V). To directly test the importance of the warm-adapted microbiota in a pathological context, we used mice that were ovariectomized at 16 weeks of age and recurrently transplanted with fecal microbiota of either warmth-exposed or RT-kept mice (OvaTransp34°C or OvaTranspRT; Figure S4A). Both microbiota-transplanted groups of mice were maintained at RT to isolate the microbiota effect. The PCA of the transplanted mice suggested microbiota similarities to the respective donors (Figure S4B). These observations were supported by the conserved microbial signature described earlier, including changes in the *Lactobacillus otu2644* and *Muribaculaceae otu2596*, which were maintained in the transplanted groups (Figure S4C).

The recurrent microbiota transplantation did not affect the body weight gain, nor did it change the food intake (Figures S4D and S4E). However, tibia measurements before and after the transplantation showed higher BV in the OvaTransp34°C than that of the OvaTranspRT mice (Figures 4A–4C and 4E). The increased tibia BV was associated with greater connectivity density delta before versus after microbiota transplantation (Figure 4D) in the OvaTransp34°C compared with the delta in the OvaTranspRT without affecting the trabecular thickness, trabeculae space and number (Figure S4F), and the cortical BV and width (Figures 4F–4H). The bone strength was improved at different levels during the three-point bending test on the femurs (Figures 4I–4M), collectively indicating that the protective effect observed during warmth exposure on the bone loss outcome is in part phenocopied by the warm microbiota transplantation.

We also investigated whether microbiota transplantation could have an effect in non-pathological conditions, using male germ-free (GF) mice transplanted with microbiota from male donors that were exposed to warmth for 4 weeks, or kept at RT. The PCA of the microbiota from the transplanted GF mice revealed differences between the groups (Figures S4G and S4H; data not shown). Fecal warm microbiota transplantation of the young male GF mice led to higher cortical BV and width (Figures S4I and S4J), despite these measurements being done only 20 days after the transplantation, without affecting the femur length (Figure S4L). Warm microbiota transplantation in the GF mice led to a slight improvement in the bone strength parameters compared with the RT-microbiota-transplanted controls (Figure S4K). These data show that warm-adapted microbiota

(K) Representative cortical sections from each group (from 62 sections per bone of each mouse of n = 8 per group). Scale bar, 0.5 mm.
(L) Trabecular BV/TV, measured in the caudal vertebra (CA2) (normalized to body weight) of mice as in (C). Right: representative reconstruction (each consisting of 262 sections, n = 8 per group) of a vertebra used for calculation. Scale bar, 100 μm.
(M–Q) Biomechanical analysis of femur from mice as in (C) showing ultimate stress (M), Young's modulus (N), yield point (O), energy to fracture (P), and elastic energy (Q), all normalized to the body weight.
Data are shown as mean ± SD (n = 8 per group). Significance (p value) is calculated using Mann-Whitney t test, *p < 0.05; **p < 0.01; ***p < 0.001. Sham RT mice (as shown in Figure 1) are shadowed in gray.

CellPress

Cell Metabolism
Article

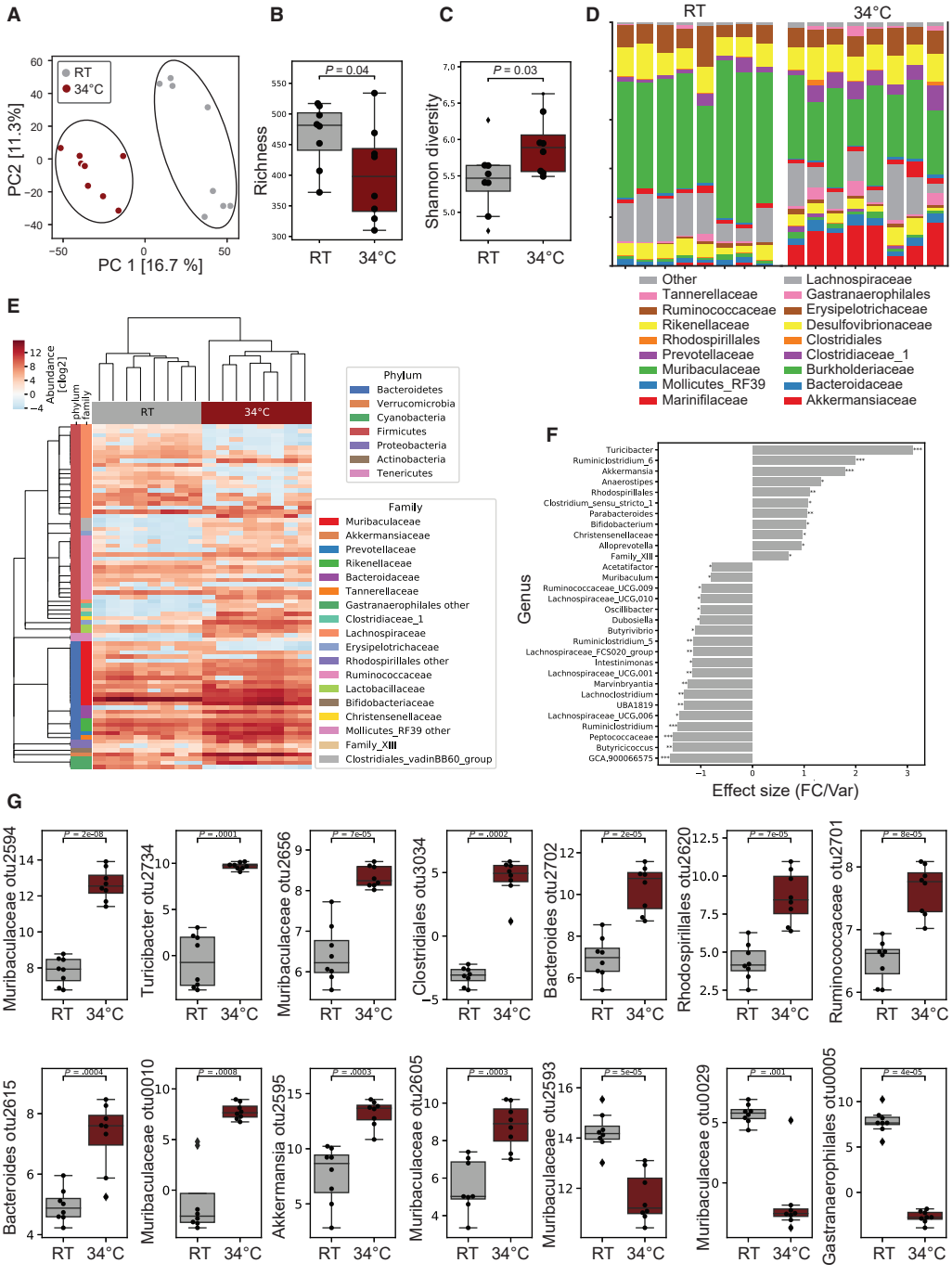

Figure 3. Warmth Exposure Changes the Gut Microbiota Composition

(A) PCA of 16S rDNA sequencing of fecal microbiota from 24-week-old female mice exposed for 2 months to 34°C or kept at RT. Each dot represents a fecal microbiota from one mouse. The analysis is based on the centric log2 ratio (CLR).

(B and C) Estimated richness (B) and Shannon diversity (C) of microbiota samples as in (A).

(D) Bar chart of the relative microbiome abundance at family level from mice as in (A).

(legend continued on next page)

Cell Metabolism
Article

CellPress

transplantation improves bone strength and physiology, with the effect being more pronounced in pathological conditions.

Warmth Exposure and Warm Microbiota Ameliorate the Ovariectomy-Induced Transcriptional Bone Remodeling

To gain insights into the magnitude and mechanisms of the bone remodeling, we performed RNA sequencing on tibias from ovariectomized and sham-operated mice exposed to 34°C and their RT controls, as well as from the ovariectomized microbiota-transplanted mice. Ovariectomy-induced severe transcriptional alterations, which were markedly reduced when the ovariectomized mice were kept at 34°C (Figures 5A and 5B). Specifically, to dissect the effect of warmth on the ovariectomy-induced transcriptional alterations, we selected the deregulated genes ($|\log_2FC| > 1$ in OvaRT versus ShamRT, and log count per million [CPM] > 0) and compared them to the changes in Ova34°C versus ShamRT. Strikingly, warmth exposure reduced the ovariectomy-induced transcriptomics changes in 90.5% of the genes partially or completely (93.2% from the upregulated and 86.4% from the downregulated) (Figure 5C), demonstrating that warmth exposure exerts a major protective effect on the transcriptional bone remodeling induced by estrogen deficiency. Reactome pathway analysis between ovariectomized mice at RT or at 34°C indicated differences in the collagen biosynthesis and degradation, associated with extracellular matrix reorganization, suggesting that warmth exposure leads to alterations in the bone remodeling pathways at the transcriptional level (Figure 5D). Comparative analysis suggested overlap between the reactomes of ovariectomized and control non-ovariectomized mice kept at 34°C when compared with their respective RT controls (Figures 5I and S5A–S5C). Specifically, out of 21 deregulated pathways between ShamRT versus 34°C, 20 pathways (95%) were found altered by warmth exposure in the ovariectomized mice (OvaRT versus 34°C).

Transplantation of the ovariectomized mice with the warm-adapted microbiota (OvaTransp34°C) also induced transcriptional alterations (FDR < 0.01 and $|\log_2FC| > 1$) in bone when compared with the RT-microbiota-transplanted controls (OvaTranspRT) (Figure 5E). To investigate if the warm-adapted microbiota could exert similar effect as the warm exposure on mitigating the ovariectomy-induced transcriptional deregulation, we specifically analyzed the altered genes (shown in Figure 5C) in the OvaTransp34°C mice compared with the OvaTranspRT controls. Interestingly, the ovariectomy-induced transcriptional changes were reduced or reverted in 59% of the total deregulated, and in 94% of the reduced genes (shown in green in Figure 5F), when the ovariectomized mice were transplanted with warm microbiota, similar to the direct effect of warmth exposure (Figures 5F and 5G). In the top 10 deregulated reactome pathways of the microbiota-transplanted ovariectomized mice, we observed a similar pattern to the warmth-exposure-induced changes (Figure 5H). These data indicate that warmth exposure and warm microbiota transplantation suppress the ovariectomy-induced transcriptional alterations.

Warmth and Warm Microbiota Enhance Periosteal Bone Formation

To gain further insights into the mechanisms by which warmth exposure increases bone strength, we investigated the number and activity of the cells responsible for the bone remodeling. During homeostasis, the activity of osteoblast and osteoclasts is at equilibrium. In the context of osteoporosis, the overall bone remodeling is increased, where the activity of the osteoclasts is superior to the one of the osteoblasts, leading to bone loss. We quantified the osteoblast activity by measuring the fluorescent calcein deposits within the bone during its formation between 2 injections, 7 days apart. The cortical bone in the midshaft of the femur showed a specific increase of the periosteal mineralized surface in the ovariectomized mice exposed to warmth compared with the RT-housed controls, without the endocortical surface and the trabecular bone mineralization (measured in the head of the femur) being affected (Figures 6A–6C and S5D). The increased osteoblast activity was confirmed by the higher levels of circulating osteocalcin in the warmth-exposed ovariectomized mice, but not in the sham-operated controls (Figures 6D and S5E). Consistent with warmth exposure, the specific increase in the periosteal mineral apposition rate (MAR) was observed in the ovariectomized mice receiving the warm-adapted microbiota (Figures 6E–6I and S5F), suggesting that similar mechanisms mediate the effects of warmth exposure and warm microbiota transplantation. The active osteoclast number was then quantified using Tartrate-resistant acid phosphatase (TRAP) staining on femur trabecular histological sections. No differences were observed after warmth exposure, or warm microbiota transplantation in any of the groups (Figures 6J–6L; data not shown). This was supported by the circulating CTX-1 levels as marker of bone resorption, which was neither changed by warmth in both ovariectomized and non-ovariectomized mice, nor in the warm microbiota-transplanted animals (Figures 6M and S5G). Notably, the bone remodeling effects were independent of the collagen deposition, bone mineral content, and circulating vitamin D levels, as we did not detect differences for these parameters between any of the groups (Figures S5H–S5K; data not shown). These data indicate that warmth exposure or warm microbiota transplantation shifts the balance between osteoblast activity and the number of active osteoclasts toward bone formation.

Warmth Exposure Increases Production of Polyamines that Affect Osteoblast Activity and Decrease Osteoclast Differentiation

To investigate the link between microbiota and bone during warmth, we performed a metagenomic analysis of the gut microbiota from 24-week-old female mice that were exposed for

(E) Hierarchical clustering associated with a heatmap comparing the CLRs of the OTUs selected for a $p < 0.05$ of mice as in (A). An idealized tree represents their taxonomic hierarchy down to genus level associated with bars that are color-coded for phylum and family. Each column represents one mouse.
(F) Effect size of all significantly changed genera calculated with aldex2 (FDR < 0.05) in samples from mice as in (A).
(G) CLRs representing relative abundance of the most changed OTUs (FDR < 0.01) by warm exposure in samples from mice as in (A). Boxplots represent median and quantiles; the whiskers show 1.5 inter quartile range and values outside the whisker's box are represented as diamonds.
Data are shown as mean ± SD (n = 8 per group). Significance in (F) and (G) is calculated using Welch t test, *$p < 0.05$; **$p < 0.01$; ***$p < 0.001$.

CellPress

Cell Metabolism
Article

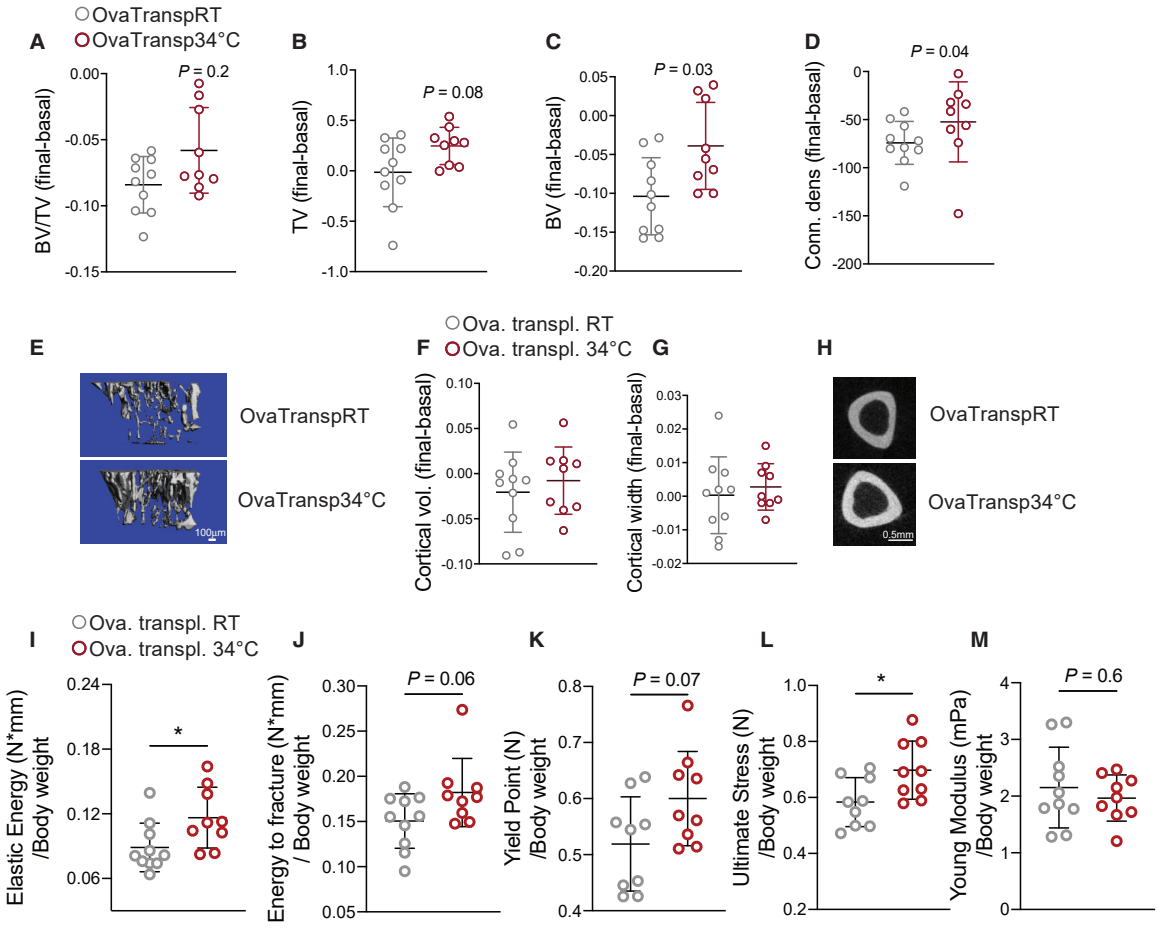

Figure 4. Warm Microbiota Transplantation Prevents Bone Loss and Improves Bone Strength

(A–D) Delta between two micro-CT measurements (day 0 and day 32 after starting the microbiota transplantation) of proximal tibias at trabecular level in 21-week-old ovariectomized, microbiota recipient female mice. The recipient mice were ovariectomized at week 16, and repetitively transplanted with fecal microbiota from 34°C exposed, or RT-kept donors (OvaTransp34°C or OvaTranspRT, respectively). The 34°C treatment of the 16-week-old female donor mice was initiated 1 month before starting the transplantations and lasted for the whole length of the experiment. BV/TV (A), BV (B), TV (C), and connectivity density (D).

(E) Representative reconstruction (each consisting of 262 sections, n = 10 per group) of trabecular bone use for the calculations. Scale bar, 100 µm.

(F–H) Cortical BV (F) and width (G) measured in midshaft of tibias from mice as in (A). (H) representative cortical section (from 62 sections per bone of each mouse of n = 10 per group). Scale bar, 0.5 mm.

(I–M) Biomechanical analysis of tibias from mice as in (A) showing elastic energy (I), energy to fracture (J), yield point (K), ultimate stress (L), and Young's modulus (M), all normalized to their body weights.

Data are shown as mean ± SD (n = 10 per group). Significance is calculated using Mann-Whitney t test, *p < 0.05; **p < 0.01; ***p < 0.001.

8 weeks to 34°C and from the RT-housed controls. Among 536 identified pathways, 134 were differentially abundant in the feces of warmth-exposed animals compared with RT controls. Within the top ten regulated pathways was the polyamine synthesis showing higher levels for the key genes responsible for polyamine production and lower levels for those involved in the polyamine degradation processes (Figures 7A, 7B, and S6A). Deeper analysis of the metagenomic data by genus suggested that expansion of *Akkermansia muciniphila* during warmth exposure, as well as the genera *Bacteroides* and *Alitsipes*, may be the main contributors to the polyamine biosynthesis (Figure S6B). Conversely, the decreased propensity of the microbiota to degrade spermine and spermidine could be attributed to the decline of the bacteria from the *Muribaculaceae* or *Lachnospirae* genera (Figure S6C). The polyamines have fast plasma turnover and rapidly reach their target tissues (Pegg, 2009). To directly test whether the metagenomic data would correlate with an actual increase in the respective polyamine metabolites, we developed an isotope dilution-based, hydrophilic interaction chromatography coupled to targeted tandem mass spectrometry (HILIC-MS/MS) method for absolute quantification of the polyamine metabolites. In agreement with the metagenomics

Cell Metabolism
Article

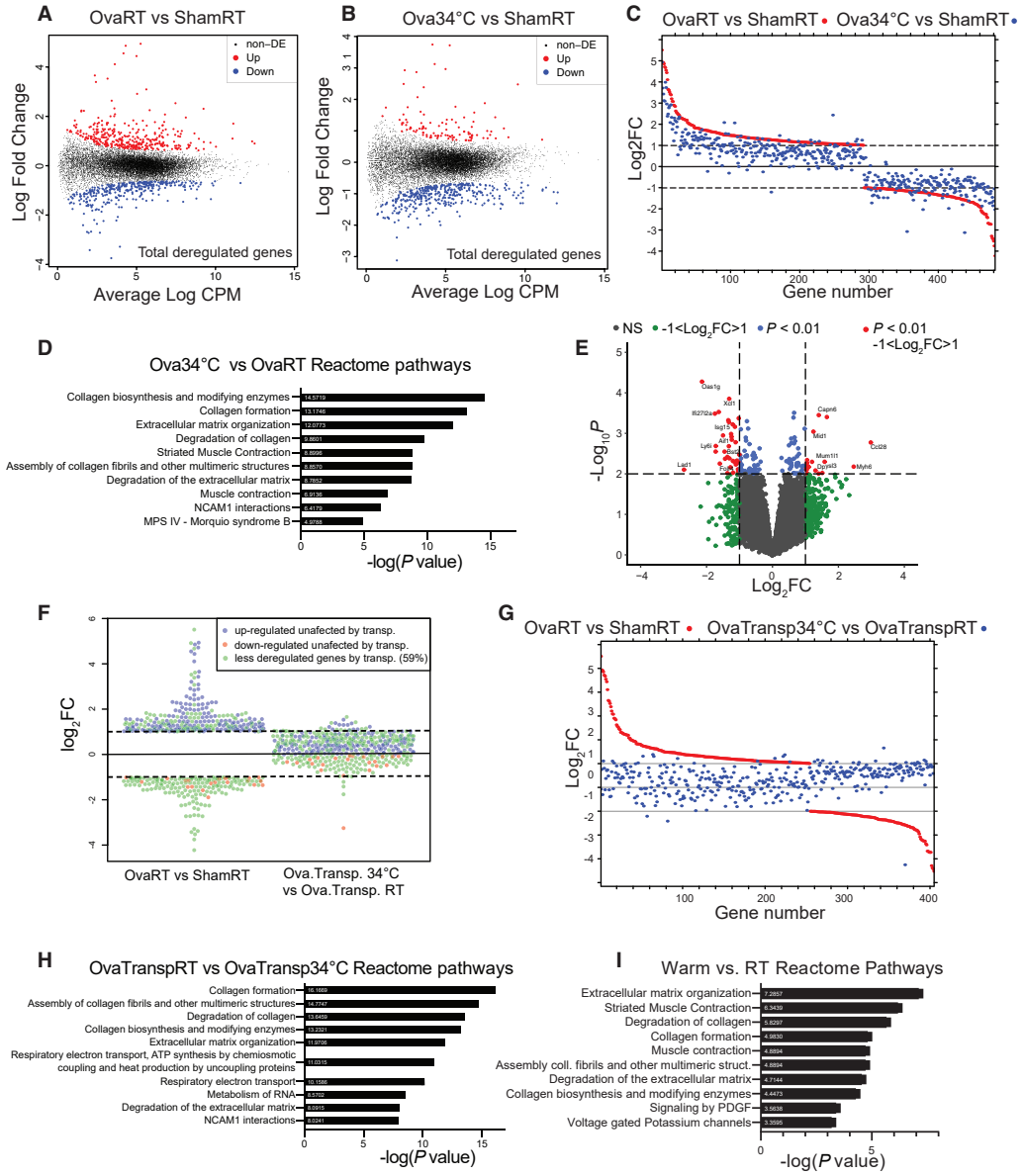

Figure 5. Warmth and Warm Microbiota Transplantation Ameliorate Ovariectomy-Induced Transcriptional Deregulation

(A) Mean-difference plot (MD-plot) of the log fold change gene expression between tibias of 24-week-old female mice that were ovariectomized or sham-operated at 16 weeks of age and then kept at RT for 2 months (OvaRT versus ShamRT, respectively) shown as average CPM. Red dots show the increased and blue show the decreased genes selected for FDR < 0.05.

(B) MD-plot of the log fold change of gene expression between tibias of 24-week-old female mice that were ovariectomized at 16 weeks of age and then kept at 34°C for 2 months (Ova34), versus ShamRT, shown as average CPM. Red dots show increased and blue show decreased genes selected for FDR < 0.05.

(C) Comparison between the log fold change of genes deregulated by ovariectomy at RT shown in red ($|\log_2 FC| > 1$; OvaRT versus ShamRT) and the same genes when exposing the ovariectomized mice at 34°C shown in blue ($|\log_2 FC| > 1$; Ova34°C versus ShamRT).

(D) Top 10 most deregulated Reactome pathways between tibias of OvaRT and Ova34°C mice.

(E) Volcano plot comparing the p value and the log fold change of gene expression between tibias of 21-week-old ovariectomized, microbiota recipient female mice (OvaTransp34°C or OvaTranspRT) as in Figures 4A–4E. Green dots, $|\log_2 FC| > 1$; blue dots, $p < 0.01$; red dots, $p < 0.01$ and $|\log_2 FC| > 1$.

(F and G) Expression analysis of the ovariectomy-altered genes ([$|\log_2 FC| > 1$] at RT [OvaRT versus shamRT]) in tibia from OvaTransp34°C mice compared with the OvaTranspRT controls (OvaTransp34°C versus OvaTranspRT). In (F), blue and red show genes (up- or downregulated, respectively) unaltered by microbiota

(legend continued on next page)

data, the concentrations of putrescine, N1-acetylputrecine, N1-acetylspermidine, and spermine were higher in feces of the warmth-exposed animals (Figures 7C, 7D, and S6D). This was coupled to higher spermine levels in the cecum of warmth-exposed mice or elevated N1-acetylspermidine and N1N12-acetylspermidine in the warm microbiota-transplanted mice (Figures 7C, S6E, and S6F).

To test the effect of polyamines on bone cellular activity, we performed an *ex vivo* experiment with spermine and spermidine supplementation in primary osteoblast or osteoclast cultures during differentiation. Since it is difficult to correlate the *in vivo* levels with those *in vitro*, we used different concentrations in the primary cultures and assessed the outcome in a dose-response manner. Supplementation of spermine and spermidine at high (but not low) doses in osteoclasts during differentiation caused downregulation of cathepsin K (*CtsK*), TRAP 5 (*Trap5b*), and matrix metalloprotease 9 (*Mmp9*), which are markers of osteoclast activity and differentiation (Figures 7E, 7F, and S6G). The decrease in expression of the osteoclast differentiation markers was associated with a reduced number of differentiated osteoclasts measured by TRAP staining (Figures 7G and S6H). These findings are in agreement with the studies in mice that oral supplementation of spermine and spermidine in an ovariectomy-induced model of osteoporosis was sufficient to prevent bone loss, measured by %BV/TV in vertebra (Yamamoto et al., 2012). The anti-osteoclast effects of spermidine, but not spermine, were observed even when these polyamines were added after differentiation, where 24 h of spermidine supplementation was sufficient to reduce the expression level of *Ctsk* and *Trap5b* (Figures S6I and S6J). Spermine increased osteoblast expression of osteocalcin (*Ocn*) and osteoprotegerin (*Opg*) in a dose-dependent manner (Figure 7H). Similarly, elevated spermidine levels augmented osteopontin (*Opn*), osteoprotegerin (*Opg*), and receptor activator of nuclear factor kappa-B ligand (*Rankl*) expression, indicating an increased osteoblast function (Figure 7I), coupled to a decrease in the *Rankl*/*Opg* ratio that could explain the decreased osteoclastogenesis. These observations were supported by an enhanced activity of alkaline phosphatase (ALP) when spermine and spermidine were added to the osteoblasts (Figures 7J–7K). These data support the observations regarding the osteoblast function *in vivo* during warmth exposure and warm microbiota transplantation, and they demonstrate that polyamines could mediate the enhanced osteoblast activity. This increase was observed despite the slight reduction of the cell viability (lower total protein and RNA) upon spermine supplementation (Figures S6K and S6L), which may result from interaction of spermine with serum from the media, producing H_2O_2 radicals by oxidative degradation of the polyamines (Wang et al., 2018).

Finally, we directly tested the necessity of the polyamine biosynthesis in mediating the warmth-induced effects on the bone *in vivo*. Polyamine supplementation in older female mice increased the yield point, elastic energy, and energy to fracture of the femur to similar values as the warmth-exposed mice (Figures 7L–7P). Conversely, we used a polyamine biosynthesis pathway inhibitor, diaminazene acetureate (DA), which prevents formation of decarboxy-S-adenosinemethionine, a metabolite that turns into spermine and spermidine (Karvonen et al., 1985). DA also blocks spermidine and spermine acetyltransferase activity (Libby and Porter, 1992; Neidhart et al., 2014), thus, inhibiting the back conversion of spermine and spermidine toward putrescine, leading to reduced acetylspermine and acetylspermidine formation. Treating warmth-exposed older female mice with the polyamine inhibitor abolished the warmth-induced increase in the yield point and elastic energy during the three-point binding test in femur, revealing similar biomechanical parameters between the warmth-exposed, DA-treated mice and the RT-housed controls (Figures 7L–7P). Moreover, the warmth-induced increase in the trabecular BV and connectivity density of tibia were reduced in the polyamine inhibitor-treated mice despite the warmth exposure, and there were no differences between RT and warmth-exposed, inhibitor-treated mice in any of the trabecular and cortical parameters (Figures S7A–S7F).

DISCUSSION

Over a century ago, Joel Asaph Allen proposed an ecogeographical model of adaptation to temperature differences for the homeothermic animals, in which the body surface area-to-volume ratio varies with the average temperature of the habitat, where higher temperatures would favor the higher ratios and heat dissipation, called the Allen's rule (Allen, 1877). In growing long bones, a cartilaginous disk called the growth plate separates the epiphysis from the metaphysis and diaphysis. A new cartilage is produced at the epiphyseal side of the growth plate, while the previously made cartilage at the metaphyseal side is replaced by new bone leading to bone elongation. With the onset of puberty in humans, the deposition of cartilage ceases and the metaphysis fuses with the epiphysis, leading to ceased longitudinal apposition and disappearance of the growth plate (Jilka, 2013; Pines and Hurwitz, 1991). During adulthood, bones undergo permanent remodeling that enables adaptation of the skeleton to the environment and in response to the continuous microfractures. This remodeling is kept in balance by precise coupling between the osteoclast and osteoblast activities. During aging, this exquisite balance is often disrupted, progressively leading to osteopathy. Our data show that the bone remodeling is largely affected by the environmental temperature and that warmth exposure leads to improved trabecular and cortical bone structure and strength. Interestingly, in mice while warmth exposure during development can indeed lead to lengthening of the bones (Racine et al., 2018; Serrat, 2013, 2014; Serrat et al., 2008, 2015), in our experiments applying the heat post-developmentally and during middle adulthood did not change the bone length (and thus surface area-to-volume ratio) but still increased the bone strength and mass. Accordingly, transplantation of the warm-adapted microbiota in older female and younger male

transplantation. Green shows genes with reduced or reverted expression when mice are transplanted with warm microbiota. (G) Comparison between the log fold changes of genes ($|\log_2 FC| > 1$) as in (C) using the groups of mice from (F): OvaRT versus ShamRT (red) and OvaTransp34°C versus OvaTranspRT (blue).
(H) Top 10 most deregulated reactome pathways between tibias from OvaTransp34°C and OvaTranspRT mice.
(I) Top 10 most deregulated reactome pathways between tibias from 34°C and RT mice.

Cell Metabolism
Article

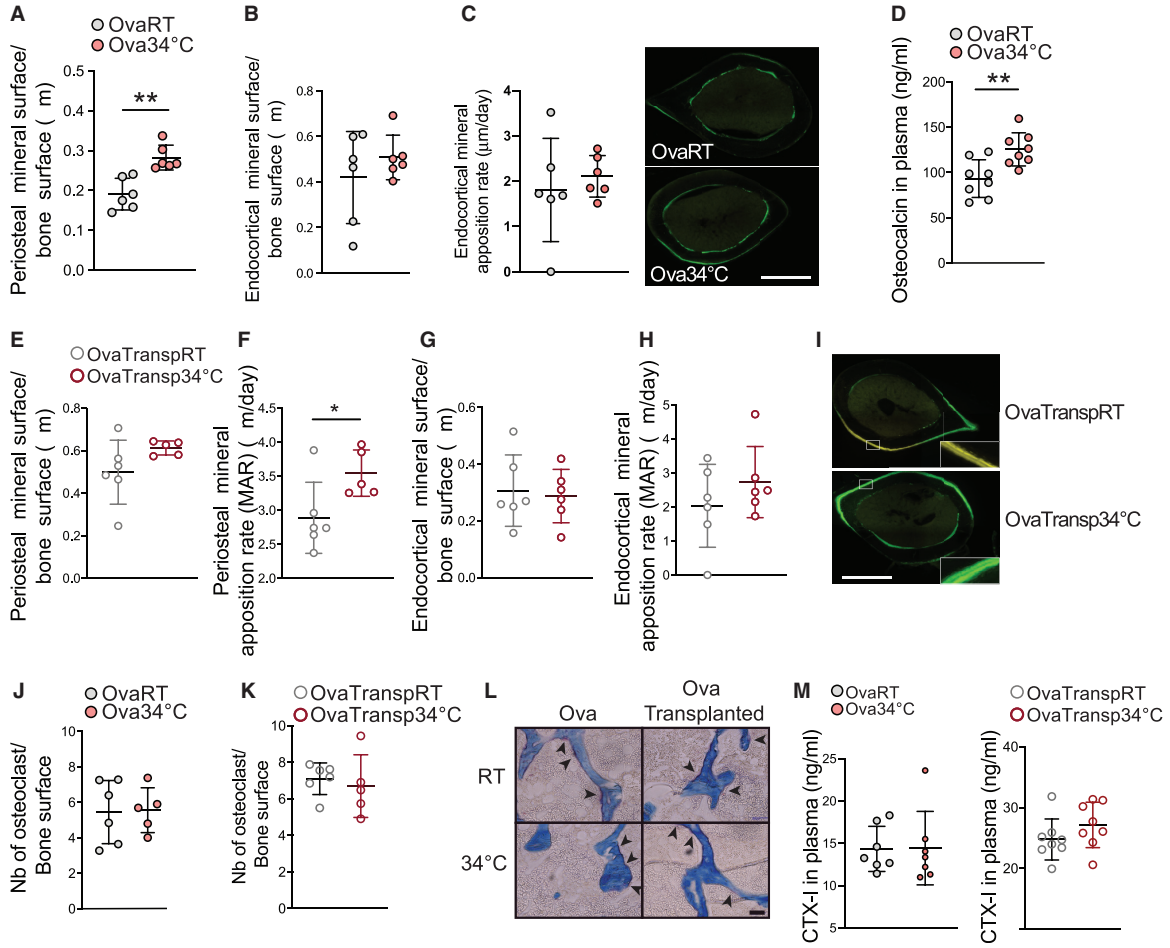

Figure 6. Warmth and Warm Microbiota Transplantation Increase Periosteal Bone Formation

(A and B) Periosteal (A) and endocortical (B) mineralized surface after calcein injection in 24-week-old female mice that were ovariectomized at 16 weeks of age and exposed for 2 months to 34°C or kept at RT.

(C) Representative images (of n = 6) of fluorescent calcein in femur midshaft used for the quantifications.

(D) Osteocalcin levels in plasma of mice as in (A).

(E–I) Periosteal mineralized surface (E), periosteal MAR (F), endocortical mineralized surface (G), and endocortical MAR (H) in tibias of 21-week-old ovariectomized, microbiota recipient female mice (OvaTransp34°C or OvaTranspRT) as in Figures 4A–4E. (I) Representative images (n = 6) of fluorescent calcein in femur midshaft used for the quantifications. Scale bar, 0.5 mm.

(J–L) TRAP staining quantification of osteoclast number in femur trabeculae of mice as in (A) shown in (J) and of mice as in (E) shown in (K). (L) Representative images (n = 6) of the quantifications shown in (J) and (K). Arrowheads correspond to the TRAP signal. Scale bar, 50 µm.

(M) CTX-1 levels in plasma of mice as in (J) and (K).

Data are shown as mean ± SD (n = 6 per group). Significance (p value) is calculated using Mann-Whitney t test, *p < 0.05; **p < 0.01; ***p < 0.001.

mice increased the bone strength and density but did not change the bone length. These data may therefore imply an extension to the Allen's rule, suggesting elongation-independent effects of warmth exposure, which predominantly favors increased bone density and strength through microbiota alterations.

The frequency of major osteoporotic fractures varies substantially depending on the country, being highest in Scandinavia and lowest in Africa. While this may partly reflect ethnic influences, it is also observed in Europe where the hip fracture rate in northern Europe is 11 times higher than in the Mediterranean area (Cheng et al., 2011; Cauley et al., 2014; Johnell et al., 1992; Eastell et al., 2016). There could be several explanations regarding the origin of these geographical differences, and it has been proposed that levels of vitamin D and calcium consumption as well as diet and genetics may be causal factors (Prentice, 2004; Yeum et al., 2016; Zengin et al., 2015). Without excluding any of the above-mentioned causes, our human metadata analysis supports a geographical gradient and shows that the osteoporosis-related hip fractures inversely correlate with the average temperatures and positively with latitude independently of

CellPress

Cell Metabolism
Article

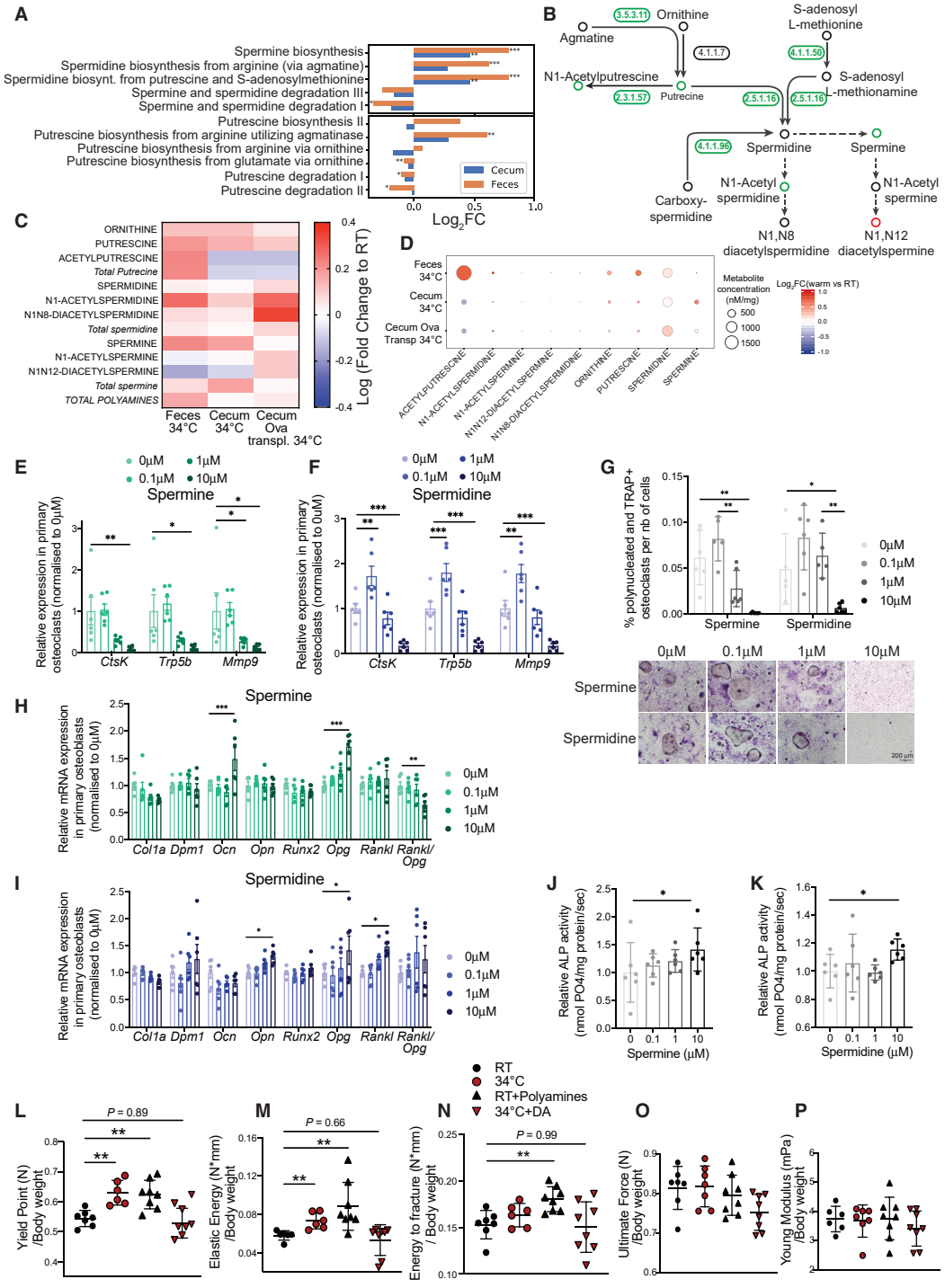

Figure 7. Microbial Production of Polyamines Mediates the Warmth Effects on the Bone

(A) Bar chart representing metagenomics analysis of the bacterial polyamine biosynthetic and degradation pathways in feces and cecum samples from 24-week-old female mice that were exposed to 34°C for 2 months or kept at RT. Significance shows FDR: *p < 0.05; **p < 0.01; ***p < 0.001.

(legend continued on next page)

Cell Metabolism
Article

vitamin D and calcium consumption, suggesting that the results we observe in mice could be translated to humans.

Our work shows that more than 90% of the ovariectomy-induced transcriptional changes in the bone are dampened by exposure to warmth and 59% by transplanting the ovariectomized mice with warm-adapted microbiota. These results suggest a major protective effect of these treatments on the overall bone alterations that underlie bone loss. The findings that the warmth exposure affects the polyamine biosynthetic pathway in the microbiota suggest a possible link between these changes and the effects on bone mass and strength and presumably other tissues that are affected by the polyamine levels. Aging is associated with decline in the polyamine levels (Scalabrino and Ferioli, 1984; Pucciarelli et al., 2012), and polyamine supplementation protects against several age-related diseases (Ramos-Molina et al., 2019; Tofalo et al., 2019), including memory impairment (Gupta et al., 2013; Frühauf et al., 2015), cardiovascular disease (Eisenberg et al., 2016), and cancer (Yue et al., 2017), while extending the lifespan of various organisms (Soda et al., 2009; Kiechl et al., 2018). Warmth-induced microbiota-mediated increases in polyamine biosynthesis may therefore be of general physiological importance that could extend well beyond bone-related research, impacting several age-related diseases and prolonging health span.

Limitations of Study

Our study does not address the upstream mechanisms by which warmth exposure alters the microbiota composition. These changes are unlikely due to a direct temperature effect as the internal body temperature of the mice was unaffected when we exposed them to 34°C. It is likely that the decreased food intake and movement during warmth exposure will jointly impact the microbiota composition to a certain extent; however, follow-up work is needed to clarify the initial triggers and pathways by which the gut microbiota responds to the increased environmental temperature. Similarly, while the study suggests a critical direct or indirect contribution of the polyamines and the gut microbiota, it does not exclude that there could be additional microbiota-related, or unrelated mechanisms by which warmth exposure increases bone strength.

STAR★METHODS

Detailed methods are provided in the online version of this paper and include the following:

- KEY RESOURCES TABLE
- RESOURCE AVAILABILITY
  - Lead Contact
  - Materials Availability
  - Data and Code Availability
- EXPERIMENTAL MODEL AND SUBJECT DETAILS
  - Mouse Models
  - Primary Cell Culture
- METHOD DETAILS
  - Ovariectomy
  - Sample Collection at Sacrifice
  - Microbiota Transplantation
  - Antibiotic Treatment
  - Polyamines Supplementation and Inhibitor Treatment
  - Micro-CT Analysis
  - Biomechanical Analysis of the Bone
  - Human Metadata Analysis
  - 16S Gut Microbiota Profiling
  - Metagenomics Sequencing
  - RNA Extraction, Reverse Transcription and Real-time qPCR
  - RNA Sequencing
  - Cecal and Fecal Concentration of Polyamines
  - Elisa
  - Bone Mineral Content
  - TRAP Staining
  - Alkaline Phosphatase (ALP) Activity Measurement
  - Bone Histomorphometric Analysis
- QUANTIFICATION AND STATISTICAL ANALYSIS
  - Data Representation and Statistical Analysis

(B) Graphical representation of the polyamine biosynthetic pathway where numbers (enzymes from keg nomenclature) represent the level of respective genes present in the gut microbiota from fecal samples of mice as in (A). Green-colored circles show increase, red-colored show decrease, and black-colored indicate unchanged concentrations after warm exposure. 3.5.3.11, agmatinase; 4.1.1.7, benzoylformate decarboxylase; 2.3.1.57, putrescine acetyltransferase/spermine-spermidine N1-acetyltransferase; 4.1.1.50, adenosylmethionine decarboxylase; 2.5.1.16, spermidine synthase; 4.1.1.96, carboxynorspermidine decarboxylase.
(C and D) Heatmap (C) or heatmap associated with absolute polyamine levels (D), showing fold change of polyamines measured using HILIC-MS/MS in feces or cecum samples from 24-week-old female mice that were exposed to 34°C for 2 months versus RT controls (34°C versus RT; feces 34°C and cecum 34°C); or cecum of 21-week-old ovariectomized, microbiota recipient female mice (cecum Ova transpl34°C).
(E and F) Relative mRNA expression levels in cultured primary osteoclasts subjected to different spermine (E) or spermidine (F) concentrations, measured by qPCR.
(G) Quantification of the polynucleated and $TRAP^+$ differentiated osteoclasts normalized to the total number of cells in presence of spermine or spermidine. Below: representative images (from 6 wells per condition) from TRAP staining of osteoclasts differentiated in presence of spermine or spermidine. Scale bar, 200 μm.
(H and I) Relative mRNA expression levels in cultured primary osteoblasts subjected to different spermine (H) or spermidine (I) concentrations, measured by qPCR.
(J and K) Relative alkaline phosphatase (ALP) activity in osteoblast culture after spermine (J) or spermidine (K) supplementation at different concentrations.
(L–P) Biomechanical analysis using three-point bending test of femur from 23-week-old female mice that were RT kept (RT), warm exposed (34°C), supplemented with freshly prepared polyamine mix and RT kept (RT-polyamines), or provided with 50 μm DA and kept at 34°C (34°C-DA), starting at 16 weeks of age until sacrifice. Polyamines and DA were supplemented in drinking water every second day. The panels show yield point (L), elastic energy (M), energy to fracture (N), ultimate force (O), and Young's modulus (P) that are normalized to their body weight values at sacrifice.
Data are shown as mean ± SD (n = 8 per group). Significance is calculated based on one-way ANOVA, *p < 0.05; **p < 0.01; ***p < 0.001.
Significance (p value) in all panels except (A) and (L)–(P) is calculated using Mann-Whitney t test, *p < 0.05; **p < 0.01; ***p < 0.001.

SUPPLEMENTAL INFORMATION

Supplemental Information can be found online at https://doi.org/10.1016/j.cmet.2020.08.012.

ACKNOWLEDGMENTS

We thank Claes Wollheim and the members of our lab for discussions and critical reading of the manuscript, and Serge Ferrari, Tony Teav, and Hector Gallart-Ayalla for technical expertise and advice. This work is part of a project that has received funding from the European Research Council (ERC) under the European Union's Horizon 2020 research and innovation program (ERC Consolidator grant agreement no. 815962, Healthybiota) and from the Clayton Foundation for biomedical research.

AUTHOR CONTRIBUTIONS

Conceptualization, C.C. and M.T.; Methodology, C.C., S.K., M.C., N.H., B.B., N.B., and M.T.; Investigation, C.C., S.K., M.C., N.H., J.B., N.S.Z., M.S., S.F., and N.B.; Writing, C.C. and M.T.; Resources, N.B., A.M., and M.T.; Funding Acquisition, M.T.; Supervision, M.T.

DECLARATION OF INTERESTS

M.T. and C.C. disclose that they are inventors of a submitted patent application for treatment of bone diseases. All other authors declare no competing interests.

Received: February 19, 2020
Revised: June 25, 2020
Accepted: August 18, 2020
Published: September 10, 2020

REFERENCES

Alhilli, F., and Wright, E.-A. (1983). The effects of changes in the environmental-temperature on the growth of tail bones in the mouse. Br. J. Exp. Pathol. *64*, 34–42.

Allen, J. (1877). The influence of physical conditions in the genesis of species. Radical Rev. *1*, 108–140.

Aramaki, T., Blanc-Mathieu, R., Endo, H., Ohkubo, K., Kanehisa, M., Goto, S., and Ogata, H. (2020). KofamKOALA: KEGG ortholog assignment based on profile HMM and adaptive score threshold. Bioinformatics *36*, 2251–2252.

Ashoub, M.A. (1958). Effect of two extreme temperatures on growth and tail-length of mice. Nature *181*, 284.

Balk, E.M., Adam, G.P., Langberg, V.N., Earley, A., Clark, P., Ebeling, P.R., Mithal, A., Rizzoli, R., Zerbini, C.A.F., Pierroz, D.D., et al. (2017). Global dietary calcium intake among adults: a systematic review. Osteoporos. Int. *28*, 3315–3324.

Boskey, A.L., and Coleman, R. (2010). Aging and bone. J. Dent. Res. *89*, 1333–1348.

Bushnell, B. (2020). BBmap. https://www.osti.gov/biblio/1241166-bbmap-fast-accurate-splice-aware-aligner.

Callahan, B.J., McMurdie, P.J., Rosen, M.J., Han, A.W., Johnson, A.J., and Holmes, S.P. (2016). DADA2: high-resolution sample inference from Illumina amplicon data. Nat. Methods *13*, 581–583.

Caporaso, J.G., Lauber, C.L., Walters, W.A., Berg-Lyons, D., Lozupone, C.A., Turnbaugh, P.J., Fierer, N., and Knight, R. (2011). Global patterns of 16S rRNA diversity at a depth of millions of sequences per sample. Proc. Natl. Acad. Sci. USA *108*, 4516–4522.

Caporaso, J.G., Lauber, C.L., Walters, W.A., Berg-Lyons, D., Huntley, J., Fierer, N., Owens, S.M., Betley, J., Fraser, L., Bauer, M., et al. (2012). Ultra-high-throughput microbial community analysis on the Illumina HiSeq and MiSeq platforms. ISME J. *6*, 1621–1624.

Caspi, R., Billington, R., Ferrer, L., Foerster, H., Fulcher, C.A., Keseler, I.M., Kothari, A., Krummenacker, M., Latendresse, M., Mueller, L.A., et al. (2016). The MetaCyc database of metabolic pathways and enzymes and the BioCyc collection of pathway/genome databases. Nucleic Acids Res. *44*, D471–D480.

Cauley, J.A., Chalhoub, D., Kassem, A.M., and El-Hajj Fuleihan, Gel-H. (2014). Geographic and ethnic disparities in osteoporotic fractures. Nat. Rev. Endocrinol. *10*, 338–351.

Cheng, S.Y., Levy, A.R., Lefaivre, K.A., Guy, P., Kuramoto, L., and Sobolev, B. (2011). Geographic trends in incidence of hip fractures: a comprehensive literature review. Osteoporos. Int. *22*, 2575–2586.

Chevalier, C., Stojanović, O., Colin, D.J., Suarez-Zamorano, N., Tarallo, V., Veyrat-Durebex, C., Rigo, D., Fabbiano, S., Stevanović, A., Hagemann, S., et al. (2015). Gut microbiota orchestrates energy homeostasis during cold. Cell *163*, 1360–1374.

Cox-York, K.A., Sheflin, A.M., Foster, M.T., Gentile, C.L., Kahl, A., Koch, L.G., Britton, S.L., and Weir, T.L. (2015). Ovariectomy results in differential shifts in gut microbiota in low versus high aerobic capacity rats. Physiol. Rep. *3*, e12488.

Demontiero, O., Vidal, C., and Duque, G. (2012). Aging and bone loss: new insights for the clinician. Ther. Adv. Musculoskelet. Dis. *4*, 61–76.

Devlin, M.J., Cloutier, A.M., Thomas, N.A., Panus, D.A., Lotinun, S., Pinz, I., Baron, R., Rosen, C.J., and Bouxsein, M.L. (2010). Caloric restriction leads to high marrow adiposity and low bone mass in growing mice. J. Bone Miner. Res. *25*, 2078–2088.

Eastell, R., O'Neill, T.W., Hofbauer, L.C., Langdahl, B., Reid, I.R., Gold, D.T., and Cummings, S.R. (2016). Postmenopausal osteoporosis. Nat. Rev. Dis. Primers *2*, 16069.

Eisenberg, T., Abdellatif, M., Schroeder, S., Primessnig, U., Stekovic, S., Pendl, T., Harger, A., Schipke, J., Zimmermann, A., Schmidt, A., et al. (2016). Cardioprotection and lifespan extension by the natural polyamine spermidine. Nat. Med. *22*, 1428–1438.

Fabbiano, S., Suárez-Zamorano, N., Rigo, D., Veyrat-Durebex, C., Stevanovic Dokic, A.S., Colin, D.J., and Trajkovski, M. (2016). Caloric restriction leads to browning of white adipose tissue through type 2 immune signaling. Cell Metab. *24*, 434–446.

Fabregat, A., Sidiropoulos, K., Viteri, G., Forner, O., Marin-Garcia, P., Arnau, V., D'Eustachio, P., Stein, L., and Hermjakob, H. (2017). Reactome pathway analysis: a high-performance in-memory approach. BMC Bioinformatics *18*, 142.

Fernandes, A.D., Macklaim, J.M., Linn, T.G., Reid, G., and Gloor, G.B. (2013). ANOVA-like differential expression (ALDEx) analysis for mixed population RNA-Seq. PLoS One *8*, e67019.

Ferris, R.L., Blumenschein, G.R., Fayette, J., Guigay, J., Colevas, A.D., Licitra, L., Harrington, K., Kasper, S., Vokes, E.E., Even, C., et al. (2018). Two-year update From CheckMate 141: outcomes with Nivolumab (Nivo) vs Investigator's choice (IC) in recurrent or metastatic (R/M) squamous cell carcinoma of the head and neck (SCCHN) in the overall population and PD-L1 subgroups. International Journal of Radiation Oncology*Biology*Physics *100*, 1317.

Frühauf, P.K., Ineu, R.P., Tomazi, L., Duarte, T., Mello, C.F., and Rubin, M.A. (2015). Spermine reverses lipopolysaccharide-induced memory deficit in mice. J. Neuroinflamm. *12*, 3.

Gupta, V.K., Scheunemann, L., Eisenberg, T., Mertel, S., Bhukel, A., Koemans, T.S., Kramer, J.M., Liu, K.S.Y., Schroeder, S., Stunnenberg, H.G., et al. (2013). Restoring polyamines protects from age-induced memory impairment in an autophagy-dependent manner. Nat. Neurosci. *16*, 1453–1460.

Hamrick, M.W., Ding, K.H., Ponnala, S., Ferrari, S.L., and Isales, C.M. (2008). Caloric restriction decreases cortical bone mass but spares trabecular bone in the mouse skeleton: implications for the regulation of bone mass by body weight. J. Bone Miner. Res. *23*, 870–878.

Harland, S.C. (1960). Effect of temperature on growth in weight and tail-length of inbred and hybrid mice. Nature *186*, 446.

Hsu, E., and Pacifici, R. (2018). From osteoimmunology to osteomicrobiology: how the microbiota and the immune system regulate bone. Calcif. Tissue Int. *102*, 512–521.

Cell Metabolism
Article

CellPress

Hyatt, D., Chen, G.L., Locascio, P.F., Land, M.L., Larimer, F.W., and Hauser, L.J. (2010). Prodigal: prokaryotic gene recognition and translation initiation site identification. BMC Bioinformatics *11*, 119.

Iwaniec, U.T., Philbrick, K.A., Wong, C.P., Gordon, J.L., Kahler-Quesada, A.M., Olson, D.A., Branscum, A.J., Sargent, J.L., DeMambro, V.E., Rosen, C.J., and Turner, R.T. (2016). Room temperature housing results in premature cancellous bone loss in growing female mice: implications for the mouse as a preclinical model for age-related bone loss. Osteoporos. Int. *27*, 3091–3101.

Jilka, R.L. (2013). The relevance of mouse models for investigating age-related bone loss in humans. J. Gerontol. A Biol. Sci. Med. Sci. *68*, 1209–1217.

Johnell, O., Gullberg, B., Allander, E., and Kanis, J.A.; MEDOS Study Group. (1992). The apparent incidence of hip fracture in Europe: a study of national register sources. Osteoporos. Int. *2*, 298–302.

Jones, R.M., Mulle, J.G., and Pacifici, R. (2017). Osteomicrobiology: the influence of gut microbiota on bone in health and disease. Bone *115*, 59–67.

Kaiyala, K.J., Morton, G.J., Thaler, J.P., Meek, T.H., Tylee, T., Ogimoto, K., and Wisse, B.E. (2012). Acutely decreased thermoregulatory energy expenditure or decreased activity energy expenditure both acutely reduce food intake in mice. PLoS One *7*, e41473.

Kaliannan, K., Robertson, R.C., Murphy, K., Stanton, C., Kang, C., Wang, B., Hao, L., Bhan, A.K., and Kang, J.X. (2018). Estrogen-mediated gut microbiome alterations influence sexual dimorphism in metabolic syndrome in mice. Microbiome *6*, 205.

Kang, D.D., Li, F., Kirton, E.S., Thomas, A., Egan, R.S., An, H., and Wang, Z. (2019). MetaBAT 2: an adaptive binning algorithm for robust and efficient genome reconstruction from metagenome assemblies. PeerJ *7*, e7359.

Karvonen, E., Kauppinen, L., Partanen, T., and Pösö, H. (1985). Irreversible inhibition of putrescine-stimulated S-adenosyl-L-methionine decarboxylase by berenil and pentamidine. Biochem J. *231*, 165–169.

Kasper, S., Gillison, M.L., Blumenschein, G., Fayette, J., Guigay, J., Colevas, A.D., Licitra, L., Harrington, K., Vokes, E.E., Even, C., et al. (2018). Nivolumab (Nivo) vs Investigator's choice (IC) for platinum-refractory (PR) recurrent or metastatic (R/M) squamous cell carcinoma of the head and neck (SCCHN; CheckMate 141): outcomes in first-line (1L) R/M Patients (Pts) and updated safety and efficacy. Oncol. Res. Treat. *41*, 96.

Kiechl, S., Pechlaner, R., Willeit, P., Notdurfter, M., Paulweber, B., Willeit, K., Werner, P., Ruckenstuhl, C., Iglseder, B., Weger, S., et al. (2018). Higher spermidine intake is linked to lower mortality: a prospective population-based study. Am. J. Clin. Nutr. *108*, 371–380.

Kieser, S., Brown, J., Zdobnov, E.M., Trajkovski, M., and McCue, L.A. (2020). Atlas: a Snakemake workflow for assembly, annotation, and genomic binning of metagenome sequence data. BMC Bioinformatics *21*, 257.

Li, L., Rao, S., Cheng, Y., Zhuo, X., Deng, C., Xu, N., Zhang, H., and Yang, L. (2019). Microbial osteoporosis: the interplay between the gut microbiota and bones via host metabolism and immunity. MicrobiologyOpen *8*, e00810.

Libby, P.R., and Porter, C.W. (1992). Inhibition of enzymes of polyamine backconversion by pentamidine and berenil. Biochem Pharmacol. *44*, 830–832.

Madeira, F., Park, Y.M., Lee, J., Buso, N., Gur, T., Madhusoodanan, N., Basutkar, P., Tivey, A.R.N., Potter, S.C., Finn, R.D., and Lopez, R.D. (2019). The EMBL-EBI search and sequence analysis tools APIs in 2019. Nucleic Acids Res. *47*, W636–W641.

Markle, J.G., Frank, D.N., Mortin-Toth, S., Robertson, C.E., Feazel, L.M., Rolle-Kampczyk, U., von Bergen, M., McCoy, K.D., Macpherson, A.J., and Danska, J.S. (2013). Sex differences in the gut microbiome drive hormone-dependent regulation of autoimmunity. Science *339*, 1084–1088.

Martín-Fernández, J.A., Barcelo-Vidal, C., and Pawlowsky-Glahn, V. (2003). Dealing with zeros and missing values in compositional data sets using nonparametric imputation. Math. Geol. *35*, 253–278.

Mcmillan, P.J., Dewri, R.A., Joseph, E.E., Schultz, R.L., and Deftos, L.J. (1989). Rapid changes of light microscopic indices of osteoclast-bone relationships correlated with electron microscopy. Calcif. Tissue Int. *44*, 399–405.

Meyer, C.W., Ootsuka, Y., and Romanovsky, A.A. (2017). Body temperature measurements for metabolic phenotyping in mice. Front. Physiol. *8*, 520.

Mosekilde, L. (2000). Age-related changes in bone mass, structure, and strength - effects of loading. Z. Rheumatol. *59*, 1–9.

Neidhart, M., Karouzakis, E., Jüngel, A., Gay, R.E., and Gay, S. (2014). Inhibition of spermidine/spermine N1-acetyltransferase activity: a new therapeutic concept in rheumatoid arthritis. Arthritis Rheumatol. *66*, 1723–1733.

Nurk, S., Meleshko, D., Korobeynikov, A., and Pevzner, P.A. (2017). metaSPAdes: a new versatile metagenomic assembler. Genome Res *27*, 824–834.

Ohlsson, C., and Sjögren, K. (2015). Effects of the gut microbiota on bone mass. Trends Endocrinol. Metab. *26*, 69–74.

Ohlsson, C., and Sjögren, K. (2018). Osteomicrobiology: a new cross-disciplinary research field. Calcif. Tissue Int. *102*, 426–432.

Parfitt, A.M. (1988). Bone histomorphometry: proposed system for standardization of nomenclature, symbols, and units. Calcif. Tissue Int. *42*, 284–286.

Parks, D.H., Imelfort, M., Skennerton, C.T., Hugenholtz, P., and Tyson, G.W. (2015). CheckM: assessing the quality of microbial genomes recovered from isolates, single cells, and metagenomes. Genome Res *25*, 1043–1055.

Parvaneh, K., Jamaluddin, R., Karimi, G., and Erfani, R. (2014). Effect of probiotics supplementation on bone mineral content and bone mass density. Sci. World J. *2014*, 595962.

Pegg, A.E. (2009). Mammalian polyamine metabolism and function. IUBMB Life *61*, 880–894.

Pines, M., and Hurwitz, S. (1991). The role of the growth plate in longitudinal bone growth. Poult. Sci. *70*, 1806–1814.

Prentice, A. (2004). Diet, nutrition and the prevention of osteoporosis. Public Health Nutr. *7*, 227–243.

Pucciarelli, S., Moreschini, B., Micozzi, D., De Fronzo, G.S., Carpi, F.M., Polzonetti, V., Vincenzetti, S., Mignini, F., and Napolioni, V. (2012). Spermidine and spermine are enriched in whole blood of nona/centenarians. Rejuvenation Res. *15*, 590–595.

Quast, C., Pruesse, E., Yilmaz, P., Gerken, J., Schweer, T., Yarza, P., Peplies, J., and Glöckner, F.O. (2013). The SILVA ribosomal RNA gene database project: improved data processing and web-based tools. Nucleic Acids Res. *41*, D590–D596.

Racine, H.L., Meadows, C.A., Ion, G., and Serrat, M.A. (2018). Heat-induced limb length asymmetry has functional impact on weight bearing in mouse hindlimbs. Front. Endocrinol. *9*, 289.

Ramos-Molina, B., Queipo-Ortuño, M.I., Lambertos, A., Tinahones, F.J., and Peñafiel, R. (2019). Dietary and gut microbiota polyamines in obesity- and age-related diseases. Front. Nutr. *6*, 24.

Reginster, J.Y., and Burlet, N. (2006). Osteoporosis: a still increasing prevalence. Bone *38*, S4–S9.

Romsos, D.R., Ferguson, D., and Vander Tuig, J.G. (1985). Effects of a warm environment on energy balance in obese (Ob/Ob) mice. Metab. Clin. Exp. *34*, 931–937.

Scalabrino, G., and Ferioli, M.E. (1984). Polyamines in mammalian ageing: an oncological problem, too? A review. Mech. Ageing Dev. *26*, 149–164.

Serrat, M.A. (2013). Allen's rule revisited: temperature influences bone elongation During a critical period of postnatal development. Anat. Rec. (Hoboken) *296*, 1534–1545.

Serrat, M.A. (2014). Environmental temperature impact on bone and cartilage growth. Compr. Physiol. *4*, 621–655.

Serrat, M.A., King, D., and Lovejoy, C.O. (2008). Temperature regulates limb length in homeotherms by directly modulating cartilage growth. Proc. Natl. Acad. Sci. USA *105*, 19348–19353.

Serrat, M.A., Schlierf, T.J., Efaw, M.L., Shuler, F.D., Godby, J., Stanko, L.M., and Tamski, H.L. (2015). Unilateral heat accelerates bone elongation and lengthens extremities of growing mice. J. Orthop. Res. *33*, 692–698.

Sieber, C.M.K., Probst, A.J., Sharrar, A., Thomas, B.C., Hess, M., Tringe, S.G., and Banfield, J.F. (2018). Recovery of genomes from metagenomes via a dereplication, aggregation and scoring strategy. Nat. Microbiol. *3*, 836–843.

Sjögren, K., Engdahl, C., Henning, P., Lerner, U.H., Tremaroli, V., Lagerquist, M.K., Bäckhed, F., and Ohlsson, C. (2012). The gut microbiota regulates bone mass in mice. J. Bone Miner. Res. *27*, 1357–1367.

Skipper, S., and Perktold, J. (2010). statsmodels: econometric and statistical modeling with python. In Proceedings of the 9th python in science conference https://conference.scipy.org/proceedings/scipy2010/pdfs/seabold.pdf.

Soda, K., Dobashi, Y., Kano, Y., Tsujinaka, S., and Konishi, F. (2009). Polyamine-rich food decreases age-associated pathology and mortality in aged mice. Exp. Gerontol. *44*, 727–732.

Sözen, T., Özışık, L., and Başaran, N.Ç. (2017). An overview and management of osteoporosis. Eur. J. Rheumatol. *4*, 46–56.

Steinegger, M., and Söding, J. (2018). Clustering huge protein sequence sets in linear time. Nat. Commun. *9*, 2542.

Suárez-Zamorano, N., Fabbiano, S., Chevalier, C., Stojanović, O., Colin, D.J., Stevanović, A., Veyrat-Durebex, C., Tarallo, V., Rigo, D., Germain, S., et al. (2015). Microbiota depletion promotes browning of white adipose tissue and reduces obesity. Nat. Med. *21*, 1497–1501.

Tofalo, R., Cocchi, S., and Suzzi, G. (2019). Polyamines and gut microbiota. Front. Nutr. *6*, 16.

Tsai, Y.F., Hsu, L.H., Wu, C.C., Cai, W.H., Yang, K.C., and Fan, F.Y. (2017). Long-term oral toxicity and anti-osteoporotic effect of sintered dicalcium pyrophosphate in rat model of postmenopausal osteoporosis. J. Med. Biol. Eng. *37*, 181–190.

Wahl, D.A., Cooper, C., Ebeling, P.R., Eggersdorfer, M., Hilger, J., Hoffmann, K., Josse, R., Kanis, J.A., Mithal, A., Pierroz, D.D., et al. (2012). A global representation of vitamin D status in healthy populations. Arch. Osteoporos. *7*, 155–172.

Wang, L.L., Liu, Y., Qi, C., Shen, L.Y., Wang, J.Y., Liu, X.J., Zhang, N., Bing, T., and Shangguan, D.H. (2018). Oxidative degradation of polyamines by serum supplement causes cytotoxicity on cultured cells. Sci. Rep. *8*, 10384.

Wu, Y.W., Simmons, B.A., and Singer, S.W. (2016). MaxBin 2.0: an automated binning algorithm to recover genomes from multiple metagenomic datasets. Bioinformatics *32*, 605–607.

Yamamoto, T., Hinoi, E., Fujita, H., Iezaki, T., Takahata, Y., Takamori, M., and Yoneda, Y. (2012). The natural polyamines spermidine and spermine prevent bone loss through preferential disruption of osteoclastic activation in ovariectomized mice. Br. J. Pharmacol. *166*, 1084–1096.

Yeum, K.J., Song, B.C., and Joo, N.S. (2016). Impact of geographic location on vitamin D status and bone mineral density. Int. J. Environ. Res. Public Health *13*, 184.

Yue, F., Li, W., Zou, J., Jiang, X., Xu, G., Huang, H., and Liu, L. (2017). Spermidine prolongs lifespan and prevents liver fibrosis and hepatocellular carcinoma by activating MAP1S-mediated autophagy. Cancer Res. *77*, 2938–2951.

Zengin, A., Prentice, A., and Ward, K.A. (2015). Ethnic differences in bone health. Front. Endocrinol. (Lausanne) *6*, 24.

Ziętak, M., Kovatcheva-Datchary, P., Markiewicz, L.H., Ståhlman, M., Kozak, L.P., and Bäckhed, F. (2016). Altered microbiota contributes to reduced diet-induced obesity upon cold exposure. Cell Metab. *23*, 1216–1223.

Cell Metabolism
Article

CellPress

STAR★METHODS

KEY RESOURCES TABLE

REAGENT or RESOURCE	SOURCE	IDENTIFIER
Chemicals, Peptides, and Recombinant Proteins		
Calcein	Sigma-Aldrich	C0875
RNA-later	Invitrogen	AM7020
Neomycin-streptomycin-penicillin	Sigma-Aldrich	P4083
Vancomycin	Sigma-Aldrich	V2002
Metronidazole	Sigma-Aldrich	M3761
Bacitracin	Sigma-Aldrich	11702
Ciprofloxacine HCL	Alkaloid	2000314
CEFAZ	Alkaloid	1046371
Spermine for *in vivo*	Sigma-Aldrich	85590
Spermidine for *in vivo*	Sigma-Aldrich	S2626
Diaminazene Acetureate	Sigma-Aldrich	D7770
Trizol	Thermo Fisher Scientific	15596018
High-Capacity cDNA Reverse Transcription Kit	Applied Biosystems	4368813
Power-up SYBR Green	Applied Biosystems	A25742
aMEM medium	bioconcept	1-23P10-M
100X Penicillin Streptomycin	GIBCO	15140
100x glutamine	GIBCO	25030
amino-acids mix	BioConcept	5-12K01-H
Recombinant murine M-CFS	Peprotech	31502
Recombinant murine sRANK Ligand	Peprotech	315-11C
Spermine for cell culture	Sigma-Aldrich	S4264
Spermidine for cell culture	Sigma-Aldrich	S0266
Fast violet B salt	ChemCruz	sc-215029B
Sirius red dye reagent: Direct red 80	Sigma-Aldrich	P744
Critical Commercial Assays		
PowerFecal DNA Kit	QIAGEN	12830-50
5Prime HotMaster mix	Quantabio	2200400
MiSeq reagent kit V2	Illumina	MS-102-2003
TruSeq Nano DNA Library Prep Kit	Illumina	20015964
TruSeq RNA Library Prep Kit v2	Illumina	RS-122-2001
Calcitriol (INN) Elisa kit	Abbexa	abx 513030
Osteocalcin Elisa Kit	Immutopics (quidel)	60-1305
RatLaps CTX-I EIA	Immunodiagnostic Systems	AC-06F1
Pierce BCA Protein assay kit	Thermo Scientific	23225
Deposited Data		
Raw shotgun-metagenome data of female mice	This study	PRJNA647832
Raw amplicon data of male mice	This study	PRJNA648020
Raw amplicon data of female mice	This study	PRJNA647833
Raw RNA seq data	This study	PRJNA648022
SILVA database v132	(Quast et al., 2013)	N/A
Reactome pathways database	(Fabregat et al., 2017)	N/A

(*Continued on next page*)

Continued

REAGENT or RESOURCE	SOURCE	IDENTIFIER
Resources for the metagenomic analysis	This study	https://github.com/SilasK/WarmMicrobiota
Resources for the 16SrDNA analysis	This study	https://github.com/SilasK/WarmMicrobiota
Resources for the human correlation analysis	This study	https://dx.doi.org/10.6084/m9.figshare.0.12696407
Targeted Metabolomic data	This study	https://dx.doi.org/10.6084/m9.figshare.12696419
Experimental Models: Organisms/Strains		
C57BL/6J mice	Janvier Labs	SC-C57J-M
Germ-free mice on C57BL/6J background	Germ-free Clean Animal Facility, University of Bern, Switzerland	N/A
Oligonucleotides		
Primer for 16S rDNA library preparation: 806 Reverse Primer GGACTACNVGGG TWTCTAAT - 515 Forward Primer GTG YCAGCMGCCGCGGTAA.	515F-806R barcoded primers Integrated DNA Technologies (IDT)	10776320 (plate5) and 10776323 (plate6)
Primer for 16S rDNA library sequencing: read1, 5′- TATGGTAA TTGTGTGCCAGCMGCCGCGGTA A-3′, read2, 5′- AGTCAGTCAGCCG GACTACHVGGGTWTCTAAT3′ and index read, 5′- ATTAGAWACCCBD GTAGTCCGGCTGACTGACT3′	Illumina	N/A
Primer used for the cell culture characterization: See Table S1	This study	N/A
Software and Algorithms		
VivaCT40 associated software	Scanco system; Zurich, Switzerland	N/A
Instron 1114 associated software	Instron, High Wycombe, UK	N/A
Amplicon sequencing plipline	https://github.com/SilasK/16S-dada2	N/A
Statistical 16S data analysis	https://github.com/SilasK/microbiome-analysis	N/A
Sci-kit bio, compositional data analysis	http://scikit-bio.org/	N/A
Metagenomic reads analysis: metagenome-atlas v2	(Kieser et al., 2020)	N/A
MetaCyc Pathways	(Caspi et al., 2016)	N/A
TopHat v.2 software	John Hopkins university	N/A
RSeQC V2.3.3	N/A	http://rseqc.sourceforge.net/
PicardTools1.92	N/A	https://broadinstitute.github.io/picard/
R/Bioconductor package EdgeR v.3.4.2	N/A	https://www.bioconductor.org/packages/release/bioc/html/edgeR.html
Raw LC-MS/MS data was processed using the Agilent Quantitative analysis software (version B.07.00)	MassHunter Agilent technologies	N/A
Metaexpress (5.1.41) software	Molecular devices	N/A
Leica Q image analyzer	Leica	N/A
Bioquant osteo software	Bioquant	N/A

RESOURCE AVAILABILITY

Lead Contact

Further information and requests for resources and reagents should be directed to and will be fulfilled by the Lead Contact, Mirko Trajkovski (Mirko.Trajkovski@unige.ch)

Cell Metabolism
Article

CellPress

Materials Availability

All materials used in this study are either commercially available or obtained through collaboration, as indicated.

Data and Code Availability

All sequencing data generated in this study is deposited at the Sequence Read Archive (SRA) of the National Center for Biotechnology Information. The 16S rDNA sequencing of the female and the male mice have accessions SRA: PRJNA647833 and SRA: PRJNA648020, respectively. Shotgun metagenomics data is available under the id SRA: PRJNA647832 and the RNA seq data under SRA: PRJNA648022. The data for targeted metabolomics and the correlation analysis in human are deposited in the open access repository figshare: https://doi.org/10.6084/m9.figshare.12696419 and https://doi.org/10.6084/m9.figshare 0.12696407, respectively. The scripts used for the analysis of the 16S rDNA, metagenomc and human epidemiology data are available at https://github.com/SilasK/WarmMicrobiota.

EXPERIMENTAL MODEL AND SUBJECT DETAILS

Mouse Models

All C57BL/6J mice were purchased from Janvier Labs and were kept in a specific pathogen-free facility (SPF) in individually ventilated cages, 2 mice per cage. All mice were in a 12-h day/night cycle and fed a standard chow diet (SDS RN3). Upon arrival and before the start of the experiment, mice were allowed to acclimatize in the new environment for 1 week. GF mice on C57BL/6J background were obtained from the GF clean animal facility of the University of Bern (in collaboration with A.M.) and transplanted with donor microbiota immediately upon arrival. At the start of the experiments, the male mice were at 8 weeks, and females were at 16 weeks of age. Animals were equally allocated into groups based on their body weight to ensure equal starting points, and otherwise randomly. Warmth exposure was done at 34°C in a light and humidity-controlled climatic chamber (TSE, Germany) in SPF conditions using individually ventilated cages. The 34°C-like pair-fed animals were kept at room temperature (RT) and fed an equal amount to the warm exposed animals. This was equivalent to ~25% less than RT ad libitum fed, and the food was provided each day at 6pm. No signs of stress or suffering we detected in any of the mice. All animal experiments were approved by the Swiss federal and Geneva cantonal authorities for animal experimentation (Office Vétérinaire Fédéral and Commission Cantonale pour les Expériences sur les animaux de Genève).

Primary Cell Culture

Three male C57Bl/6J mice of 3 weeks old were sacrificed and their tibias, femurs and humeri were collected. After epiphyses excisions, the bone marrow was flushed, collected in αMEM 10% FBS and pooled from each bone for osteoclasts differentiation. The rest of the bone was kept for the osteoclast isolation. For the osteoclasts, after filtration through a 70 μm filter, the cells were plated in T75 in αMEM 10% FBS + 10ng/ml MCFS. After incubation for 24h at 37°C and 5% CO2, the supernatant was collected and the cells were seeded as 200 000 cells/ml in αMEM + 10% FBS + 30ng/ml MCFS. After 48h, the differentiation was initiated by adding 100ng/ml RANKL to the medium as well as spermine or spermidine at the indicated concentration (0-0.1-1-10 μM). After 14 days, RNA was extracted and cells were fixed for 1h at RT in 3.7% formaldehyde for TRAP staining. Alternatively, cells were kept in differentiating medium for 14 days and spermine and spermidine were added for 24h before RNA extraction and TRAP staining. For the osteoblasts, the bones were cut in small pieces and incubated in αMEM 10% FBS + 1mg/ml Collagenase II for 90°C at 37°C with shaking. The cells were rinsed and then incubated in αMEM10%FBS medium at 37°C with 5%CO2, and split a couple of times for proliferation before seeding them to 70 000cells/ml in differentiating medium (αMEM 10%FBS + 50μg/ml ascorbic acid + 10mM β-glycerophospate) supplemented with spermine or spermidine (at 0; 0.1; 1 and 10 μM). After 7 days of treatment, cells were harvested for RNA extraction and ALP measurements, and after 25 days of treatment for Sirius red or Alizarin red measures. The following chemical compounds were used: aMEM medium (bioconcept ref 1-23P10-M supplemented with 25mM NaHCO3, 100X Penicillin Streptomycin (Gibco Ref: 15140), 100x glutamine (Gibco Ref: 25030) and 3.75 ml amino-acids mix (BioConcept ref: 5-12K01-H)), recombinant murine M-CFS (peprotech ref 31502), recombinant murine sRANK Ligand (Peprotech ref 315-11C), Spermine (Sigma ref S4264), Spermidine (Sigma Ref: S0266).

METHOD DETAILS

Ovariectomy

Mice were anesthetized with Xylazine/Ketamine (mixture of 100 mg/kg ketamine and 16 mg/kg xylazine) and shaved below the ribs on the back side. Betadine was applied on the area for appropriate disinfection. After a 1-2 cm incision through the skin and the muscle layer just below the ribs, the ovary was localized, the fallopian tube ligated with dissolving suture and the ovary removed. The muscle layer was sutured with dissolving suture, the wound closed with staples and disinfected. The same procedure was performed on the other side. A dose of Tamgesic was administered 4 hours after the surgery, and the staples were removed 7 days after the surgery under isoflurane anesthesia. The sham-operated animals underwent the same procedure, without ligating the fallopian tube and the ovary excision.

CellPress

Cell Metabolism
Article

Sample Collection at Sacrifice

To measure the dynamic indices of bone formation, mice received subcutaneous injections of calcein in saline solution at 9 and 2 days before euthanasia. 500 μl of blood was taken from terminally anesthetized mice in tubes with 10 μl of 0.5 mM EDTA, 4 μl of aprotinin (1.3%) and 4 μl of DPP-IV (10mM) and plasma stored at -80°C. Samples for RNA isolation were stored in RNAlater solution (Invitrogen ref AM7020). Bone samples for the CT-scan analysis were stored in a humid package at -20°C, and the samples for histology in 3.8% formaldehyde. All other samples snap frozen in liquid nitrogen. The tail length was measured with a ruler from the tip of the tail to the border between the fur and the skin.

Microbiota Transplantation

Upon arrival, 8 weeks old male GF mice were handled in aseptic conditions and immediately colonized by gavaging them with cecal content of the appropriate donor. The donors were male C57Bl/6J mice that were exposed to 34°C, or kept at RT for 4 weeks starting at 8 weeks of age. 500 μl of freshly collected cecal contents from donors were pooled and suspended in 5 ml of anaerobic PBS, to make a gavage mixture for each group of colonized mice. Each mouse was orally gavaged with 100 ul of the solution upon arrival and 2 days later. Animals were kept for 7 days in dirty cages from the respective donors and then switched to sterilized cages.

For microbiota transplantation of the ovariectomized mice, we used female C67Bl/6J recipients with conventional microbiota already present, and the ovariectomy was done at 16 weeks of age. The donors for these experiments were female mice that were exposed to 34°C for 4 weeks starting at 16 weeks of age. Fresh fecal pellets from the donors were freshly collected every 2 days and immediately homogenized in 1 ml of anaerobic PBS. After a short centrifugation (300g, 30sec), the supernatant was then immediately gavaged to the respective recipient. In this condition, one cage of donors (1 pellet per mouse from both mice) was used to repopulate 1 cage of recipients. Each recipient received 200 μl of the donor mixture every 2 days during 4 weeks.

Antibiotic Treatment

16-weeks-old female mice were treated with fresh antibiotics and kept at either room temperature or 34°C for 7 weeks (RT-Abx and 34°C-Abx respectively). Antibiotics cocktail was composed of 100 μg/ml neomycin, 50 μg/ml streptomycin, 100 U/ml penicillin, 50 μg/ml vancomycin, 100 μg/ml metronidazole, 100 μg/ml CEFAZ, 125 μg/ml Ciprofloxine hydrocholoride, 1 mg/ml bacitracin provided in the drinking water changed twice per week (Chevalier et al., 2015; Suárez-Zamorano et al., 2015)

Polyamines Supplementation and Inhibitor Treatment

6-weeks old C57BL/6J female mice were given a mixture of Spermine (Sigma-Aldrich) and Spermidine (Sigma-Aldrich) freshly dissolved in drinking water at concentration of 0,5mM from each compound every second day during additional 45 days at room temperature. Diaminazene Acetureate (Sigma-Aldrich) was supplemented in drinking water at a concentration of 50μM every second day during 45 days to the 16-weeks old C57BL/6J female mice that are kept at 34°C with temperature-controlled chamber in conventional facility. Food and water were given to the mice in ad libitum.

Micro-CT Analysis

The limbs were scanned in vivo before the ovariectomy to determine the basal state using a micro-CT (VivaCT40/ Scanco system; Zurich, Switzerland). After Xylazine/Ketamine anaesthesia, limb were scanned for 18 min. Final scans were performed post mortem on isolated bones. Subsequent analysis was done using micro-CT software. For the femoral and tibial trabecular region, we analyzed one hundred slices starting from 50 slices below the distal growth plate. Femoral and tibial cortical structure was assessed through 60 continuous CT slides (600 μm) from the bone midshaft. Images were segmented using an adaptative-iterative threshold approach, rather than a fixed threshold. Morphometric variables were computed from binarized images using direct 3D technique that does not rely on prior assumptions about the underlying structure (5). For trabecular bone regions, we assessed the bone volume/total volume (BV/TV). For cortical bone at the femoral and tibial midshaft, we measured the cortical bone volume (mm3) and the average cortical thickness named cortical width (μm). The lengths of the femurs were also measured from the CT-scans.

Biomechanical Analysis of the Bone

For the 3-points bending test to address the biomechanical parameters, tibias were placed on two supports separated by a distance of 9.9 mm and load was applied to the midpoint of the shaft (creating a 3-points bending). Mechanical resistance to failure (displacement and load applied) was measured using a servo-controlled electromechanical system (Instron 1114, Instron, High Wycombe, UK) with actuator displaced at 2 mm/minute. Ultimate force (maximal load, measured in Newtons [N]), Yield point (N), stiffness (elastic energy, N/mm), and energy to fracture (surface under the curve of the plastic region, N*mm) were calculated. Young's modulus (MPa) was determined by the previously described equation (Mcmillan et al., 1989).

Human Metadata Analysis

We correlated the age-standardized incidence of hip fracture (per 100'000 inhabitants) per country using the data obtained from Cauley et al. (2014) with the country's average day temperature (1961–1990, Climate Change Data, World Bank Group), or the distance from the equator (latitude) of their capitals. We accounted for the effect of calcium intake and Vitamin D serum levels (Wahl et al., 2012; Balk et al., 2017) using partial-correlation analysis. This dataset contains age-standardized incidence of hip fracture and latitude for 62 countries, temperature for 60 countries, vitamin D serum level for 38 countries and the calcium levels for 49 countries. The

Cell Metabolism
Article

regression was performed using statsmodels (Skipper and Perktold, 2010). All code is available as specified in the Key Resources Table.

16S Gut Microbiota Profiling

At the end of the experiment fecal samples were collected in sterile tubes and immediately frozen and kept at -80°C. Cecal samples were collected after sacrifice of the mice, snap frozen and conserved at -80°C. Fecal and cecal bacterial DNA was extracted using the PowerFecal DNA Kit (Qiagen, Ref. 12830-50) and the 16SrDNA library was built following the standardized protocol from the earth microbiome project (Caporaso et al., 2011, 2012). DNA was amplified with QuantaBio 5Prime HotMasterMix using barcoded universal bacterial primers targeting variable region V4 of 16SrRNA gene (515F-806R barcoded primers, Illumina): 806 Reverse Primer GGACTACNVGGGTWTCTAAT - 515 Forward Primer GTGYCAGCMGCCGCGGTAA. 2 ng of template was used and the PCR conditions included an initial denaturation at 94°C for 3', followed by 35 cycles of denaturation at 94°C for 45", annealing at 50°C for 1', and extension at 72°C for 90", with a final extension at 72°C for 10'. Each PCR was done in triplicates and later combined and quality checked on an agarose gel. Each PCR amplification was then quantified with Quant-iT PicoGreen dsDNA Assay with SpectraMax Gemini XPS microplate reader and pooled to an equal amount of 200 ng per sample to form the library. The library was purified using QIAquick PCR purification Kit (Qiagen, Ref. 28104), and sequenced from both ends on Illumina MiSeq (kit v2) to generate 2x250bp paired-end reads (Illumina, San Diego, CA, USA). Eighteen picometers of the library were mixed with PhiX DNA (10%) and were loaded on a MiSeq Reagent kit V2 (500 cycles) together with customized sequencing primers; read1, 5'-TATGGTAATTGTGTGC CAGCMGCCGCGGTAA-3′, read2, 5'-AGTCAGTCAGCCGGACTACHVGGGTWTCTAAT-3′ and index read, 5′-ATTAGAWACC CBDGTAGTCCGGCTGACTGACT-3′. 250 bp paired-end sequencing was performed on the MiSeq platform (Illumina, USA) in the iGE3, Institute of Genetics and Genomics in Geneva, CMU, University of Geneva. Sequencing results were obtained and de-multiplexed using standard method supplied by the MiSeq, Illumina.

Reads were processed using a pipeline based on dada2 v 1.8.0 (Callahan et al., 2016) (code accessible here : https://github.com/SilasK/16S-dada2). In short, the reads were quality filtered with the parameters (truncLen="180,100", and maxEE=2), dereplicated, merged, and chimeras removed. sequences with length outside of 253+-7 were removed. The resulting operational taxonomic units were given numbers and were annotated with the SILVA database v132 (Quast et al., 2013). Richness and Shannon diversity were calculated after rarefaction. Compositional data analysis was performed on OTUs with at least 1 count on average using aldex2 (Fernandes et al., 2013) for the OTU, genus and family level. The reported p values are calculated using the welch test within aldex2 and were corrected for multiple testing with the Benjamini-Hochberg procedure. Principal component analysis was performed on the centered $\log_2$ ratios after multiplicative replacement of the zero values (Martín-Fernández et al., 2003).

Metagenomics Sequencing

Paired-end metagenomic libraries were prepared from 100 ngDNA using TruSeq Nano DNA Library Prep Kit (Illumina) and size selected at about 350 bp. The pooled indexed library was sequenced in a HiSeq4000 instrument at the iGE3 facility (University of Geneva).Metagenomics reads were processed using atlas v2 (Kieser et al., 2020). In short, using tools from the BBmap suite v37.78 (Bushnell, 2020), reads were quality trimmed, and contaminations from the mouse genome were filtered out. Reads were error corrected and merged before assembly with metaSpades v.1.13 (Nurk et al. 2017). Contigs were binned using metabat2 (Kang et al., 2019) and maxbin2 (Wu et al., 2016) and their predictions were combined using DAS Tool (Sieber et al., 2018). The predicted metagenome assembled genomes (MAGs), which had at least 50% completeness and < 10% contamination based on the estimation by checkM (Ferris et al., 2018; Kasper et al., 2018; Parks et al., 2015) were clustered (95% average nucleotide identity) resulting in 147 representative genomes (referred later as genomes). The genes of each genome were predicted using prodigal (Hyatt et al., 2010) and clustered using linclust (Steinegger and Söding, 2018) to a non-redundant gene catalog. The 2.3M genes were annotated using KofamScan (Aramaki et al., 2020) and InterProScan 5 (Madeira et al., 2019). Using pygenomeprop (https://github.com/Micromeda/pygenprop) the presence of genomes were annotated to contain complete or partial MetaCyc Pathways (Caspi et al., 2016). The genomes were quantified by the median of coverage in 1kb windows along the genome. MetaCyc pathways and Kegg orthologs (KO) were quantified as the sum of the relative abundance of the genomes containing them. Welch test was used for testing significant differences in pathway abundances between the groups.

RNA Extraction, Reverse Transcription and Real-time qPCR

Upon collection, tissues were stored in 1ml RNAlater and immediately processed for RNA extraction for the bone tissues or stored at -80°C. For RNA extraction, tissues were placed in 2 ml Eppendorf tubes containing 1 ml Trizol (Thermo Fisher Scientific) and mechanically disaggregated using the bead-based TissueLyser equipment (Qiagen) by shaking for 40 seconds at 30 Hz in presence of a silicate bead for the bone and a metal bead for the other tissues. After brief centrifugation to remove tissue debris (3 minutes at 12000g at 4°C), 200 µl chloroform was added, samples were shaken and centrifuged for 15 minutes at 12000g at 4°C. The chloroform phase was collected, mixed with 500 µl isopropanol and centrifuged again as before. The pellet obtained was washed twice with 70% ethanol and ultimately resuspended in 50 µl PCR-grade water. RNA from cell culture was extracted using 1ml of Trizol using the standard protocol. For retro-transcription we used High-Capacity cDNA Reverse Transcription Kit (Applied Biosystems) with 1 µg RNA per sample. qPCR were done on a LightCycler 480 machine (Roche) with SYBR Green-based detection (Applied Biosystem, Power-up). The primer sequences are shown in the Supplementary Data, as Table S1.

CellPress

Cell Metabolism
Article

Results were calculated using standard curve method and normalized to the TATA box binding protein (TBP) housekeeping gene, and shown as fold change relative to the control group.

RNA Sequencing

Next Gen Sequencing of mRNA transcripts was done on Ilumina MiSeq 2500 platform at the sequencing facility of the Institute of Genetics and Genomics of Geneva (iGE3), University of Geneva. RNA was isolated from entire tibias. For the experiment comparing the ovariectomized mice transplanted with warm- or RT-microbiota (Ova. Transp. RT and Ova transp. 34°C), each group contained 4 samples where each sample correspond to one mice. For the experiment comparing Ovarectomized and sham operated mice exposed to 34°C or RT (OvaRT, Ova 34°C, shamRT and sham34°C), each group was a sample pooled from 5 mice. Libraries for the sequencing were prepared with poly-A selection according to Ilumina TrueSeq protocol. The reads were mapped with the TopHat v.2 software to the UCSC mm10 reference on new junctions and known junctions' annotations. Biological quality control and summarization were done with RSeQC-2.3.3 and PicardTools1.92.

The differential expression analysis was performed with the statistical analysis R/Bioconductor package EdgeR v.3.4.2 for the genes annotated in mm10. Briefly, the counts were normalized according to the library size and filtered. The genes above 1 count per million reads (cpm) (in experiment with replicate, in at least 3 samples) were kept for the further analysis. After normalization of the counts, transcript abundances were compared in pairwise condition in a modified Fischer exact test (as implemented in edgeR). p values of the differentially expressed genes were corrected for multiple testing error with a 5% FDR (false discovery rate), using the Benjamini-Hochberg (BH) correction. Genes were called differentially expressed between any given two conditions when their false-discovery rate was <0.05 and their fold-change >2. Transcripts with log(cpm)>0 and $p \leq 0.05$ were subsequently subjected to pathway analysis using Reactome pathways database (Fabregat et al., 2017), reporting the enrichment ratio (# DEGs/Total Genes in dataset) and FDR-adjusted pvalue computed by Fisher exact test.

Cecal and Fecal Concentration of Polyamines

Feces and cecum content samples were pre-weighed directly in the lysis tubes (soft tissue homogenizing CK 14 tubes, Bertin Technologies, Rockville, MD, US) and extracted (using ceramic beads) by adding ice-cold MeOH:H_2O (4:1; v:v) spiked with internal standards in the Cryolys Precellys 24 sample Homogenizer (2 x 20 seconds at 10000 rpm, Bertin Technologies, Rockville, MD, US). Homogenized tissue extracts were centrifuged for 15 minutes at 21000 g at 4°C and the resulting supernatant was transferred to LC-MS vials for the injection into the LC-MS system. For feces, the sample amount normalization was based on weight whereas the cecum content was extracted entirely (whole cecum per specimen). Thirteen-point calibration curves were generated by the addition of IS mixture (25 μL) to each calibrator (i.e. standard mixture) (75 μL), vortexed and transferred to LC-MS vials for the injection.

Extracted samples were analyzed by Hydrophilic Interaction Liquid Chromatography coupled to tandem mass spectrometry (HILIC - MS/MS) in positive mode using a 6495 triple quadrupole system (QqQ) interfaced with 1290 UHPLC system (Agilent Technologies). The chromatographic separation was carried out in an Acquity BEH Amide, 1.7 μm, 100 mm × 2.1 mm I.D. column (Waters, Massachusetts, US). Mobile phase was composed of A = 50 mM ammonium formate and 0.1 % FA in water and B = 50 mM ammonium formate, 0.1 % formic acid in ACN/H2O (8:2; v:v). The linear gradient elution from 100% B (0-1.5 min) down to 60% B was applied (1.5 min - 12 min) and these conditions were held for 4 min, followed by the initial chromatographic conditioning during the 5 min post-run for column re-equilibration. The flow rate was 400 μL/min, column temperature 40°C and sample injection volume 2μl. ESI source conditions were set as follows: dry gas temperature 230°C, nebulizer 35 psi and flow 14 L/min, sheath gas temperature 400°C and flow 12 L/min, nozzle voltage 500 V, and capillary voltage 4000 V. Dynamic Multiple Reaction Monitoring (dMRM) was used as acquisition mode with a total cycle time of 500 ms. Optimized collision energies for each metabolite were applied.

Raw LC-MS/MS data was processed using the Agilent Quantitative analysis software (version B.07.00, MassHunter Agilent technologies). For absolute quantification, calibration curves and the stable isotope-labeled internal standards (IS) were used to determine the response factor. Linearity of the standard curves was evaluated for each metabolite using a thirteen-point range; in addition, peak area integration was manually curated and corrected where necessary.

Elisa

1,25-dihydroxycholecalciferol was measured with Abbexa Calcitriol (INN) Elisa kit (ref: abx 513030) in 1:10 diluted plasma samples. Osteocalcin was measured with Immutopics (quidel) Elisa KIT ref 60-1305 in 1:11 diluted plasma samples. CTX-I was measured with RatLaps CTX-I EIA Immunodiagnostic Systems (ref: AC-06F1) from undiluted plasma samples. All measures were done according to manufacturers' instructions.

Bone Mineral Content

Tibias were dried in oven for 3 days at 60°C. The dry weight of each bone was recorded (w_i) and the tibias were burned and reduced to ashes with a furnace set at 800°C for 1h. The weight of the remaining ashes was measured (w_f), and the ratio between the weight of the bone ash and the dry weight (w_f/w_i) was calculated to determine the bone mineral content (Tsai et al., 2017)

TRAP Staining

Cells were fixed with 3.7% Formol (formaldehyde) for 1h at RT and rinsed with water. The staining solution was freshly prepared by mixing equal amount of Fast violet B salt (ChemCruz ref sc-215029B) solution in acetate buffer (7mg/ml), and Naphtol AS-TR phos-

Cell Metabolism
Article

phate disodium salt (Sigma ref: N6125) solution in acetate buffer (2mg/ml, 225mM sodium acetate, 75mM acetic acid and 4mM NaOH). Cells were incubated overnight at 4°C with the staining solution, rinsed with water, incubated 30 min at RT in Sodium Fluorine (4.2g/L H2O). and rinsed with water once again before being processed for imaging and analysis. Images were acquired with ZeissAxio Observer ZI and ImagexpressXL (Molecular devices). The total cells per well were quantified with Metaexpress (5.1.41) software, and the number of differentiated osteoclasts manually (defined as multinucleated and $TRAP^+$ cells).

Alkaline Phosphatase (ALP) Activity Measurement

Cells were rinsed with cold PBS and scraped in 500µl H2O. After short sonication (2x15sec-10kHtz), samples were centrifuged at 10 000rpm for 15min at 4°C. 100µl of the supernatant was collected and incubated for 10min at 37°C, while the rest of the supernatant was kept for measuring the protein concentration. The reactive solution was as the following: 10mM p-nitrophenylphosphate, 560mM 2-amino-2-methyl-1-propanol, 1mM MgCl2, pH 10.5. 900µl of the reactive solution was added to the pre-heated 100ul sample and time monitored until sample turned yellow (approx. 7min). The reaction was stopped with 200ul of 1M NaOH and the time recorded. Absorbance of the sample was measured at 405nm, and the concentration of the remaining protein was measured using Pierce BCA Protein assay kit (Thermo scientific ref 23225). The ALP activity was obtained with the following formula: ALP activity (nmol PO4/mg of prot/sec) = [(OD x 1000)/ time(sec)]/protein (mg/ml).

Bone Histomorphometric Analysis

After 24 hours of fixation in 3.8% Formol, bones were dehydrated in absolute ethanol for 3 days followed by overnight incubation in acetone at -20°C before being embedded in methyl-methacrylate (Merck). 8µm thick transversal sections of the midshaft, and sagittal section of the proximal femur were cut with Leica RM 22 65 microtome (Leica Corp Microsystems AG) and mounted unstained for the evaluation of fluorescence from the calcein deposition. Histomorphometric measurements were performed on the secondary spongiosa of the proximal tibia metaphysis and on the endocortical and periosteal bone surfaces in the middle of the tibia using Leica Q image analyzer (Leica) at 40x magnification, and Bioquant osteo software. All parameters were calculated and expressed according to standard formulas and nomenclatures (Parfitt, 1988): mineral apposition rate (micrometers per day), mineralizing surface per bone surface (percentage) and bone formation rate (cubic micrometers per square micrometer per day). Osteoclast surface per bone surface and numbers were evaluated after TRAP staining performed following the same protocol as for the cell culture staining on free floating slides and followed by a Methylene blue counterstaining and mounted with Permount (fisher chemical ref: SP15-100). Sirius red staining was performed with Sirius red dye reagent (Direct red 80 Sigma #P744, in saturated aqueous picric acid (1.3% in H2O) at concentration of 0.1% w/v).

QUANTIFICATION AND STATISTICAL ANALYSIS

Data Representation and Statistical Analysis

Plots include each datapoint, mean and ± Standard deviation (SD). All p values, n (number of animals) and each applied statistical test is specified in the figure legends. To compare two different groups we applied Mann-Whitney t test. To compare more than two groups we applied One-Way ANOVA with Tukey's multiple comparison test. All experiments were reproduced at least twice, and shown are the representative data. *In vivo* measurements were done without blinding, while the histomorphometric and biomechanical measurements were done with blinding. No data were excluded from the analysis. Where available, group sizes were calculated based on power calculations of 0.8. Results were considered significant when $p < 0.05$ in the respected statistical test and represented significance as *p <0.05; **p <0.01; ***p <0.001.

We analyzed the data using Prizm Version 8.4.3., and assembled the figures in Adobe Illustrator. We generated the graphical abstract in Powerpoint, using some of the illustrations available at Servier Medical Art.

The comprehensive mouse gut metagenome catalog

4.1 Subspecies, Viruses & Plasmids from the mouse gut metagenome

Title: Comprehensive mouse gut metagenome catalog reveals major difference to the human counterpart

Authors: Silas Kieser, Evgeny M Zdobnov & Mirko Trajkovski

Status: Submited. Here we show the original version of this articles, a revised version is available as pre-print from *bioRxiv*, 2021

Mouse is the most used model for studying the impact of microbiota on its host, but the repertoire of species from the mouse gut microbiome remains largely unknown. We took on the challenge to create a comprehensive catalog of genomes from the mouse gut. We predicted bacterial and viral genomes from over a thousand public mouse metagenomes as well as our own. We also included reference genomes isolated from the mouse microbiome. We compared the resulting catalog of metagenome-assembled genomes and reference genomes to the Unified catalog of genomes from the human gut and uncovered major differences in the species composition. Our catalog increases our knowledge of the mouse microbiota gene repertoire by ten-fold and allows comprehensive analysis of the mouse gut microbiome at an unprecedented depth.

Contribution statement

I wrote the code, analysed, and interpreted the data, and generated the figures. E.Z. and M.T. guided the project and supervised the work. All authors conceptualized the study and wrote the paper.

Comprehensive mouse gut metagenome catalogue reveals major difference to the human counterpart

Silas Kieser[1,2,3], Evgeny M. Zdobnov[3,4,5,*] and Mirko Trajkovski[1,2,5,*]

[1]Department of Cell Physiology and Metabolism, Faculty of Medicine, Centre Medical Universitaire, Geneva, Switzerland.

[2]Diabetes Center, Faculty of Medicine, Centre Medical Universitaire, Geneva, Switzerland.

[3]Swiss Institute of Bioinformatics, Geneva, Switzerland.

[4]Department of Genetic Medicine and Development, University of Geneva, Geneva, Switzerland.

[5]Institute of Genetics and Genomics in Geneva (iGE3), University of Geneva, Geneva, Switzerland.

*e-mail: Evgeny.Zdobnov@unige.ch , Mirko.Trajkovski@unige.ch

Keywords: Mouse, Human, Microbiome, Metagenome, Genome, Gut, Gene catalogue, Species, Sub-species, Plasmids, Viruses

Abstract

Mouse is the most used model for studying the impact of microbiota on its host, but the repertoire of species and subspecies from the mouse gut microbiome remains largely unknown. Here, we constructed a Comprehensive Mouse Gut Metagenome (CMGM) catalogue by assembling all currently available mouse gut metagenomes. We recovered 33'109 metagenome-assembled genomes (MAGs) from bacteria, 3470 plasmids, and over 120'000 viral contigs, together encoding 78 million proteins. We integrated all MAGs into 1449 species, of which 71.7% are newly identified, and 4007 subspecies. Rarefaction analysis indicates a comprehensive sampling of species and subspecies. 300 species represent newly identified genera, and we discovered 8 new families. CMGM enables an unprecedented coverage of mouse faecal and cecum metagenomes reaching 94%. Comparing CMGM to the human gut microbiota shows an overlap of only 18% at species, and 11% at the gene level, demonstrating that human and mouse gut microbiota are largely distinct.

Introduction

Mouse is the most used model for studying the microbiota importance due to several factors: availability of samples from different parts of the gastrointestinal tract, treatment options, controlled housing environment and diet, defined genetic background, and ethical considerations. However, the mouse gut microbiota has been poorly characterized, and only a fraction of the diversity observed by 16S rDNA sequencing is represented by genomes in public databases[1]. The majority of the studies on the mouse microbiome are performed by sequencing variable regions of the 16S, sometimes mislabelled as metagenomics. While this technique has allowed a general overview into the microbiota and information down to the genus level, it is not suited for identifying species for most of the organisms[2]. Different species from the same genus and even subspecies from the same species can exert contrasting functions[3], stressing the importance of annotating the gene content at a low taxonomic level.

Shotgun metagenomics allows studying the full microbiota diversity of an environment, including uncultured microorganisms, viruses, and plasmids. However, its interpretation is limited by the availability of reference genomes. Previous efforts led to the creation of a gene catalogue of the mouse metagenome (MGC v1)[4], by sequencing faecal samples from mice with different genotypes and housed in different conditions. This catalogue enables the functional annotation of genes and allows a 50% mapping rate of faecal sequences. However, the mapping rate of sequences from cecum samples is only 37%, and the catalogue does not contain genomic references. Recently developed algorithms enable assembly of genomes from metagenomes, leading to a recovery of new species from the human gut and other environments[5–9]. The integrated mouse gut metagenomic catalogue (iMGMC)[10] increased the fraction of reads mapped to genes compared to the MGC v1, however, mapping to the recovered metagenome-assembled genomes (MAGs) remains at about 40%[10]. Accordingly, many mouse genomes remain unclassified with the current state-of-the-art, and none of the approaches so far provide information of the microbiota on a subspecies level.

Here we report a Comprehensive Mouse Gut Metagenome (CMGM) collection that contains genomes generated by assembling gut microbiomes sequenced by us and all publicly available mouse metagenomes. This resource improves the mapping rate of genomic reads from mouse faecal and cecum metagenomes to over 94% and provides full classification on the level of subspecies, viruses, and plasmids. This nearly complete catalogue of the mouse gut bacterial species allows comparison between the newly assembled mouse gut microbiomes and the human counterpart, highlighting major differences between human and mouse in both species' composition and their abundance.

Results

Assembly of high-quality genomes from mouse gut metagenomes

We selected all metagenomic datasets associated with the mouse intestinal tract that are sequenced with a paired-end layout from the NCBI sequence read archive (accessed December 2019). To these, we added samples generated by our lab resulting in 1464 datasets (Extended Data Table 1). Each sample was processed using metagenome-atlas[11], which handles pre-processing, assembly, and binning of the metagenome datasets. The resulting MAGs were filtered based on fragmentation (N50>5000) and a quality score calculated from the output of checkM[12] as 'completeness minus 5 times contamination'. Bins with a quality score of <50 were excluded, resulting in 33'109 MAGs from which 11'373 (34%) had high quality (Quality score >90, Fig. 1b, Extended Data Fig. 1a). We included 776 complete mouse-associated bacterial genomes retrieved from RefSeq belonging to 331 species (Extended Data Table 2), which also includes genomes from mouse specific culture collections: Oligo-mouse-microbiota[13] (12 genomes), and Mouse Gut Microbial Biobank (mGMB, 41 genomes)[14]. As the genomes of the mouse Intestinal Bacterial Collection (miBC, 53 genomes)[1] were not available, we assembled them from the raw reads. Surprisingly, some reference genomes had contamination values of 100%, suggesting that the sequenced genomes consist of multiple strains. In total, 13 reference genomes did not pass the quality filtering,

and we included 816 reference genomes in the CMGM collection, resulting in a total of 33'925 genomes.

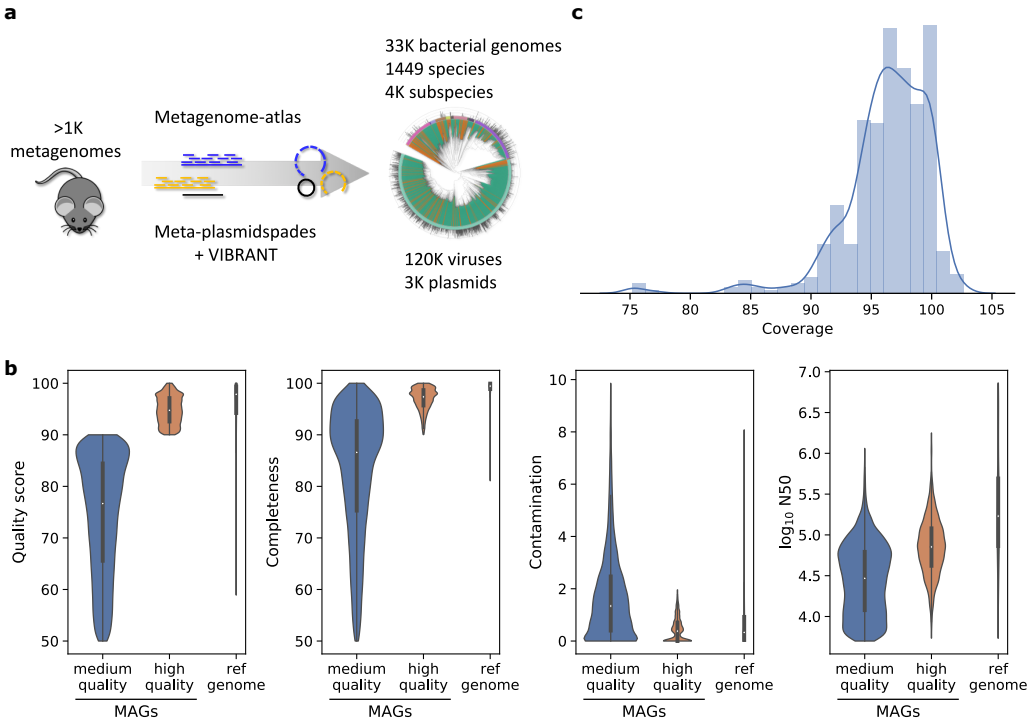

Fig. 1| Many metagenome-assembled genomes have comparable quality to reference genomes
a, Scheme of the workflow. **b,** Violin plots showing the quality score, completeness, contamination estimated using checkM and the $\log_{10}$ N50 from the assembly for the reference genomes and MAGs present in CMGM. **c,** Coverage of reference genomes by MAGs (n=494).

While MAGs were more fragmented and had a lower median quality score than the reference genomes, the quality score and N50 of the high-quality MAGs were comparable to the values for the references (Fig. 1b). For 60% of the reference genomes, we recovered MAGs that align to them with high coverage and identity (ANI >95%, IQR 94-99%, Fig. 1c). This validates our metagenome assembly approach to recover "reference quality" genomes *de novo*. Some of the remaining differences might be attributed to strain variation, as the coverage is higher for more similar genomes (Extended Data Fig. 1b).

Since we assembled genomes from individual samples, the same strain could have been recovered multiple times, especially if different gut locations of the same

mouse were sampled. To remove this potential redundancy, we clustered the genomes based on the average nucleotide identity (ANI) calculated using bindash[15]. 95% ANI was used as threshold to delineate genomes from the same species[16,17]. For each species cluster, the genome with the highest quality and

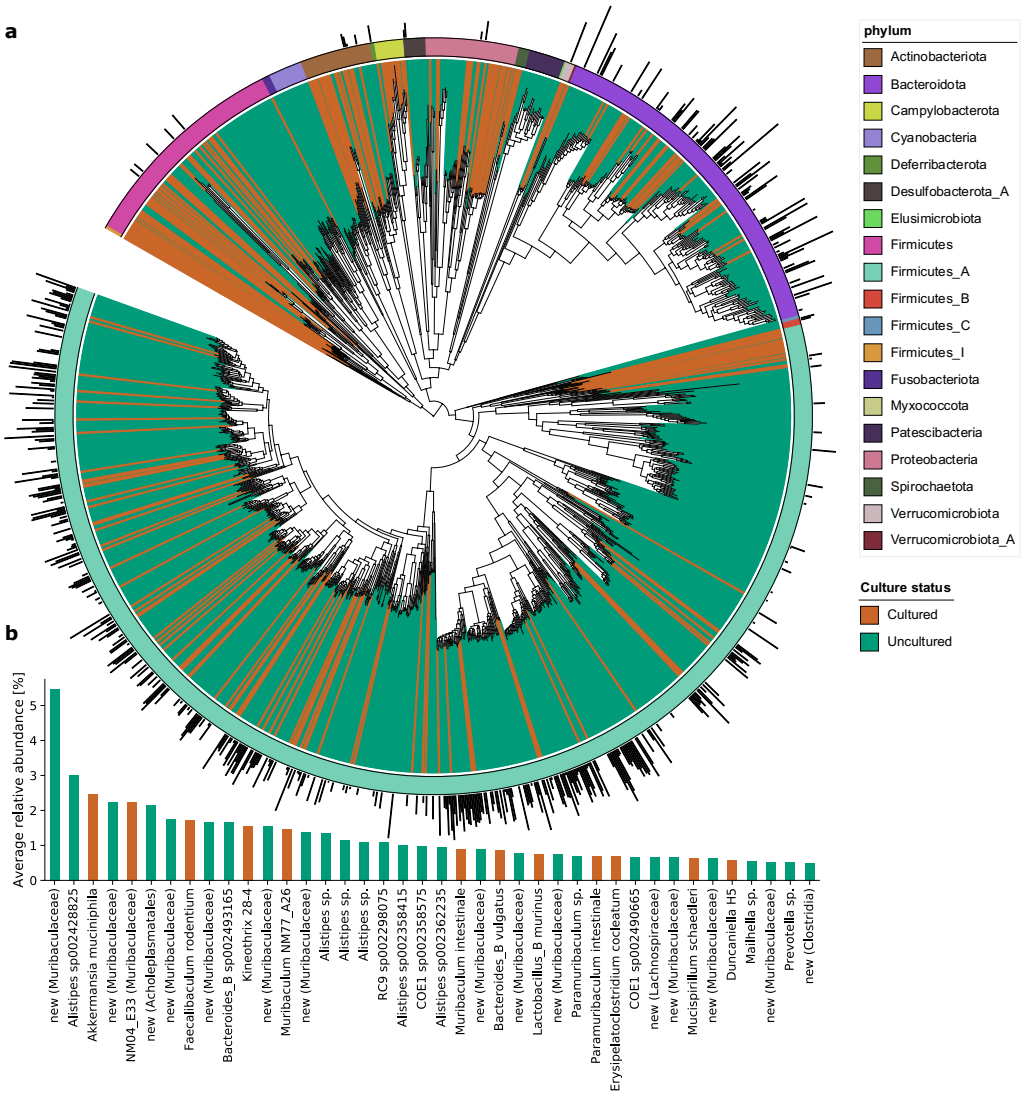

Fig. 2| The mouse gut microbiome is predominantly uncultured. **a,** Maximum-likelihood phylogenetic tree of the 1449 bacterial species detected in the mouse gut. Clades are colored by culture status. The color ring indicates the phylum attribution and the bar in the outer ring indicates the median abundance in mouse gut microbiome (centered log ratio). Values < 0 are omitted. **b**, Bar plot of the 40 most abundant species in the mouse gut microbiome colored by cultured status.

lowest fragmentation was selected as representative, but reference genomes were preferred over MAGs. The species representatives were annotated using the genomic taxonomy database (GTDB[18,19]). Species that contain a reference genome of an isolate were counted as cultured, even when they might not be available from official culture collections. Similarly, species named after an isolated strain in GTDB were annotated as cultured.

Majority of the species from the mouse gut are uncultured

The CMGM genome collection represents 1449 species (Fig. 2a), of which 71.7% have not been previously identified. 76.4% of the CMGM species are uncultured, with 17.5% having a mouse-specific cultured strain. 300 represent the first species for their genus, and we discovered 8 new families. 218 species do not have a cultured species at the order level. Since many of the most abundant species are uncultured (Fig. 2b), the sum of cultured species accounts on average for less than 20% of the mouse metagenome. 4607 genomes contain one or multiple full-length 16S gene sequences, which allowed us to link 51% of the 1449 species in the CMGM catalogue to a 16S sequence. This represents over 50% advance over the latest reports linking 484 genomes from the mouse gut to 16S sequences[10].

We used StrainDrep[20] to further split the 33'925 genomes into 4007 subspecies. We observed clear clusters, for which the genome with the highest quality was chosen as representative (Extended Data Fig. 2). Subspecies contain a specific subset of genes (Extended Data Fig. 2). In datasets with faeces and cecum samples of the same mouse, genomes from the same species belong also to the same subspecies/strain. This indicates that our approach consistently recovers dominant strains/subspecies.

To assemble viruses and plasmids from metagenomic and genomic datasets, we used a pipeline based on metaplasmid-spades[21] and VIBRANT[22]. The assembled plasmids and viral contigs were dereplicated into non-redundant catalogues. We recovered 120'983 viral contigs, 1128 of which are complete circular and 3106 are of high or medium quality as estimated by VIBRANT. 88% of the contigs were classified as lytic, 8.6% as lysogenic, and 3.7% are integrated prophages. The

Plasmid catalogue consists of 3470 circular plasmids including 48 plasmids which were recovered from the 53 assembled genomes of the miBC[1].

Evaluation of the CMGM catalogues

Rarefaction analysis shows that the number of species reached a saturation point at 1036 when considering species with at least two conspecific genomes (Fig. 3a). This indicates that the CMGM catalogue contains all species commonly living in the mouse gut. However, more rare species remain to be discovered, as the rarefaction curves with singletons (species which were recovered only in one sample) did not converge. Strikingly, rarefaction analysis reached a saturation

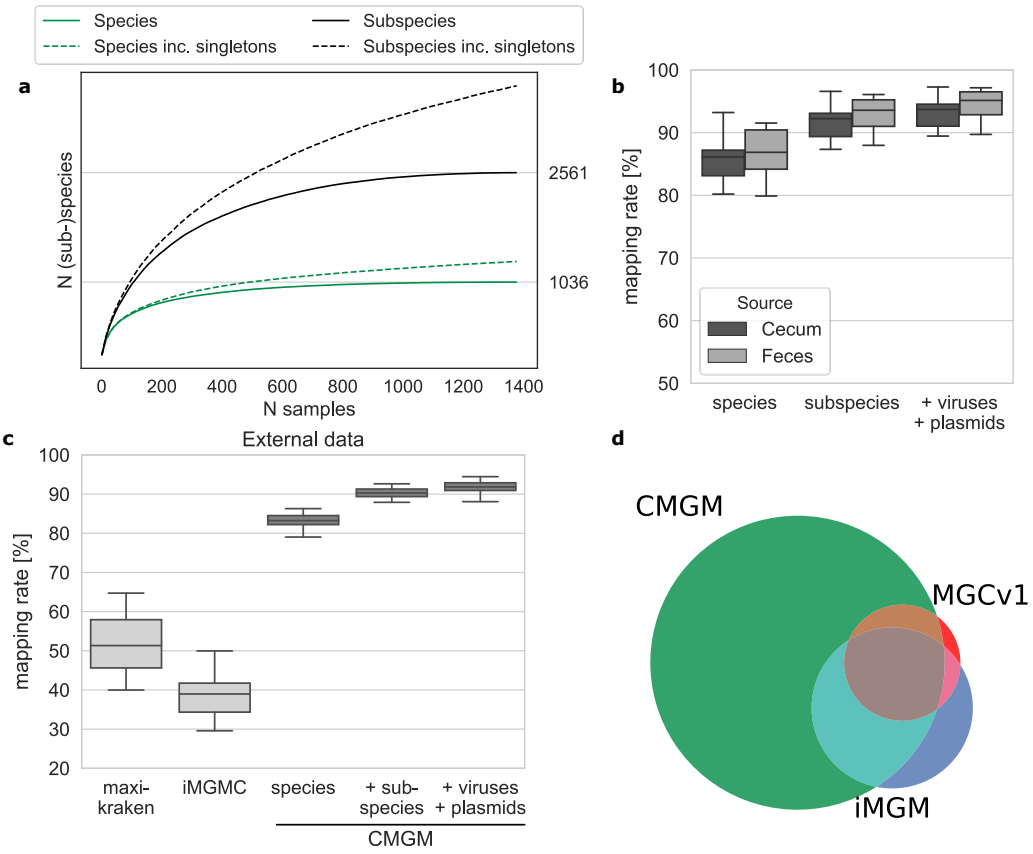

Fig. 3| CMGM catalog provides close-to-complete coverage of the mouse microbiome

a, Rarefaction curves of species and subspecies. **b,c**, Comparison of mapping rates on assembled genomes, plasmids and viruses of the mouse gut metagenome on internal (b) and external data (c). **d,** Overlap of different gene catalogs from the mouse metagenome.
CMGM: this study, iMGM: Lesker et al. 2020, MGCv1: Xiao et al 2015

point at 2561 subspecies (Fig. 3a), indicating that the CMGM catalogue also contains all subspecies commonly found in the mouse gut.

CMGM achieves a mapping rate of the mouse metagenome of 95.1% for faecal and 93.7% for cecum samples. Specifically, the mouse microbiome diversity captured by the CMGM species covers 86% of reads from both faecal and cecum samples (Fig. 3b). Microbiome profiling using the subspecies representatives increased the mapping rate by 6% compared to species alone. Viruses and plasmids added 1.5% of mapped reads (Fig. 3b).

To independently evaluate the mapping rate of the CMGM catalogue, we used an external dataset of cecum samples, which was explicitly left out from this catalogue, and not contained in previous ones. The CMGM species covered 83% of the metagenomic reads, twice as many compared to the previous genome collection from the mouse gut[9] (Fig. 3c). The addition of subspecies and extra-chromosomal elements increased the mapping rate by 7% and 1.5%, respectively. In total, 91.8% of reads from an external sample were mapped by CMGM, which is over 40% increase compared to the maxi-kraken database that contains all RefSeq genomes from bacteria, archaea, protist, fungi, and viruses.

We predicted over 260 million genes from the assembled contigs and clustered them to generate the CMGM protein catalogue. This non-redundant protein catalogue contains 78 million proteins, over 10 times more than the previous mouse gene collections[4,10] (Fig. 3d). 83.1% of our gene catalogue could be annotated, and 49.7% of genes are linked to 8077 Kegg annotations. To facilitate further comparisons, we produced the CMGM gene catalogue clustered at 90 and 50% amino acid identity.

To test the applicability of the CMGM, and propose how this catalogue allows discovering compelling biological insights, we compared mice from three different providers fed a high fat-fed diet (HFD) for 7-8 weeks to control mice on chow diet[4] (N=67). We used aldex2 with a linear model to account for the different mouse providers. Many *Becteroidota* species were significantly decreased and species from the phylum *Firmicutes* increased (Extended Data Fig. 3A). Interestingly, Shannon diversity did not decrease with HFD (Extended Data Fig.

3B). This example suggests that using the CMGM catalogue as reference for metagenomic studies enables discovering precise and comprehensive changes of species induced by a treatment or a disease. It also sets the ground for reanalysis of the existing datasets for uncovering species that are involved or altered by the condition of interest.

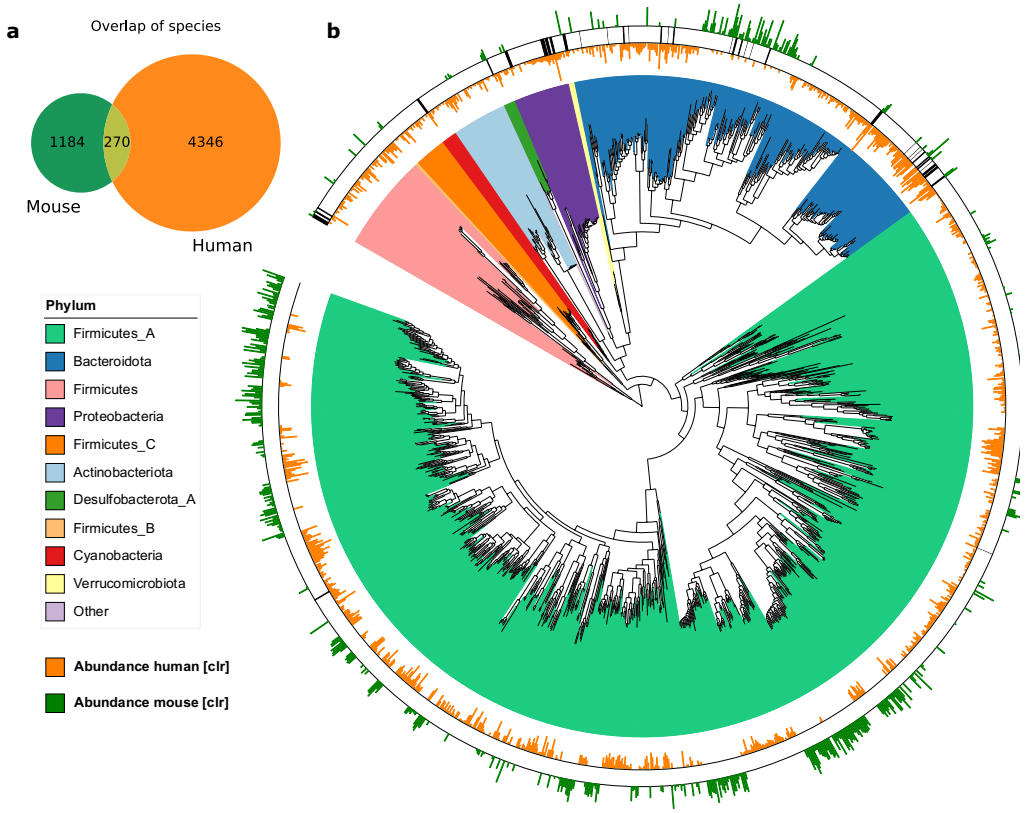

Fig. 4| Human and mouse guts harbor distinct bacterial species. **a,** Venn diagrams of the overlap between mouse and human gut microbiota at the species level. **b,** Phylogenetic tree of abundant species (centered log ratio, clr >0) in either human or mouse microbiome. Clades are colored by phylum attribution. The black bars in the middle ring indicate shared species between human and mouse (ANI > 95%). The bar plot in the inner ring indicates the median abundance in human microbiome (inverted axis), and the bar plot in the outermost ring the abundance in the mouse microbiome (values clr < 0 are omitted).

Comparison between human and mouse gut microbiomes

Studying mice microbiota and its impact on the host as a proxy for humans implies their similarities. However, 16S rDNA profiling and gene catalogues don't allow a

comprehensive analysis of the analogy between human and mouse microbiota down to species level. Also, much fewer species from the mouse gut are sequenced than from the human gut[23]. The CMGM catalogue, together with the recent creation of genome collections from the human gut[24], renders this comparison possible. Here, we compared the species representatives from CMGM to the ones from the unified human gut genomes[24] and applied the same criteria as for clustering (ANI > 95%). From the 1449 CMGM species, 18.29% (270) were identified in the human gut microbiota (Fig. 4a, Extended Data Fig. 5). The shared species account on average for 15.6% of the mouse and 29.6% of the human gut microbiome.

When low abundant species (centred log-ratio (CLR) <0) are left out from this comparison only 45 species were shared (Fig. 4b, Extended Data Fig. 4, Extended Data Table 3) that corresponds to an overlap of 10% of abundant species. Curiously, 27 of the 45 shared species belong to the phylum *Bacteroidota*, whereas only two of them are from the phylum *Firmicutes_A*. Only 12 species are abundant in both microbiomes (CLR >0), 10 of which belong to the phylum *Bacteroidota*. 10 out of the 12 most abundant species have cultured representatives. These data reveal major differences between human and mouse microbiota at the species level.

To investigate the functional repertoire of the human and mouse microbiome, we compared the CMGM protein catalogue to the unified human gut protein (UHGP)[24] at 90% amino acid identity. Similar as in MGCv1[4], only a fraction of genes could be annotated with Kegg orthologs (50% in CMGM and 13% in UHGP). Comparison based on this set of 8077 functional annotations indicates an overlap of 99% between the human and mouse microbiome. However, if all 78mio genes are taken into account, the overlap drops to 10.8%, corroborating the limited overlap of species between these two microbiomes.

We compared CMGM and UHGG[24] at higher taxonomic resolutions based on the GTDB taxonomy. In GTDB, if a taxonomic group is polyphyletic, it is split into several sister clades based on relative evolutionary divergence[18], which permits more robust comparisons and correlations. The new clades are usually named

with an alphabetical suffix, for example, the phylum Firmicutes is split into 12 sister phyla. More than half of the species in both microbiomes belong to the phyla Firmicutes_A. *Firmicutes_A* and *Bacteroidota* (*Bacteroidetes*) are the most abundant phyla in both human and mouse microbiomes (Fig. 5a). Overall, 17 phyla have representatives in both human and mouse microbiome. 5 phyla including *Synergistota* and *Eremiobacterota* are only found in human and not in mice microbiota. In contrast, the phylum *Deferribacterota* and the two species *Chlamydia muridarum* and *Chlamydophila psittaci* which represent an own phylum, are specific to mice. No archaea were reconstructed from the mouse gut metagenome, whereas 0.4 % of the genomes in the UHGG belong to this domain.

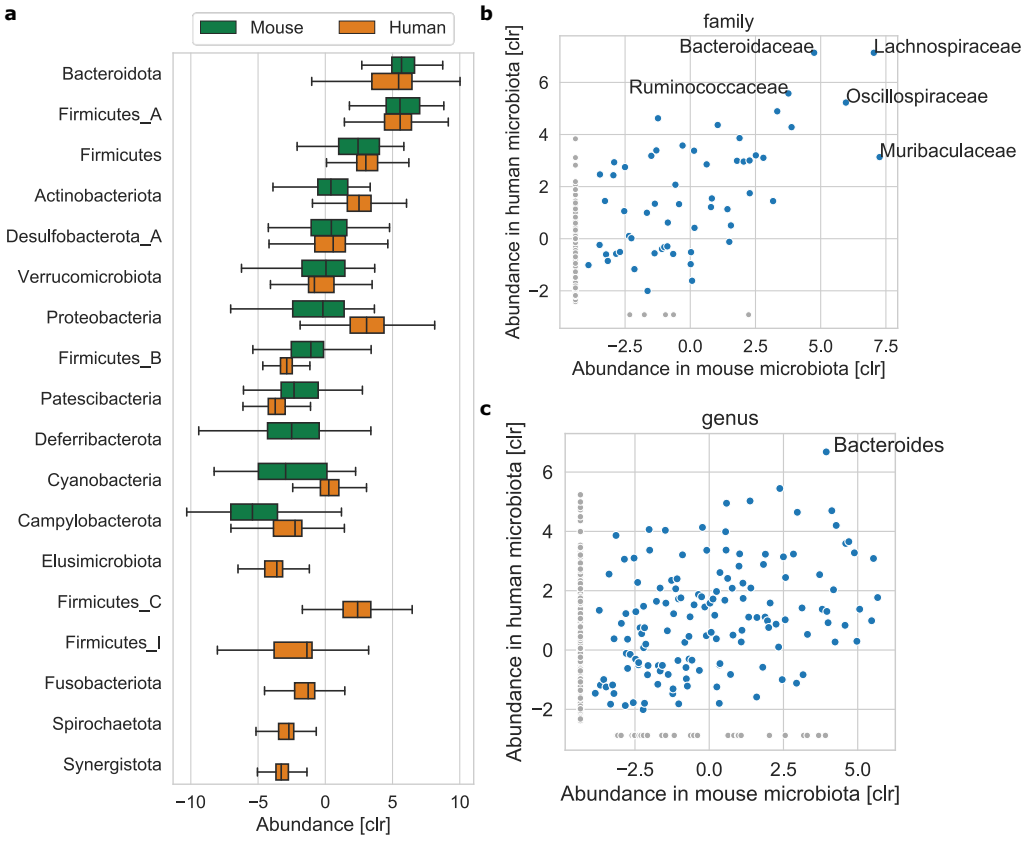

Fig. 5| Human and mouse microbiomes are similar at higher taxonomic level.
a, Phylum abundances in human and mice microbiota. **b,c,** Correlation of average abundance of families (b) and genera (c) in human and mice microbiotas. CLR = centred log ratio.

At the family level, humans and mice share 91 of the 105 defined taxa, whose

average abundance in human and mouse microbiota are correlated (r=0.63, Fig. 5b). The families *Lachnospiraceae*, *Oscillospiraceae*, and *Ruminococcaceae*, have high abundance in both human and mice. The family *Muribaculaceae* is 60 times more abundant in mice than in humans, whereas *Bacteroidaceae* is 10 times less. While at the genus level, 227 of 273 of taxa are shared (83% overlap), the abundance of the genera showed only a very limited correlation (r=0.37, Fig. 5c), in line with the results based on 16S rDNA seqiencing[25]. These data show that even when at higher taxonomic levels (phylum to family) the mouse and human microbiome show similarities, there are major differences of the genera abundances and a very limited overlap at the species level. This is further supported by comparing the influence of age and obesity on the microbiome of mouse and human, which shows that host-adaption is the strongest difference (Extended Data Figure 5).

Discussion

We generated a comprehensive catalogue of the mouse gut metagenome: 33'925 genomes, 78 million protein sequences, over 120'000 viral contigs, and 3470 plasmids. This resource now enables mapping of over 95% of faecal and 93% of cecum samples. From the 1449 genomic defined species, 71% are newly identified and 51% could be linked to a full-length 16S sequence. Integrated into databases of 16S genes, these sequences can help to link the functional repertoire of the genome with the 16S gene, therefore leveraging the use of amplicon sequencing. Three-quarters of the species are uncultured, and some do not have a representative at the order level. Hence, the CMGM catalogue is a valuable basis for targeted culturing of these missing strains.

The CMGM is the first collection containing plasmids and viruses. Expectedly most of the viral contigs represent fragments of viruses as they are recovered from unfiltered metagenomic reads. Higher diversity might be recovered in filtered virome samples from the mouse gut. The CMGM catalogue is also the first that contains in-depth information down to the subspecies level. Although it is possible to use single nucleotide polymorphisms to detect genotype-diversity in metagenome samples, such approaches make it hard to link the genotype to the

functional repertoire. On the other hand, the CMGM subspecies are naturally linked to a specific subset of genes.

Saturation in the rarefaction analysis shows that the CMGM catalogue contains all main species and subspecies commonly living in the mouse gut. Nevertheless, we cannot exclude that new samples may contain diversity that is not part of the CMGM, for example, species present in single samples or wild mice. However, CMGM is built by assembling all publicly available data from the mouse strains that are most experimentally used, thus comprehensively representing the microbiome of laboratory mice.

Comparing the mouse microbiota to the human counterpart reveals overlap and correlation of the average abundance from phylum down to family level. As suggested by amplicon sequencing[25], the genera are qualitatively the same but quantitatively different. We observed no correlation between their average abundances in human and mouse microbiota, despite identifying 83% of shared genera. Whereas a comprehensive and precise comparison at species level between the two microbiomes was not previously feasible[2,26], the comparison of CMGM with the UHGG collection reveals an overlap of only 10% of the abundant species. These findings effectively challenge our view on the analogy between human and mouse microbiota and may impact the experimental designs and approaches for studying the gut microbiota. Different ways can be envisaged to overcome these challenges. For example, advanced transplanting human gut microbiota into germ-free mice to create 'humanized' mouse models that would be kept in gnotobiotic conditions, or complementing the work by exploring additional animal models [27]. To leverage data produced using conventional mice, it will be worth finding functional homologues between the species adapted to mouse and human microbiota e.g. by identifying 'guilds'[28], groups of species that use the same type of resources in a similar way. The functionally annotated species in the CMGM collection lays the basis for such work. The knowledge of the genomes and a nearly complete mapping rate is a basis for precise analysis on higher taxonomic levels and function. Also, the studies included in the CMGM might contain biological insights that were not accessible previously, for example

because they relate to previously unknown species. The integration with human genome catalogues allows easy comparison at higher taxonomic level.

In summary, CMGM increases our knowledge of the mouse microbiota gene repertoire by ten-fold and is the first to identify the subspecies present in the mouse gut microbiota, which together with the majority of newly identified species allows comprehensive analysis of the mouse gut microbiome at an unprecedented depth. This work uncovers major differences between the mouse and human gut microbiome identities.

Author contributions

S.K. wrote the code, analysed, and interpreted the data, and generated the figures. E.Z. and M.T. guided the project, interpreted the data and supervised the work. All authors conceptualized the study and wrote the paper.

Acknowledgements

We are grateful to Christopher Rands for critical reading of the manuscript, and to all members from our labs for discussions. This project has received funding from the European Research Council (ERC) under the European Union's Horizon 2020 research and innovation programme (ERC Consolidator Grant agreement No. 815962, Healthybiota) to M.T.

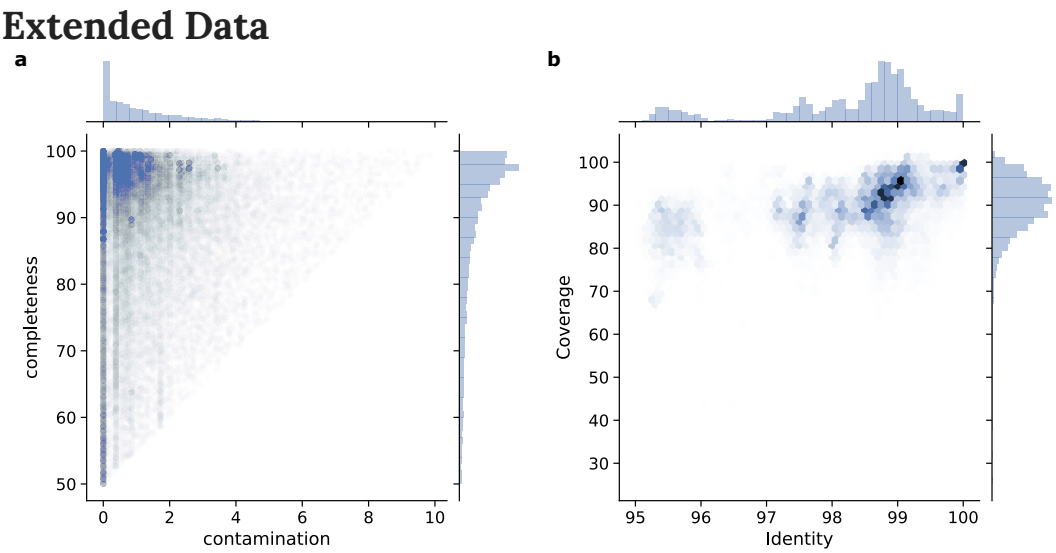

Extended Data Fig. 1| Quality estimates of MAGs at a genome level. **a,** Distribution of the MAGs included in the CMGM collection according to their completeness and contamination estimated with checkM. MAGs with 'completeness -5×contamination`< 50 were excluded. **b,** Density plot of the coverage vs. identity of the MAGs alignments to 494 reference genomes.

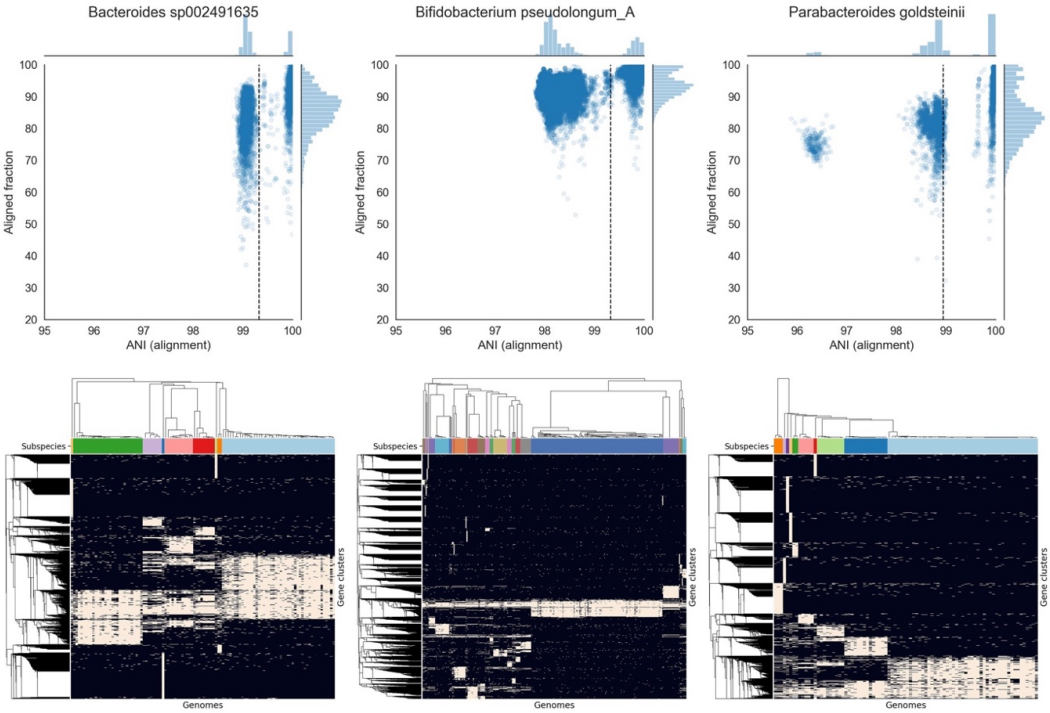

Extended Data Fig. 2| Subspecies clustering.
Example of subspecies clustering of three species with > 50 genomes. Top panels: Distribution of intra-species pairwise alignments with respect to average nucleotide identity (ANI) and aligned fraction. The dashed lines indicate the automatically selected threshold for sub-species clustering. Lower panels: presence/absence matrix of subspecies-specific gene clusters (GC50). Genomes are arranged by the dendrograms build from the pairwise ANI values. Gene clusters are ordered by dendrograms based on Jaccard distance.

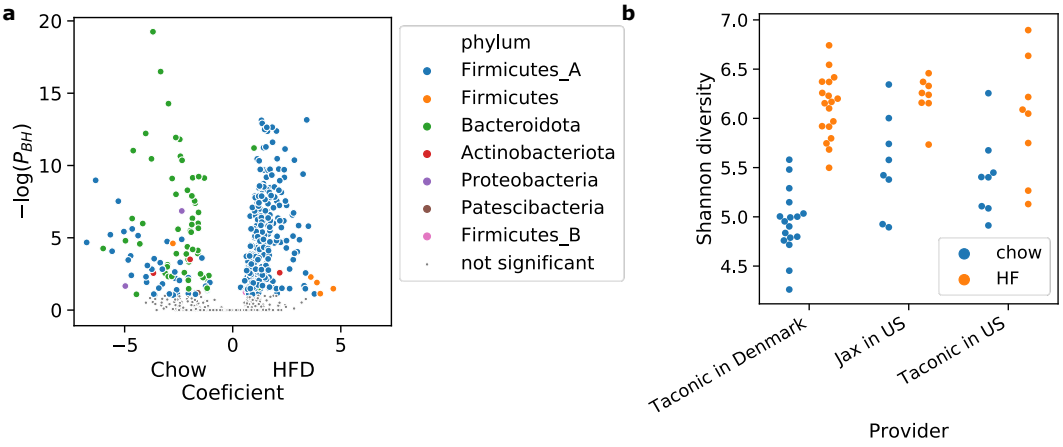

Extended Data Fig. 3| Bacterial changes induced by a high fat diet.
a, Volcanoplot of coefficients associated with high-fat diet of the generalized linear model and the associated p-values corrected using Benjamini-Hochberg-correction. **b**, Shannon diversity of the same samples stratified by Provider.

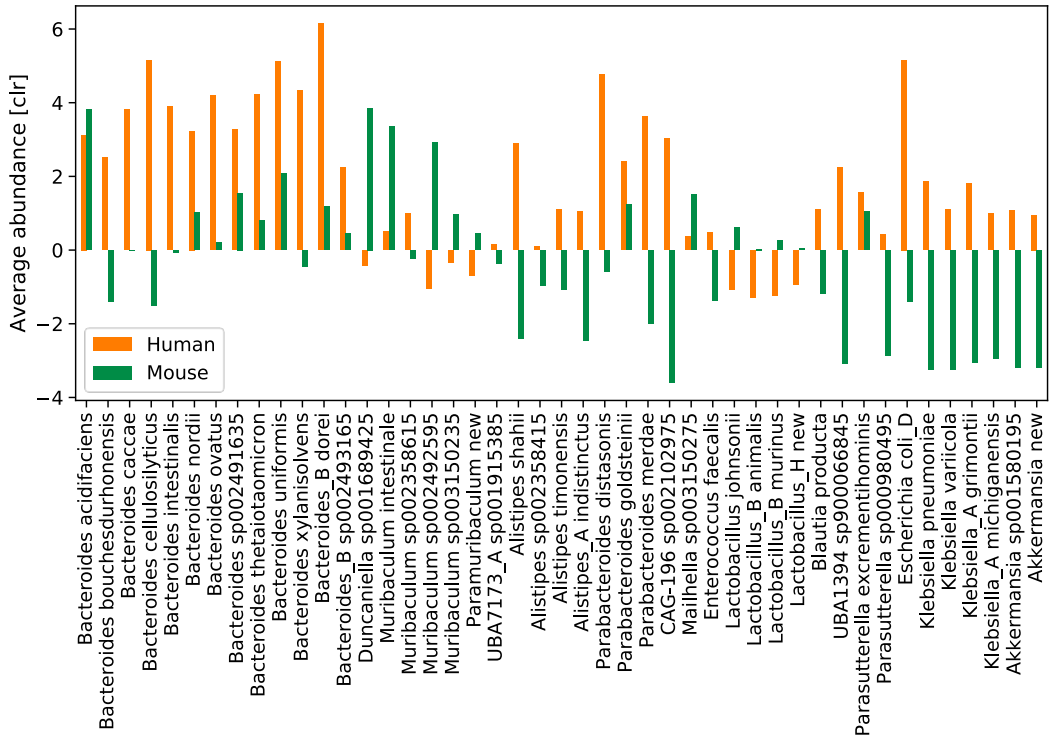

Extended Data Fig. 4| Species present in both human and mouse microbiomes.
Bar plot of the 45 species shared between human and mouse microbiome with a minimal abundance of centred log-ratio (CLR) >0 in either of the two microbiomes. The species are ordered according to their taxonomy. Negative CLR values indicate abundance that is lower than the geometrical mean of species.

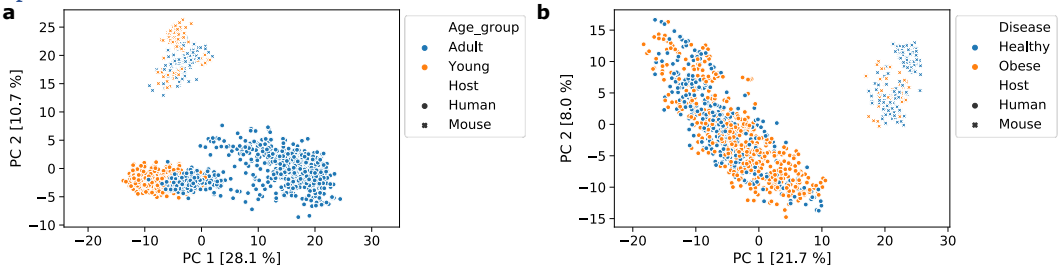

Extended Data Fig. 5| PCA of human and mouse metagenome samples.
Principal component analysis based on the robust Atchison distance based on the family abundance of mouse and human samples. **a,** Human samples come from healthy European adults or infants. Young` for mice signifies less than 12 weeks of age. **b,** Human samples come from adults that are either healthy or obese defined as Body Mass Index (BMI) > 30 kg m^{-2}. In mice, obesity is induced by high-fat diet.

Extended Data Table 1 | Metagenome samples used to construct CMGM.
The table shows the metagenome samples used for the generation of CMGM. The CMGM_Id corresponds to the SRA read id, except for the samples sequenced by our lab. The table contains information retrieved from NCBI that was available for most of the samples: Name, description, Link to bioproject, collection data, country, and submission centre. The column 'Source' specifies the organ from which the sample was taken. If the information was available in any of the metadata. Samples under the bioproject accession PRJNA646351 were sequenced for this study.

Link:
https://ezmeta.unige.ch/CMGM/v0.1/Creation/input_data/curated_metadata_SRAruns.xlsx

Extended Data Table 2 | Reference genomes associated with the mouse gut.
The table shows the assembly information of reference genomes associated with the mouse gut. These genomes were filtered for completeness and contamination before integration into CMGM. The columns `Isolated` and `Cultured` label if the genome is Isolated and cultured. The `coaction` describes if the genome is part of a mouse-specific culture collection. The genomes of the miBC collection are assembled for this study.

Link:

https://ezmeta.unige.ch/CMGM/v0.1/Creation/input_data/all_mouse_associated_ReferenceGenomes.tsv

Extended Data Table 3 | Core shared species between the human and the mouse microbiota.
The table shows detailed information about the 45 species shared between human and mouse microbiota with a minimal abundance of cantered log-ratio (CLR) >0 in either of the microbiomes, related to Extended Data Figure 4. The table contains the taxonomy and the cultivation status as well as the abundance in

relative and CLR. The number of subspecies in CMGM are indicated in the last column.

Link:

https://ezmeta.unige.ch/CMGM/v0.1/Comparison_with_Human_Microbiome/Shared_core_Species.xlsx

Online Methods

Sequencing of metagenomic data of mice

The sample collection and metagenomic sequencing were approved by the Swiss federal and Geneva cantonal authorities for animal experimentation (Office Vétérinaire Fédéral and Commission Cantonale pour les Expériences sur les animaux de Genève). Animals were on C57Bl/6J background, commercially available through Charles River, France. The mice experiment is detailed in[29]. Paired-end metagenomic libraries were prepared from 100 ngDNA using TruSeq Nano DNA Library Prep Kit (Illumina) and size selected at about 350 bp. The pooled indexed library was sequenced in a HiSeq4000 instrument at the iGE3 facility (University of Geneva).

Collection of public metagenome and genomic data

We searched the sequence read archive (SRA) of the National Center for Biotechnology Information (NCBI) for all publicly available paired-end metagenome runs from the mouse microbiome. We specifically excluded samples from human origin and amplicon sequences and different body parts than the gut. We extracted 1414 metagenome runs belonging to 43 projects. Metadata was retrieved using BioServices[30] and curated (Extended Data Table 1). We retrieved 776 assemblies from RefSeq who were linked to a biosample collected from mouse (Extended Data Table 2). We excluded reference genomes collected from other body parts than the gut or faeces.

Metagenome assembly and binning

Metagenomics and genomic reads were processed using the metagenome-atlas v2.3[11] pipeline with the command 'atlas run genomes'. The configuration file is available at the 'Code availability' section. In short, using tools from the BBmap suite v37.78[31], reads were quality trimmed, and contaminations from the mouse genome were filtered out. Reads were error corrected and merged before they were assembled with metaSpades v3.13[32]. Contigs were binned using metabat2 v 2.14[33] and maxbin2 v2.2[34], and their predictions were combined using DAS Tool v 1.1.1[35]. For the assembly of the 53 genomes of the mouse intestinal bacterial collection, we used the assembly workflow of metagenome-atlas and set 'spades_preset: normal' which uses the basic spades as assembler. The quality of the genomes was estimated using checkM v1.1[12].

Genome filtering and species clustering

We used StrainDrep v0.1[20] to filter and cluster genomes into species. For the configuration file see the 'Code availability' section. In short, genomes with an estimated quality of 'completeness-5*contamination' <50 or N50<=5000 were excluded. All Pair-wise ANI above 0.8 were calculated using bindash[15] and missing values were filled with the minimum value observed. Hierarchical clustering was performed with average linkage and a threshold of 95% using scipy[36]. For each species cluster, the genome with the highest score based on the following formula was selected as the representative.

Score= Completeness - 5×Contamination + 0.5×log(N50) + 100×isIsolate

Where Completeness and Contamination are estimated using checkM v1.1[12], N50 is the N50 score of the assembly contiguity, and 'isIsolate' is 1 for isolates and 0 for MAGs, to ensure that isolated genomes are preferred over MAGs even if they have lower quality.

Phylogenetic and taxonomic analysis

The species representatives were annotated using the genomic taxonomy database toolkit (GTDB-tk v1.2[18]). A maximum-likelihood tree based on the 120 bacterial marker genes from GTDB was built using fasttree v2.1 [37] and rooted at the midpoint. The phylogenetic trees are visualized with iTOL v5[38] and the

annotations were prepared using table2itol (https://github.com/mgoeker/table2itol). The Pearson correlation between the abundance of taxonomic groups in the human and mouse microbiota was performed with scipy v1.4.1[36].

Inferring cultured status

Species that contain a reference genome included in the CMGM catalogue are counted as cultured from a mouse origin. If GTDB-tk[18] was able to annotate the species to a reference with ANI >95%, we counted the species as cultured from a non-murine source. In both cases, if the reference genome was excluded from RefSeq (i.e. metagenome-assembled genomes) or labelled as uncultured we counted the species as isolated but not cultured.

Quantification

We used bbsplit[31] with the parameters 'ambiguous2=best minid=0.9' to map metagenomic reads to the references with 90 identity. The mapping rates were calculated as a fraction of the reads mapped to the reads used from the bbsplit log file. For most quantification, the mapped reads per genome were summed and the centred log ratio (CLR) was calculated using the sci-kit bio package (http://scikit-bio.org/) after imputing zeros using a multiplicative replacement approach. When relative abundance was used as a measure, we estimated the genome coverage as the median of blocks of 1000bp. For viruses and plasmids, the coverage over the whole contig was used. For the quantification, we used 31 cecum and 28 faecal samples from mice from our lab[29,39] as well as 184 faecal samples from the MGC v1[4]. For comparison, we quantified reads using kraken2[40] with the maxikraken2 database (lomanlab.github.io/mockcommunity/mc_databases.html, March 2019). The abundance estimation of species in the human microbiome is based on the quantification in 13132 samples[8]. We used aldex2 v1.18 for differential abundance analysis using the default parameters. Shannon diversity was calculated using the package scikit-bio (http://scikit-bio.org/) based on the relative abundance.

Gene prediction and clustering

Genes were predicted using prodigal v2.6[41] on all the assembled contigs. For the metagenome assemblies, we used the anonymous mode and for genome assemblies the parameters '–p normal --closed -m'. For the reference genomes, we downloaded the gene predictions from RefSeq. All predicted gene products were clustered using linclust[42] at 100% average amino acid identity (AAI), 0.8 coverage, and the parameters ' --kmer-per-seq 80 --cov-mode 1'. Genes were linked to the contigs and to the genomes they belong to and annotated using EggNOGmapper v2[43], which uses DIAMOND[44] to map genes to the EggNOG DB v5[45]. The catalogue was further subclustered using the same parameters as above but 90, and 50% AAI. We calculated the overlap between the 90% clustered catalogue with previous mouse gene catalogues, or the UHGP-90[24] using [42] at 90 AAI. Code availability: https://github.com/metagenome-atlas/genecatalog_atlas

Subspecies clustering

Subspecies were identified using StrainDrep v0.1[20]. In short, we calculated all intra-species pairwise genome alignments using minimap2v 2.17[46] and computed the average nucleotide identity (ANI). We used hierarchical clustering based on average linkage using scipy v1.4.1[36]. The optimal number of subspecies was automatically selected based on the maximal silhouette score. As the silhouette score can only be calculated for two or more groups, we classified species having over 95% of pair-wise comparisons with ANI > 99.5% as a single subspecies. Similar to the species clustering, for each subspecies cluster, the genome with the highest score was selected as representative genome.

The genes present in the genomes from a given species were mapped to gene clusters outlined above at 90% AAI. Gene clusters present in more than 80% of all the genomes of a subspecies were considered as this subspecies' core genes. Gene clusters that are part of the core genes in more than 80% of the subspecies are correspondingly considered as this species core genes and the genes present in a subspecies that are not part of the species core genes are subspecies specific.

Assembly of viruses and plasmids

We assembled circular contigs from our metagenome and genome datasets using (meta-)plasmid-spades v3.13[21]. The circular contigs from all samples were de-replicated using dedupe[31] and filtered for specificity to virus or plasmids using viralverify (github.com/ablab/viralVerify). In addition, we used VIBRANT v 1.2.0[22] to scan for viral fragments in our metagenome-assemblies. Viral fragments were dereplicated using bbsketch[31] based on Average amino acid identity >=99%. VIBRANT estimates the quality of vial contigs and classifies them as lytic, lysogenic. Prophages were also detected using VIBRANT.

Data Availability

The metagenomic samples sequenced for this study are available from the NCBI sequence read archive under the project id PRJNA646351. The assemblies generated in this study are deposited under study accession PRJNA646353. Reference genomes, MAGs, viruses, and plasmids used in this study together with their annotations are available at https://ezmeta.unige.ch/CMGM/v0.1. The configuration files and the metadata of the samples used for the construction of CMGM are available through the same link.

References

1. Lagkouvardos, I. *et al.* The Mouse Intestinal Bacterial Collection (miBC) provides host-specific insight into cultured diversity and functional potential of the gut microbiota. *Nat. Microbiol.* **1**, 16131 (2016).

2. Johnson, J. S. *et al.* Evaluation of 16S rRNA gene sequencing for species and strain-level microbiome analysis. *Nat. Commun.* **10**, 1–11 (2019).

3. Costea, P. I. *et al.* Subspecies in the global human gut microbiome. *Mol. Syst. Biol.* **13**, 960 (2017).

4. Xiao, L. *et al.* A catalog of the mouse gut metagenome. *Nat. Biotechnol.* **33**, 1103–1108 (2015).

5. Parks, D. H. *et al.* Recovery of nearly 8,000 metagenome-assembled genomes substantially expands the tree of life. *Nat. Microbiol.* **2**, 1533–1542 (2017).

6. Stewart, R. D. *et al.* Assembly of 913 microbial genomes from metagenomic sequencing of the cow rumen. *Nat. Commun.* **9**, 870 (2018).

7. Pasolli, E. *et al.* Extensive Unexplored Human Microbiome Diversity Revealed by Over 150,000 Genomes from Metagenomes Spanning Age, Geography, and Lifestyle. *Cell* **176**, 649-662.e20

(2019).

8. Almeida, A. *et al.* A new genomic blueprint of the human gut microbiota. *Nature* **568**, 499–504 (2019).

9. Nayfach, S., Shi, Z. J., Seshadri, R., Pollard, K. S. & Kyrpides, N. C. New insights from uncultivated genomes of the global human gut microbiome. *Nature* **568**, 505–510 (2019).

10. Lesker, T. R. *et al.* An Integrated Metagenome Catalog Reveals New Insights into the Murine Gut Microbiome. *Cell Rep.* **30**, 2909-2922.e6 (2020).

11. Kieser, S., Brown, J., Zdobnov, E. M., Trajkovski, M. & McCue, L. A. ATLAS: a Snakemake workflow for assembly, annotation, and genomic binning of metagenome sequence data. *BMC Bioinformatics* **21**, 257 (2020).

12. Parks, D. H., Imelfort, M., Skennerton, C. T., Hugenholtz, P. & Tyson, G. W. CheckM: assessing the quality of microbial genomes recovered from isolates, single cells, and metagenomes. *Genome Res.* **25**, 1043–55 (2015).

13. Garzetti, D. *et al.* High-Quality Whole-Genome Sequences of the Oligo-Mouse-Microbiota Bacterial Community. *Genome Announc.* **5**, e00758-17 (2017).

14. Liu, C. *et al.* The Mouse Gut Microbial Biobank expands the coverage of cultured bacteria. *Nat. Commun.* **11**, (2020).

15. Zhao, X. BinDash, software for fast genome distance estimation on a typical personal laptop. *Bioinformatics* **35**, 671–673 (2019).

16. Jain, C., Rodriguez-R, L. M., Phillippy, A. M., Konstantinidis, K. T. & Aluru, S. High throughput ANI analysis of 90K prokaryotic genomes reveals clear species boundaries. *Nat. Commun.* **9**, 5114 (2018).

17. Olm, M. R. *et al.* Consistent metagenome-derived metrics verify and define bacterial species boundaries. *bioRxiv* 647511 (2019). doi:10.1101/647511

18. Parks, D. H. *et al.* A standardized bacterial taxonomy based on genome phylogeny substantially revises the tree of life. *Nat. Biotechnol.* **36**, 996–1004 (2018).

19. Parks, D. H. *et al.* A complete domain-to-species taxonomy for Bacteria and Archaea. *Nat. Biotechnol.* 1–8 (2020). doi:10.1038/s41587-020-0501-8

20. Kieser, S. StrainDrep github.com/SilasK/StrainDrep.

21. Antipov, D., Raiko, M., Lapidus, A. & Pevzner, P. A. Plasmid detection and assembly in genomic and metagenomic datasets. *Genome Res.* gr.241299.118 (2019). doi:10.1101/gr.241299.118

22. Kieft, K., Zhou, Z. & Anantharaman, K. VIBRANT: Automated recovery, annotation and curation of microbial viruses, and evaluation of virome function from genomic sequences. *bioRxiv* 855387 (2019). doi:10.1101/855387

23. Hugenholtz, F. & de Vos, W. M. Mouse models for human intestinal microbiota research: a critical evaluation. *Cellular and Molecular Life Sciences* **75**, 149–160 (2018).

24. Almeida, A. *et al.* A unified catalog of 204,938 reference genomes from the human gut microbiome. *Nat. Biotechnol.* 762682 (2020). doi:10.1038/s41587-020-0603-3

25. Krych, L., Hansen, C. H. F., Hansen, A. K., van den Berg, F. W. J. & Nielsen, D. S. Quantitatively

Different, yet Qualitatively Alike: A Meta-Analysis of the Mouse Core Gut Microbiome with a View towards the Human Gut Microbiome. *PLoS One* **8**, e62578 (2013).

26. Hugenholtz, F. & de Vos, W. M. Mouse models for human intestinal microbiota research: a critical evaluation. *Cell. Mol. Life Sci.* **75**, 149–160 (2018).

27. Nguyen, T. L. A., Vieira-Silva, S., Liston, A. & Raes, J. How informative is the mouse for human gut microbiota research? *DMM Dis. Model. Mech.* **8**, 1–16 (2015).

28. Root, R. B. The Niche Exploitation Pattern of the Blue-Gray Gnatcatcher. *Ecol. Monogr.* **37**, 317–350 (1967).

29. Chevalier, C. *et al.* Gut Microbiota Orchestrates Energy Homeostasis during Cold. *Cell* **163**, 1360–1374 (2015).

30. Cokelaer, T., Pultz, D., Harder, L. M., Serra-Musach, J. & Saez-Rodriguez, J. BioServices: a common Python package to access biological Web Services programmatically. *Bioinformatics* **29**, 3241–3242 (2013).

31. Bushnell, B. BBmap. Available at: https://sourceforge.net/projects/bbmap/. (Accessed: 10th January 2018)

32. Nurk, S., Meleshko, D., Korobeynikov, A. & Pevzner, P. A. metaSPAdes: a new versatile metagenomic assembler. *Genome Res.* **27**, 824–834 (2017).

33. Kang, D. *et al.* MetaBAT 2: an adaptive binning algorithm for robust and efficient genome reconstruction from metagenome assemblies. 0–10 (2019). doi:10.7287/peerj.preprints.27522v1

34. Wu, Y.-W., Simmons, B. A. & Singer, S. W. MaxBin 2.0: an automated binning algorithm to recover genomes from multiple metagenomic datasets. *Bioinformatics* **32**, 605–607 (2016).

35. Sieber, C. M. K. *et al.* Recovery of genomes from metagenomes via a dereplication, aggregation and scoring strategy. *Nat. Microbiol.* **3**, 836–843 (2018).

36. Virtanen, P. *et al.* SciPy 1.0: fundamental algorithms for scientific computing in Python. *Nat. Methods* **17**, 261–272 (2020).

37. Price, M. N., Dehal, P. S. & Arkin, A. P. FastTree 2 - Approximately maximum-likelihood trees for large alignments. *PLoS One* **5**, e9490 (2010).

38. Letunic, I. & Bork, P. Interactive Tree Of Life (iTOL) v4: recent updates and new developments. *Nucleic Acids Res.* **47**, W256–W259 (2019).

39. Fabbiano, S. *et al.* Functional Gut Microbiota Remodeling Contributes to the Caloric Restriction-Induced Metabolic Improvements. *Cell Metab.* **28**, 907-921.e7 (2018).

40. Wood, D. E., Lu, J. & Langmead, B. Improved metagenomic analysis with Kraken 2. *Genome Biol.* **20**, 257 (2019).

41. Hyatt, D. *et al.* Prodigal: prokaryotic gene recognition and translation initiation site identification. *BMC Bioinformatics* **11**, 119 (2010).

42. Steinegger, M. & Söding, J. Clustering huge protein sequence sets in linear time. *Nat. Commun.* **9**, 2542 (2018).

43. Huerta-Cepas, J. *et al.* Fast Genome-Wide Functional Annotation through Orthology

Assignment by eggNOG-Mapper. *Mol. Biol. Evol.* **34**, 2115–2122 (2017).

44. Buchfink, B., Xie, C. & Huson, D. H. Fast and sensitive protein alignment using DIAMOND. *Nat. Methods* **12**, 59–60 (2015).

45. Huerta-Cepas, J. *et al.* eggNOG 5.0: a hierarchical, functionally and phylogenetically annotated orthology resource based on 5090 organisms and 2502 viruses. *Nucleic Acids Res.* **47**, D309–D314 (2019).

46. Li, H. Minimap2: pairwise alignment for nucleotide sequences. *Bioinformatics* **34**, 3094–3100 (2018).

4.2 CMGM enables comparative analysis of mouse metagenomes by relating functional changes to driver species

This section shows how the comprehensive mouse gut metagenome catalog (CMGM) can be used to analyze mouse metagenome data on both a functional and a species level and to relate the changes to treatments of the host. It shows also how to relate changes in the microbiome's functional potential to the responsible species. This analysis was is part of the revised manuscript available from bioRxiv.

To illustrate how this catalog allows discovering compelling biological insights, we analyzed the metagenome from mice exposed to cold ambient air temperature. Cold exposure is a stimulus that activates the classical brown fat and promotes beige cell development within the subcutaneous white adipose tissue (Cannon & Nedergaard, 2017; Chechi et al., 2013; Stojanović et al., 2018). As such, it is an extensively used intervention for enhancing thermogenic and mitochondrial activity in adipose tissues, leading to decreased adipose tissue amount and improved glycemic status. We (Chevalier, Stojanović, et al., 2015) and others (Ziętak et al., 2016) showed that cold exposure leads to a marked shift of the microbiota composition observed by 16S analysis, which is in itself sufficient to improve the insulin sensitivity, induce tolerance to cold, increase the energy expenditure and lower the fat content– an effect in part mediated by activation of the brown fat (Chevalier, Stojanović, et al., 2015; Ziętak et al., 2016) and browning of the white fat depots in the cold microbiota-transplanted mice (Chevalier, Stojanović, et al., 2015; Cypess et al., 2015; Ghorbani et al., 1997; Guerra et al., 1998; Kopecky et al., 1995). These results indicate an existence of a microbiota-fat signaling axis; however, the signaling cascades mediating this process remain poorly understood. As noticed previously (Chevalier, Stojanović, et al., 2015), here we confirmed that *Akkermansia muciniphila*, the only representative of the phylum *Verrucomicrobiota* was eliminated by cold exposure (Fig. 4.1A). The species NM07-P-09 *sp004793665* (the most abundant species from the phylum *Actinobacteriota*) and the *Muribaculaceae* species UBA7173 *sp002491305* were even more significantly decreased ($P_{BH} < 1e^{-4}$, Fig. 4.1A). We found that cold exposure leads to an increase of the family *Lachnospiraceae* and a decrease of the families *Muribaculaceae*, and *Oscillospiraceae*. On a functional level, cold

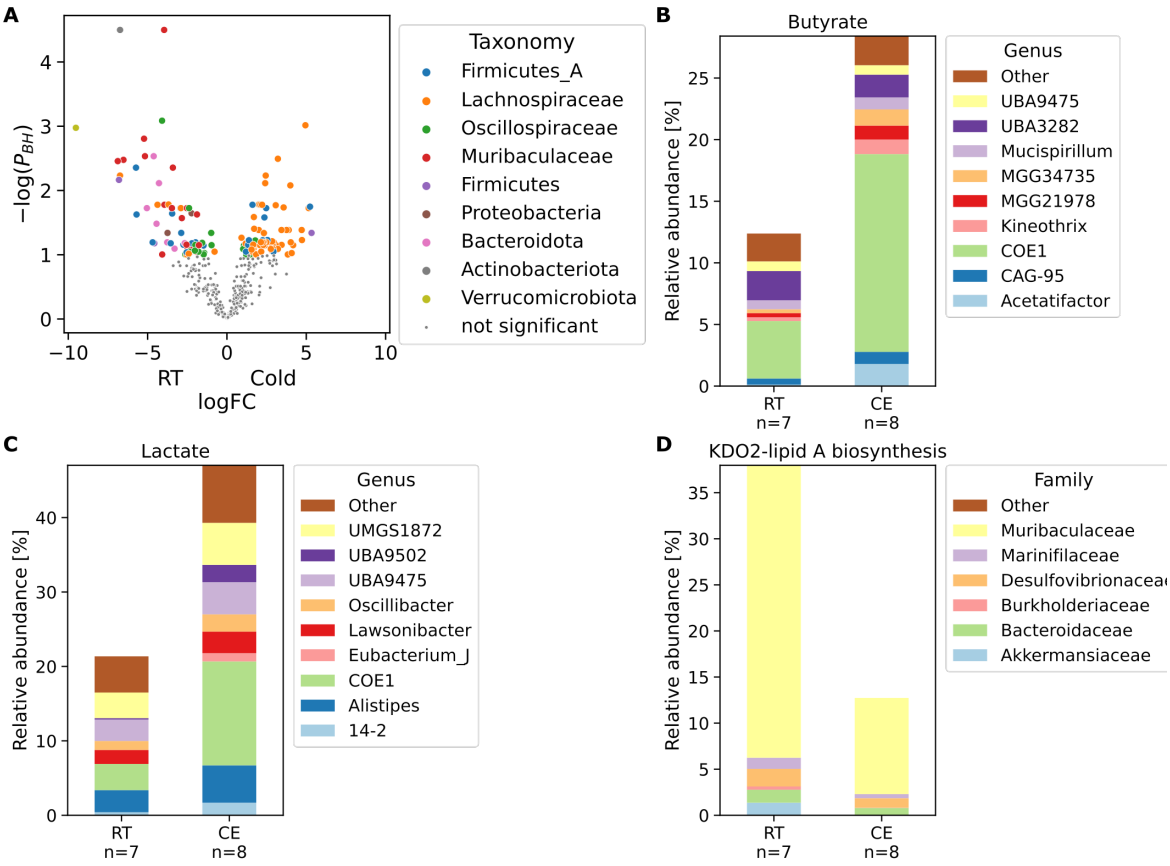

Fig. 4.1 **CMGM links functional changes to driver species**
a, Volcano plot of species changes in mouse cecal microbiota upon cold exposure. Significantly changed species are colored by their phylum. PBH: P-value corrected for multiple testing using Benjamini-Hochberg procedure. **b–d**, Bar plots of significantly changed pathways in mouse cecal microbiota upon cold exposure. The contribution to the relative abundance of each module is partitioned by genus b+c and family d.
CE: Cold exposure, RT: Room temperature control

exposure led to a doubling of butyrate and lactate production. These changes were mainly due to the increase of the family *Lachnospiraceae*, specifically the increase of the uncultured genus *COE1* (Fig. 4.1B, C). To address whether these uncovered metagenomic changes are indeed reflected in differences of the actual metabolite levels, we looked at the germ-free mice transplanted with microbiota from the cold-exposed mice or from their RT-kept controls. Transplantation of the cold-adapted microbiota led to an increase in the production of butyrate, lactate, propionate, and succinate in the recipients' cecum com-

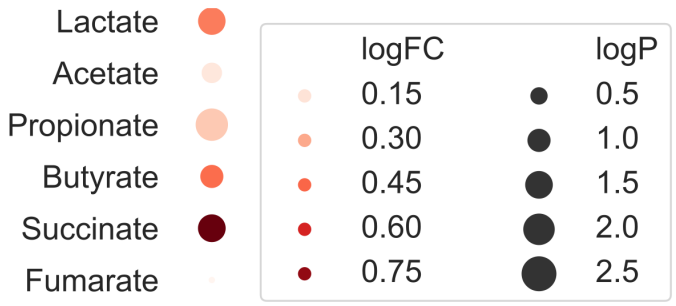

Fig. 4.2 **Metabolite changes by cold-adapted microbiome**
Dot-plot of metabolite changes in ceca of germ-free mice transplanted with cold-adapted microbiota compared to RT-microbiota transplanted controls (Data from Chevalier, Stojanović, et al., 2015).

pared to germ-free mice inoculated with microbiota from control mice (Fig. 2). Interestingly, the increased lactate was also measured in the cecum and serum of mice with an intermittent fasting feeding regime (G. Li et al., 2017), which has been shown to induce browning via the induction of the Vascular endothelial growth factor (Kim et al., 2017). Similarly, succinate is linked to the increase of thermogenesis (Mills et al., 2018). We found a decrease of the prokaryotic succinate dehydrogenase, which metabolizes succinate to fumarate, suggesting a mechanistic link between the cold-induced microbiota changes and the adipose tissue browning.

We also observed a decrease in **Lipopolysaccharide** (LPS) synthesis, both in an LpxL-LpxM–dependent and –independent way, primarily attributed to the cold-induced reduction of *Muribaculaceae* (Fig. 4.1D). LPS administration leads to reduced core body temperature and heat release, correlated with mitochondrial dysfunction (Okla et al., 2015). In contrast, genetic deletion of the LPS receptor, the toll-like receptor 4 (TLR4), leads to resistance against high caloric diet-induced obesity, improved glucose tolerance and insulin sensitivity, and adipose tissue browning (Fabbiano et al., 2018). These findings suggest an additional possible link between the cold-induced microbiota changes and adipose tissues both at mechanistic and bacterial level, contributing to improved insulin sensitivity and browning of the white fat

This example illustrates the CMGM catalog's usability as a reference for metagenomic studies, enabling discovering precise and comprehensive changes of species and the related function induced by a treatment or a disease. The

CMGM sets the ground for reanalysis of the existing datasets for uncovering species and bacterial functions that are involved or altered by the condition of interest.

4.2.1 Methods

Sequencing of metagenomic data of mice

The mouse experiments were approved by the Swiss federal and Geneva cantonal authorities for animal experimentation (Office Vétérinaire Fédéral and Commission Cantonale pour les Expériences sur les animaux de Genève). Animals were on C57Bl/6J background, commercially available through Charles River, France. The mice experiment is detailed in (Chevalier, Stojanović, et al., 2015). Paired-end metagenomic libraries were prepared from 100 ng DNA using TruSeq Nano DNA Library Prep Kit (Illumina) and size selected at about 350 bp. The pooled indexed library was sequenced in a HiSeq4000 instrument at the iGE3 facility (University of Geneva).

Quantification

We used BBsplit (https://jgi.doe.gov/data-and-tools/bbtools)) with the parameters 'ambiguous2=best minid=0.9' to map metagenomic reads to the reference genomes with 90 identity. For most quantification, the mapped reads per genome were summed, and the centered log-ratio (CLR) was calculated using the sci-kit bio package (http://scikit-bio.org/) after imputing zeros using a multiplicative replacement approach. We used the two-sided Welch test and Benjamini-Hochberg correction to estimate the significance of changes in clr-transformed genome abundance between experimental groups. We estimated the genome coverage as the median of coverage over 1000bp blocks, to calculate relative abundance.

Functional annotation

The species representatives of both the CMGM and the UHGG were annotated using DRAM (Shaffer et al., 2020). A Kegg-module is inferred to be present if ¾ of all the steps were present in a genome. As there are no modules for short chain fatty acids in Kegg we created custom modules (see the 'Code' section). The step-coverage was calculated with DRAM for all Kegg-modules. The

metagenome-side abundance of functional modules was calculated as the sum of the relative abundances of all genomes containing a module. We used the two-sided Welch test and Benjamini-Hochberg correction to estimate the significance of changes in module abundance between experimental groups.

Code Availability

The code for the analysis of the cold-exposed microbiota is available from GitHub: https://github.com/SilasK/CMGM

Statistical analysis of microbiomes

In this chapter, I explain what I have learned about the statistical analysis of microbiome data. Many of the concepts relate to **compositional data analyis** CoDa. I summarize important concepts that were developed firstly for amplicon sequencing and show their applications on *metagenome data*.

5.1 How *not* to interpret microbiome data?

Regardless of the sequencing technology and workflow used for quantifying a microbiome, the typical output is an abundance table, a table with non-negative values, integers most of the time, also known as *counts*. We obtain counts as the output of most amplicon or metagenomics analysis which might tempt us to interpret them as counting organisms or that the counts somehow relate to the number of organisms in the sample.

Most of the time, we only sequence a fraction of the (biological) sample of the microbiome, which distorts the data in many ways. To begin with, the number of reads obtained from different samples can vary in the orders of magnitude. A common practice to account for this difference in **sequencing depth** is to transform the counts into **relative abundance** by dividing by the total number of reads per sample. Relative abundance can be serviceable for visualizing the microbiome but is less so for their analysis. Relative abundance profiles of microbiomes give the impression that each quantified species can be analyzed independently from the other, but that is not the case. Due to the sequencers constraining the reads to a fixed total number, the data is not only relative (to the total number of reads) but also **compositional**. Compositional means that the observed abundance of any given species is dependent on the observed abundance of all other species. For example, the decrease of an abun-

dant member of a microbial community leads to an apparent increase of lower abundant members, which can be even significant.

We had this situation when analyzing the microbiota of children with diarrhea (Kieser, Sarker, et al., 2018). We were surprised by an increase of *Streptococcus* irrespective of the pathogen causing diarrhea, which we related to the flushing out of the majority of the colonic microbiome, which makes *Streptococcus* only appear to increase. Diarrhea is an obvious example, but the compositionality leads to a *negaitve correlation* between all species that affects the interpretation of microbiome data in more subtle ways.

It is important to note that microbiomes can be quantified in absolute terms if a measure for the number of cells is available. In a landmark study Vandeputte et al. use flow cytometric enumeration to quantify the microbial load and multiply it with the relative abundance based on amplicon sequencing (Vandeputte et al., 2017). The authors show convincingly how the number of microorganisms can vary by up to ten-fold in microbiome samples of healthy individuals. Microbiome load can be a fundamental driver of the microbiome alterations in Crohn's disease. Flow cytometric enumeration needs fresh stool samples, which is difficult to obtain for larger study cohorts. However, it was shown that quantitative PCR of the 16S gene could also reliably be used to transform the relative abundance of amplicon sequencing into absolute counts (Tettamanti Boshier et al., 2020).

The fact that microbiome data is compositional is still not widely appreciated. At the beginning of my P.h.D., Gloor et al. published an article entitled "Microbiome Datasets Are Compositional: And This Is Not Optional", where they show how the compositionality of microbiome data affects all areas of data interpretation from ordination, clustering, network analysis to differential (relative) abundance determination. They highlight fatal issues with common approaches for analyzing microbiome data that do not account for its compositionality. For instance, standard statistical tests or even microbiome-specific tools such as LEfSe (Segata, Izard, et al., 2011) give biased results. Similarly, most metrics for microbiome data, such as the UniFrac distance, also suffer from this problem. In the same article, the authors also show that there are tools that explicitly take the compositionality of the data into account and can make the interpretation of microbiome data more robust.

5.2 Compositional data analysis of microbiome data

The core idea of compositional data analysis (CoDa) is to analyze (microbiome) data not as independent abundances but rather as *ratios* between species to describe a sample. The ratios are the same whether the data are counts or proportions. They are also not affected by differences in sequencing depths nor unmapped reads. The idea of compositional data analysis goes back to John Aitchison, who formalized the analysis of data that consists of proportions. He proposed to transform compositional data using the geometric mean. This transformation is called **centered log-ratio** (CLR) and is defined as

$$CLR(\vec{x}) = \log(\vec{x}) - \text{mean}(\log(\vec{x}))$$

For each sample vector $\vec{x}$ that contains either counts or relative abundance. Taking the logarithm of the species abundance transforms them to ratio to the geometric mean of the abundances or the mean of the log-transformed abundances. Because the logarithm of zero is undefined, one needs to deal with the zeros before applying the log. A zero in a count table does not necessarily mean that a species is absent from a sample. It is also possible that a low-abundant species is not detected due to undersampling or other systemic biases (Silverman et al., 2020). In this respect zeros should be treated as missing values. Fortunately, there are many acceptable ways to deal with the missing values in sequencing data. The most basic approach is to impute a small numeric value; 0.65 is commonly used. Multiplicative replacement adjusts these imputed values to preserve the relative multivariate structure of the data (J. A. Martín-Fernández et al., 2003; Palarea-Albaladejo & Josep Antoni Martín-Fernández, 2015). Counts can be modeled as a probability distribution, where zero is a possible outcome (Fernandes et al., 2014) or estimated using matrix completion Martino et al. Noteworthy, zeros are less a problem in metagenomics data compared to amplicon data because of spurious mapping of reads to genomes, which makes zeros in count tables very unlikely.

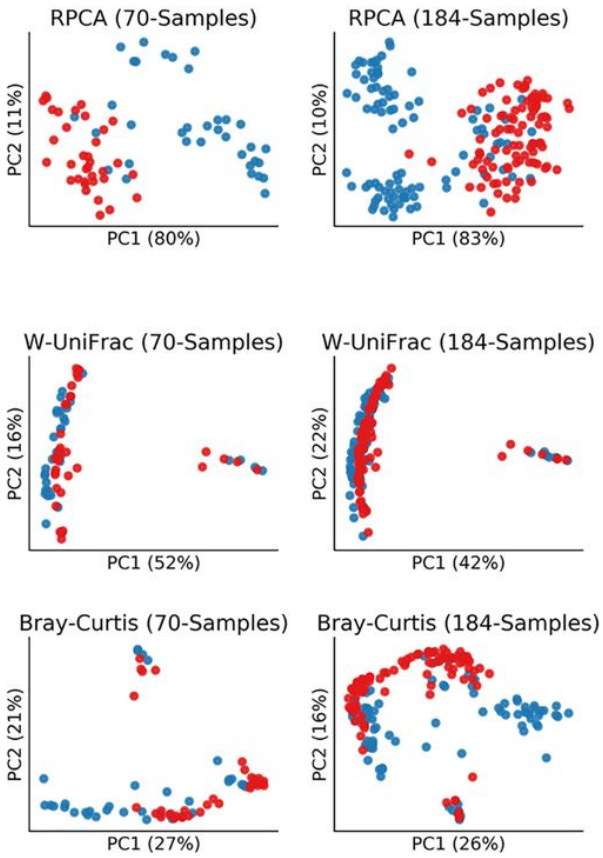

Fig. 5.1 Ordination plots of a dataset Robust Aitchison PCA (RAPCA), PCA based on Aitchison distance with zero-imputation based on matrix completion (Martino et al., 2019), compared to PCoAs based on the weighted unifrac or the Bray-Curtis distance. RAPCA is able to discriminate bwetewen the two groups (red and blue) even with lower samples (left column). Source (Martino et al., 2019).

5.2.1 Ordination and multivariate statistics

The CLR.transformation makes the data symmetric and *linearly related*, so that they can be easily be interpreted by traditional statistics and machine-learning algorithms. What is more, the simple difference between two data points becomes a meaningful □-diversity metric, sometimes named **Aitchison distance**. The Aitchison distance is a proper linear distance, making it ideal for multivariate analysis, clustering, and ordination. Ordination refers to the representation of all samples of a study in a single plot. It is usually the first step of an (exploratory) microbiome analysis. The highly dimensional data needs to be transformed into a low-dimensional, preferably two-dimensional, space. However,

the dimensional reduction should keep as much as possible of the variability to visually or statistically discriminate between groups and identify outliers. As the typical distance metrics, such as Jensen-Shannon, Bray-Curtis, and UniFrac, are not linear distances, this has to be achieved using a *principal coordinate analysis* (PCoA), which not only takes time to calculate but is also sensitive to inclusion or exclusion of samples (Wong et al., 2016). PCoA, based on standard metrics, discriminates mainly on the most abundant members of a community, which might not affect the most discriminatory species between groups (Gloor et al., 2017; Martino et al., 2019). Another major problem for the ordination of microbiome datasets is sparsity, the fact that most species are absent from most samples. Sparsity can lead to a distortion of gradients in the ordination plot using standard distant metrics, often referred to as the Horseshoe-effect (Kuczynski et al., 2010; Morton et al., 2017).

In contrast, the Aitchison distance can be used in a **principal component analysis** (PCA), which is not only swift to calculate, but also robust to sparsity (Wong et al., 2016; Morton et al., 2017), meaning that the exploratory analysis is reproducible even if additional samples are included or outliers excluded (Figure 5.1).Both principal *component* analysis and principal *coordinate* analysis identify the most important components of the data. In addition, PCA identifies which species contribute to which extent to the components; these values are referred to as the **feature loadings**. They allow the direct identification of species that contribute the most to the differences in the datasets, for example, which species contribute the most to differences between clusters separated by the PCA. It is possible to plot the feature loadings on the same plot as the PCA-transformed data, enhancing exploratory data analysis efficiently.

5.2.2 Differencial abundance analysis

CLR transformed abundances can directly be used for differential abundance analysis. Even if the plot of CLR values might seem unalike a plot with relative abundance, its interpretation is intuitive (Figure 5.2). Higher CLR values represent a higher abundance of a species in a sample, whereas negative values represent low abundances. The difference between the mean of the two groups can be intuitively interpreted as the log-fold-change between the two groups. The CLR-transformed values are approximatively normally distributed, which renders the use of the parametric tests justified, which have more power

than assessing the significance of relative abundance values using the non-parametrical tests.

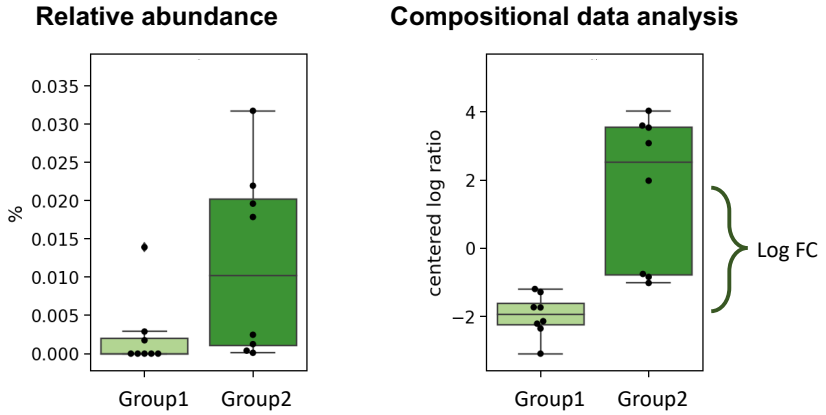

Fig. 5.2 The univariate comparison of the abundance of a species both as relative abundance and under the compositional data analysis paradigm. The significance of the relative abundance values is assessed using a Mann–Whitney U test, whereas a Welch test was used for the centered log-ratios (CLR). The difference between the average CLR of the groups is the log fold change.

Differential abundance analysis is often the final goal of microbiome analysis. After removing outliers and checking the data for inhomogeneities, one would like to identify which microbes are most significantly different between the two groups.

It is crucial to keep in mind that the CLR transformation is not an actual normalization (Quinn, Erb, et al., 2018). It does not remove the constraint and the correlation bias between the different species' abundances in a sample. The CLR-transformed data can give the impression that they refer to single species. However, the transformed data refer to the ratios of the species abundance to the geometric mean of the abundance. The geometric mean can change with the inclusion or removal of species. Therefore, slight variations of the CLR are proposed to mitigate this dependence by taking the geometric mean of all the values in the interquartile range (Wu et al., 2017).

5.2.3 Ratio based biomarker discovery

A more general approach is to calculate ratios between species or taxa directly. For instance, the ratio between the phyla *Bacteroidetes* and *Firmicutes* or be-

tween the genera *Prevotella* and *Bacteroides* are well known examples used in the field. Even when their associations with specific host phenotypes is put into question (Magne et al., 2020), these ratios represent an example of robust biomarkers that can be used to characterize microbiomes even across studies[1]. Instead of calculating all ratios between different taxa and manually testing their association with the metadata (e.g., groups), more sophisticated methods are available that search more efficiently and control the false discovery rate.

For instance, the tool `phylofactor` generalizes this idea by looking for searches for the optimal split in a phylogenetic tree to create a ratio, or balance, with the strongest association with the metadata (Washburne et al., 2019). It can identify broad clades of species that account for maximum variation or more specific clades that are most significantly associated with the metadata. This framework can build models based on multiple metadata variables. Phylofactor can identify differences between clades anywhere in the phylogenetic tree and is not limited to the annotated taxonomic levels. For instance, it can be used on taxonomically unannotated OTUs or genomes.

However, like all phylogenetic analyses, it is also constrained by the tree. Tools like `codacore` (Gordon-Rodriguez et al., 2021) can identify ratios of any combinations of species associated with the metadata. Species can be either summed, similarly as one would add the abundance of all species that exhibit the same pathway, or multiplied to capture multiplicative interactions. The more species are combined to create a ratio, the better the ratio is associated with the metadata. However, to limit over-fitting and to make the ratio more interpretable fewer species are desired. A parameter in `codacore` allows tuning how many species should be included to create a ratio resulting in easy-interpretable and robust biomarkers.

This novel machine learning framework termed **ratio based biomarker** analysis (Quinn, Gordon-Rodriguez, et al., 2021), fully accounts for the biases in (microbiome) sequencing data and allows the integration of multiple omics data. This framework presents many exciting opportunities for thorough measuring and analysis of microbiome data.

[1]However it is important to standardize the extraction protocol, which is an important confounding factor for the Bacteroidetes-Firmicutes-ratio (Magne et al., 2020).

Discussion

6.1 Genome-resolved metagenomics enhances the analysis of metagenomes with a need for reference genomes

The goal of my P.h.D. was to enable the analysis of metagenomes a need for reference genomes to study the microbiome's influence on the host's health. The core methodology I implemented is the reconstruction of genomes from metagenomes. Together with Joseph Brown and Lee Ann McCue from the Pacific Northwest National Laboratory, USA, we developed `metagenome-atlas`. This tool allows to recover genomes from metagenomes and to perform analysis based on them. It performs all steps from quality control, assembly, genome recovery, and annotation. The program was downloaded over 10'000 times and cited 19 times in the first year after its publication. Already before its publication, the open-source program was adopted by a community of users. The feedback of the users helped us to make it robust and easy to use. In our lab, we used it primarily to analyze the functional potential of the mouse gut microbiome, but it was used to analyze various types of metagenomes from anaerobic lakes to plant-associated and soil microbiomes. The simplicity to start analyzing metagenome data (We claim you can start with only three commands) makes the tool also attractive for companies.

Not surprising, `metagenome-atlas` is not the only pipeline that performs assembly and binning. For example, the pipelines `MetaWRAP`, `Sunbeam`, and `SqueezeMeta` (Uritskiy et al., 2018; Clarke et al., 2019; Tamames & Puente-Sánchez, 2019) perform similar analysis using practically the same programs. What is unique to `metagenome-atlas` is that it annotates the metagenome samples based on the

recovered MAGs with both taxonomy and functional potential. This is to say that it uses a dataset-specific genome reference. To explain why this is a crucial advantage, let me make an excursus about measuring the microbiome.

6.2 Measuring the microbiome

A fundamental step of almost every endeavor in science is measuring. We measure to compare between different experiments, samples, or even studies and draw generalizable conclusions from them. Measuring in the context of sequencing-based approaches often comes down to mapping (short-) reads to a reference (-genome) and counting the mapped reads.

Nevertheless, measuring is not straightforward, as we will see, both with 16S rDNA sequencing as metagenomics. One has to define appropriate units for quantification of the microbiome. For this, one has to consider a *tradeoff between specificity and comparability*.

6.2.1 Defining units for 16S amplicon sequencing

There is a long-standing discussion on how to define units for 16S amplicon sequencing. In a typical amplicon study, most sequences are only remotely similar to annotated species. One option is to map a sequenced amplicon to the closest matching sequence in a database of curated 16S genes, like SILVA (Quast et al., 2012). This **closed-reference** approach has the advantage that the annotated units can be compared between studies (At least the one that uses the same version of the same database). However, the mapping to the database might be ambiguous, and many new variants specific to the study might be missed. It is often much more informative to cluster all the sequenced amplicons for one study and use them as measuring units. As these clusters do not necessarily correspond to biological species, they are called **operational taxonomic units** (OTUs). This ***de novo***-clustering approach has the disadvantage that the OTUs are specific to one study, limiting the inter-study comparison.

In 1994, E Stackebrandt & Brett M. Goebel proposed 97% similarity as a species threshold for the full-length 16S gene. This threshold was adopted for amplicon sequencing (Patrick D. Schloss & Handelsman, 2005), even though this technique is based on a small fraction of the gene. More recent analyses of the

correspondence between the 16S gene and species found that 99% would be a better threshold for the full-length 16S rRNA gene and 100% for amplicon sequencing (Edgar, 2018).

However, at such a high threshold, sequencing errors create spurious OTUs unless they are appropriately dealt with. Tools, such as `DADA2` have an efficient algorithm to denoise the reads in order to distinguish sequencing errors from biological variation (Benjamin J Callahan et al., 2016). The 100% clusters of the denoised reads are also referred to as **amplicon sequence variants** (ASVs). ASVs combine the advantages of the *de novo*- and the closed-reference approach. ASVs cover all sequence variance within a dataset and are unique and consistent, allowing them to be compared across different datasets (Benjamin J. Callahan et al., 2017).

Critics of 100% ASVs point out that a genome may be split into multiple ASVs if it contains multiple copies of the 16S gene that are sufficiently diverged (Patrick D Schloss, 2021). Re-clustering of ASVs based on correlation across different samples could mitigate this problem. But it also confirms that amplicons of the 16S rRNA gene are not suited to achieve consistent species resolution as previously mentioned (Edgar, 2018; Johnson et al., 2019). In conclusion, the ASVs, are the most specific and comparable unit to measure a microbiome even though these units do not correspond precisely to species.

6.2.2 Defining units for metagenomics

Whereas in 16S amplicon sequencing, the denoised reads or ASVs *are* the units for quantification, for shotgun metagenomics reference units to which the reads can be mapped still needed to be defined. Usually, the taxonomic unit of species is used for metagenome profiling, which permits the results to be compared among studies and previous knowledge.

The main problem for metagenome quantification was, until recently, the lack of reference genomes. In the absence of good references, a tool like `mOTUs` was invaluable. This tool creates taxonomic units based on ten universal single-copy marker genes (Sunagawa et al., 2013). Because this tool is based on universal marker genes, it allows targeting virtually all (prokaryote) genomes in metagenomes and, therefore, precise estimation of their relative abundance. It is possible to create mOTUs even for low-abundant and unknown species by

assembling these genes from metagenomes and linking them through the correlation of their coverage across many samples.

As described above, genome-resolved metagenomics allows the generation of reference genomes for metagenomics. Now, the problem becomes how to map metagenomic reads efficiently to the ever-growing reference databases. In a breakthrough publication in 2014, Derrick E Wood & Steven L Salzberg showed that it is possible to circumvent the time-consuming step of precise alignment and directly assign reads to taxonomy utilizing exact k-mer-matches. The tool called `Kraken` was used to show that classifications, which previously took hours, were tractable in minutes. Notwithstanding, most k-mers are not specific to a species, which leads to the classification of many reads at higher taxonomic levels. It is shown that this problem is only aggravated with the inclusion of more and more reference genomes (Nasko et al., 2018). As an alternative to decomposing the whole genome into more or less specific k-mers, it makes sense to search for genome regions, usually genes, specific for a species. The classical tool `metaphlan` is based on this approach (Segata, Waldron, et al., 2012), and the idea was reused in a quantification tool based on the collection of recently recovered human MAGs (Nayfach et al., 2019). Mapping only to a subset of specific genes accelerates the profiling while keeping the ambiguity low.

However, all these tools depend on closed (species) databases. Insofar they have the same disadvantages as 16S OTUs that are defined based on a *closed-reference*. Even the term operational genomic unit (OGU) is used, which echoes the term OTU (Zhu, Huang, et al., 2021). Because the reference usually does not contain the exact strain(s) present in the sample, sub-optimal mapping is expected. The presence of multiple strains in a microbiome additionally complexifies quantification (See example in section 1.2.2). Finally, while the quantification on species levels is ideal for comparison with other studies, much of the subspecies diversity is ignored, showing the tradeoff between comparability and specificity again.

Dataset-specific genome reference

The problem can, naturally, be solved by the creation of **dataset-specific references** through genome-resolved metagenomics. Ideally, one would recover the genome of each strain in a sample. Limitations of the assembly and binning of low abundant genomes make this impossible. Assembly needs minimal cover-

age to correctly assemble a genome[1], and strains that are more than 98% similar are merged in the same assembly (Fritz et al., 2019).

Combining the genomes recovered from multiple samples allows complementing the catalog of genomes that serve as a reference. For instance, a strain that is low in abundance might have a nearly identical strain that is abundant in another sample. Therefore, collecting the MAGs recovered from all samples of a study allows quantifying low-abundant strains in samples where they are unrecoverable. On the other hand, it does not make sense to include every genome in the reference. The redundancy can create ambiguous results during the quantification as reads will have multiple mapping sites. Therefore MAGs are usually **de-replicated** before they are used as a reference for quantification. Genomes are usually clustered based on their ANI, and the genome with the highest quality is chosen as representative. As an alternative, one might choose the medoid, the genome that represents the cluster the best. Commonly the threshold of 95% average nucleotide identity is used for de-replication.

This is the strategy implemented in `metagenome-atlas` (Ch. 2). Each sample is assembled and binned separately (optionally using differential abundance by mapping the reads from other samples to the assembly). The bins are then de-replicated, and the best genome is chosen for each cluster. The threshold is set to the common species threshold but can be set lower to capture subspecies variation. This approach creates a *dataset-specific* reference that allows consistent quantification of all the samples. Low-abundant species can still be quantified if they are recovered in at least one sample. The annotation of the species representatives with a standard taxonomy allows comparison beyond the study. Though this method is resource-intensive, it optimizes specificity and comparability, representing similar advantages as ASVs over OTUs.

6.3 Inference of metabolic pathways and linking it to the host health and the driver species

In general, researchers are not only interested in knowing the composition of a microbiome, the “who is there?”, but also “what are they doing?” To reliably

[1]The assembly of a single prokaryote genome needed eight-fold coverage to be entirely assembled in a simulated experiment. (Fritz et al., 2019)

infer what functions microbes are presently exhibiting, one would need to sequence their expressed genes (meta-transcriptomics) or even the metabolites of the microbiome (metabolomics). The sampling of metatranscriptomics is feasible, though the transcripts are more sensitive to environmental influences and highly variable in time because cells can change gene expression rapidly to adapt to changing environmental conditions. Meta*genom*ics allows us only to answer the question "What can they do?" by inferring the functional potential of microbes.

As described in chapter 3, we developed a method based on genome-resolved metagenomics to infer the functional potential metagenomes. We analyzed 32 samples from mouse feces and cecum with `metagenome-atlas`. The tool recovered about a thousand MAGs belonging to 147 species. Then we annotated the representative genome for each species with the functional potential, especially metabolic pathways. Pathways were inferred to be present in genomes if most (threshold 80%) of the steps described for the pathway were present in the genome. We calculated the 'abundance' of a pathway as the sum of all the relative abundance of species containing the pathway. We found that warm exposure leads to a microbiome with increased polyamine synthesis. The predicted change in increased polyamines was confirmed by targeted metabolomics and could be linked to a large extent to the increase of the species *Akkermainsia muciniphila* (Figure 6.1 on the facing page). Hence, our approach not only makes it possible to identify the change in functional potential of a microbiome but also to link it to the driver species. In so far, we were able to fulfill the hopes of a genome-centric approach to functional metagenomics as described in section 1.1.2.

In contrast to other tools that calculate relative pathway abundance for the whole microbiome, our method calculates the abundances of pathways independent from each other. The rationale behind this is that an additional function in a genome does not constrain the functional potential of other functions. For example, a microbiome, where all microbes can degrade galactose and fucose, has an abundance of 1 for these two pathways and not 0.5, ignoring other pathways.

For the study in Chevalier, Kieser, et al., 2020, the pathway prediction was performed outside `metagenome-atlas` using the MetaCyc database (Caspi et al., 2016). In the meantime, we integrated `DRAM` (Shaffer et al., 2020), a robust func-

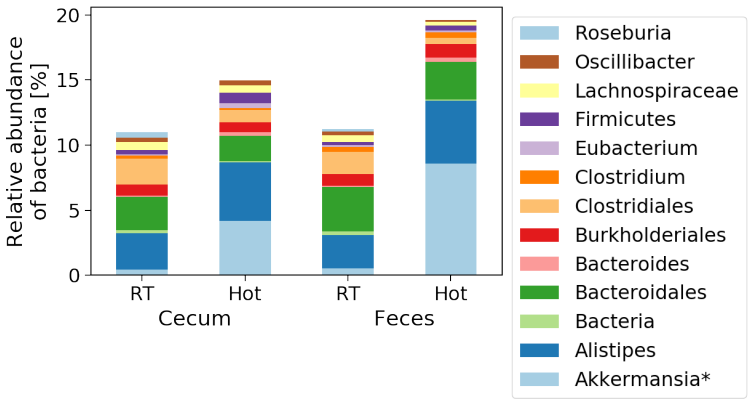

Fig. 6.1 Relative abundance of the bacteria that exhibit the pathway spermine and spermidine synthesis. The relative abundance is summed at the genus level. Source: Chevalier, Kieser, et al., 2020 Figure S6B.

tional prediction tool, into a newer version of the program that allows inferring KEGG modules (Kanehisa & Goto, 2000) and other annotations. See section 4.2 as an example.

The functional changes were assessed with a non-parametrical test based on relative abundance. According to what I described in ch. 5, it would be better to explore ways for statistical analysis of pathway abundance that take the compositional nature of microbiome data into account. One way would be to calculate the log ratio of the abundance values A:

$$\log \frac{A_{\text{pathway}}}{1 - A_{\text{pathway}}}$$

$$= \log \frac{\sum A_{\text{species with pathway}}}{\sum A_{\text{species without pathway}}}$$

Even better would be to extend the calculation of such ratios to include the Abundaces of multiple pathways. For example, the ratio between the abundance values of a synthesis and degradation pathways for a molecule could be more predictive than one pathway alone. Machine-learning tools described in sec. 5.2.3 should be perfectly suited to identify the ratios of pathways associated with the metadata automatically.

6.4 Metagenomics in a post-assembly era

At the beginning of my Ph.D., Tyson and his collaborators re-analyzed many public metagenomes and recovered nearly 8'000 genomes (Donovan H. Parks, Rinke, et al., 2017). Their publication marked the beginning of a new era of large-scale (re-)assembly in metagenomics (See Fig. 6.2). Other studies soon followed. During my thesis, three groups assembled and processed almost all publicly available human gut metagenomes (Almeida et al., 2019; Nayfach et al., 2019; Pasolli et al., 2019). Collections of genomes for the gut microbiome of farm animals were also released during my P.h.D. (Stewart et al., 2019; Glendinning et al., 2020). Each study recovers dozens of new species, and rarefaction analyses show that saturation is approaching.

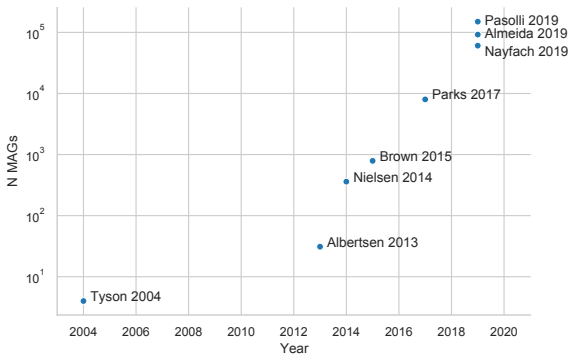

Fig. 6.2 The plot shows studies that published sets of metagenome-assembled genomes (MAGs). The list is not exhaustive but shows the general trend to increased numbers of MAGs.

As described in chapter 4, we took the challenge to create a comprehensive collection of reference genomes from the mouse gut microbiome by processing all public mouse metagenomes with `metagenome-atlas`. Rarefaction analysis shows that our collection contains practically all bacterial species living in the gut of laboratory mice. We were surprised how few species were shared between our catalog from the mouse gut and the human counterpart. This, hereto infeasible analysis, effectively challenges the views on the analogy between human and mouse microbiota.

Similarly, Lesker et al. recovered a large set of mouse metagenomes and tried to link them to 16S rDNA genes in order to enhance amplicon sequencing.

Beresford-Jones et al. created MAGs from the mouse gut and cultivated 276 new strains from the same environment.

With the accumulation of large-scale studies that recovered genomes from metagenomes, the lack of reference genomes for major host-associated microbiomes diminishes. Did we achieve our goal to enable the genome-centric analysis metagenomes, which hereto lacked reference genomes? I think it is fair to answer yes to this rhetorical question.

Accordingly, we are about to enter a **post-assembly era**, where the assembly of metagenomes is no longer necessary, and microbiomes can be profiled directly. Having comprehensive catalogs of genomes for many microbiomes is a milestone in the analysis of microbiomes[2]. If the profiling of metagenomes is simple, it becomes even more important that we use the results effectively, as I explained in chapter 5.

Does this render assembly and genomic binning unnecessary? Are pipelines, like `metagenome-atlas`, no longer useful? Surely, there are still challenges in several non-gut metagenomes. For example skin, and lung microbiomes yield low-biomass samples and are therefore difficult to assemble. Also, soil and ocean microbiomes are more complex than the typical gut microbiome, and therefore harder to assemble[3]. But even for metagenomes with good coverage, assembly and binning can give a crucial benefit to capture dataset-specific strain variation as I explained in section 6.2.2.

6.4.1 Improving current genome collections

The field has come a long way in recovering genomes from metagenomes, but there is still room to improve the current genome references: First, by improving the quality of the recovered genomes. Second, by deepening the resolution by including more strain-variation and finally, by widening the scope by including plasmids, viruses, and eukaryotes.

[2]Actually, it is included in Nature's Milestones in human microbiota research (2019)

[3]Even though, for the ocean microbiome, a significant improvement was made (Lucas Paoli et al., 2021) recently.

Recover complete genomes from metagenomes

The genomes reconstructed from metagenomes are of variable quality. While multiple genome reconstructions are available for highly prevalent species, and one can choose the best one as a representative, rare species are often represented only by one medium-quality MAG. Incomplete or "composite MAGs reduce the quality of public genome repositories" (Shaiber & Eren, 2019). Moreover, even what is called a high-quality genome is mostly an estimation based on marker genes (See section 1.2.3). The quality estimation is dependent on the marker gene set used. Therefore a bias in the marker gene set induces a bias in the genome estimation. More fundamentally, I think genome quality estimation is overused. Metagenomic binners are evaluated on the quality score of their genome predictions. Marker genes are even used during the binning by some algorithms or by tools that combine and consolidate the results of multiple binners (Sieber et al., 2018). I fear this to be an example of **Goodhart's Law**: "When a measure becomes a target, it ceases to be a good measure." (Strathern, 1997).

The fundamental problem of estimating the quality of a genome solely by assessing the presence and duplication of marker genes is that this approach is entirely blind to contigs that do not contain marker genes. A MAG may have many contigs from a wholly different species without affecting the contamination estimation. Similarly, a 'complete' genome might still be missing genome content that is not assessed by marker genes. New tools have been developed that claim to purify a MAG of this unassessed contamination (`MAGpurify`, and `conterminator` (Nayfach et al., 2019; Steinegger & Steven L. Salzberg, 2020)) or to search for additional contigs that were missed (`Spacegraphcats` and `GraphBin` (C. Titus Brown et al., 2020; Mallawaarachchi et al., 2020)). However, often it is only through manual curation that one can achieve an accurate and complete genome from metagenomes (Chen et al., 2020).

Ideally, a MAG would be assembled in one continuous sequence. For now, this only rarely happens. It is important to note that most large-scale efforts use single-sample assembly, as this approach is the most scalable. Binning methods that efficiently use differential abundance (See box on page 13) are promising ways to improve the continuity and quality of MAGs. Of note, long-read sequencing, which makes assembly much easier or even superfluous, is becoming more common. Also, culturing of microbes from metagenomes is advancing.

Both techniques have the potential to complement or even replace the recovery of genomes from metagenomes.

Including subspecies diversity

Lucas Paoli & Shinichi Sunagawa postulate that we are in the middle of a *resolution revolution* in microbiomics[4]. Increased sampling will allow us to study the microbiome in more detail in space and over time. The third dimension in which they see resolution increase is in the taxonomic dimension.

Having recovered over 30'000 genomes for the mouse gut, we were able to investigate subspecies diversity. We were able to identify subspecies with specific gene contents. We saw a consistent **strain-boundary** at 95.5% ANI for many species (ch. 4 Extended Data Fig. 2). The boundary is also visible in strain comparisons based on isolates genomes (Van Rossum et al., 2020). Below this threshold, two organisms derived from a common ancestor have practically no more genome fraction in common (Sakoparnig et al., 2021). We found many strain pairs with similarity $> 95\%$ ANI because mice are coprophages and share their microbiome with other mice within a cage. By taking the subspecies into account, we were able to increase the mapping rate of a new mouse metagenome from 83 to 90%.

Going beyond bacteria

Most of the DNA in a gut microbiome comes from bacteria. However, often overlooked are organisms from the domains archaea and eukaryotes. Eukaryotes, such as fungi and protists, can be very large compared to prokaryotes and make up a sizable fraction of a microbiome's biomass without contributing an equal fraction to the metagenome (DNA). Viruses, plasmids, and other genetic elements are also essential members of microbiomes that are easily sequenced using shotgun metagenomics.

For generating the CMGM, we not only looked for MAGs of bacteria but also viruses and plasmids. We did not assemble any genomes of archaea, which let us assume that they are not living in the mouse gut of laboratory mice. We did not look for eukaryotes. Nevertheless, we think our catalog is an important resource to perform a comprehensive analysis of the mouse gut microbiome.

[4]The study of microbiomes. Metagenomics is a subfield thereof.

The inclusion of plasmids and viruses increased the mapping rate of a mouse metagenome sample from 90% to 94%.

6.4.2 Comprehensive sets of functionally annotated genomes for the human and mouse gut

For the update of CMGM (Sec. 4.2), we annotated comprehensive sets of genomes from the mouse *and human gut*. We made the functional annotations publicly available, together with the code, to calculate pathway abundance and associate functional changes with the condition or treatment of interest. These resources enable others to benefit from the advantages of genome-resolved metagenomics and efficiently perform functional analysis of mouse and human metagenomes.

References

Abubucker, Sahar, Nicola Segata, Johannes Goll, Alyxandria M. Schubert, Jacques Izard, Brandi L. Cantarel, Beltran Rodriguez-Mueller, Jeremy Zucker, Mathangi Thiagarajan, Bernard Henrissat, Owen White, Scott T. Kelley, Barbara Methé, Patrick D. Schloss, Dirk Gevers, Makedonka Mitreva, Curtis Huttenhower (June 2012). "Metabolic Reconstruction for Metagenomic Data and Its Application to the Human Microbiome". In: *PLoS Computational Biology* 8.6. Ed. by Jonathan A. Eisen, e1002358. DOI: 10.1371/journal.pcbi.1002358.

Aitchison, John (Jan. 1982). "The Statistical Analysis of Compositional Data". In: *Journal of the Royal Statistical Society: Series B (Methodological)* 44.2, pp. 139–160. DOI: 10.1111/j.2517-6161.1982.tb01195.x.

Albertsen, Mads, Philip Hugenholtz, Adam Skarshewski, Kåre L Nielsen, Gene W Tyson, Per H Nielsen (June 2013). "Genome sequences of rare, uncultured bacteria obtained by differential coverage binning of multiple metagenomes". In: *Nature Biotechnology* 31.6, pp. 533–538. DOI: 10.1038/nbt.2579.

Almeida, Alexandre, Alex L. Mitchell, Miguel Boland, Samuel C. Forster, Gregory B. Gloor, Aleksandra Tarkowska, Trevor D. Lawley, Robert D. Finn (Apr. 2019). "A new genomic blueprint of the human gut microbiota". In: *Nature* 568.7753, pp. 499–504. DOI: 10.1038/s41586-019-0965-1.

Anderson, Stephen (1981). "Shotgun DNA sequencing using cloned DNase I-generated fragments". In: *Nucleic Acids Research* 9.13, pp. 3015–3027. DOI: 10.1093/nar/9.13.3015.

Belcour, Arnaud, Clémence Frioux, Méziane Aite, Anthony Bretaudeau, Falk Hildebrand, Anne Siegel (Dec. 2020). "Metage2Metabo, microbiota-scale metabolic complementarity for the identification of key species". In: *eLife* 9. DOI: 10.7554/eLife.61968.

Beresford-Jones, Benjamin S, Samuel C Forster, Mark D Stares, George Notley, Elisa Viciani, Hilary P Browne, Nitin Kumar, Kevin Vervier, Alexandre Almeida, Trevor D Lawley, Virginia A Pedicord (Jan. 2021). "Functional and taxonomic comparison of mouse and human gut microbiotas using extensive culturing and metagenomics". In: *bioRxiv*, p. 2021.02.11.430759. DOI: 10.1101/2021.02.11.430759.

Bowers, Robert M et al. (Aug. 2017). "Minimum information about a single amplified genome (MISAG) and a metagenome-assembled genome (MIMAG) of bacteria and archaea". In: *Nature Biotechnology* 35.8, pp. 725–731. DOI: 10.1038/nbt.3893.

Brenner, D. J. (Oct. 1973). "Deoxyribonucleic Acid Reassociation in the Taxonomy of Enteric Bacteria". In: *International Journal of Systematic Bacteriology* 23.4, pp. 298–307. DOI: 10.1099/00207713-23-4-298.

Brown, C. Titus, Dominik Moritz, Michael P. O'Brien, Felix Reidl, Taylor Reiter, Blair D. Sullivan (July 2020). "Exploring neighborhoods in large metagenome assembly graphs using spacegraphcats reveals hidden sequence diversity". In: *Genome Biology* 21.1, p. 164. DOI: 10.1186/s13059-020-02066-4.

Brown, Christopher T., Laura A. Hug, Brian C. Thomas, Itai Sharon, Cindy J. Castelle, Andrea Singh, Michael J. Wilkins, Kelly C. Wrighton, Kenneth H. Williams, Jillian F. Banfield (July 2015). "Unusual biology across a group comprising more than 15% of domain Bacteria". In: *Nature* 523.7559, pp. 208–211. DOI: 10.1038/nature14486.

Callahan, Benjamin J, Paul J McMurdie, Michael J Rosen, Andrew W Han, Amy Jo A Johnson, Susan P Holmes (July 2016). "DADA2: High-resolution sample inference from Illumina amplicon data". In: *Nature Methods* 13.7, pp. 581–583. DOI: 10.1038/nmeth.3869.

Callahan, Benjamin J., Paul J. McMurdie, Susan P. Holmes (Dec. 2017). "Exact sequence variants should replace operational taxonomic units in marker-gene data analysis". In: *ISME Journal* 11.12, pp. 2639–2643. DOI: 10.1038/ismej.2017.119.

Cannon, Barbara, Jan Nedergaard (2017). "Cell Metabolism Previews What Ignites UCP1?" In: *Cell Metabolism* 26, pp. 697–698. DOI: 10.1016/j.cmet.2017.10.012.

Caspi, Ron, Richard Billington, Luciana Ferrer, Hartmut Foerster, Carol A. Fulcher, Ingrid M. Keseler, Anamika Kothari, Markus Krummenacker, Mario Latendresse, Lukas A. Mueller, Quang Ong, Suzanne Paley, Pallavi Subhraveti, Daniel S. Weaver, Peter D. Karp (Jan. 2016). "The MetaCyc database of metabolic pathways and enzymes and the BioCyc collection of pathway/genome databases". In: *Nucleic Acids Research* 44.D1, pp. D471–D480. DOI: 10.1093/nar/gkv1164.

Chechi, Kanta, Andre C. Carpentier, Denis Richard (Aug. 2013). "Understanding the brown adipocyte as a contributor to energy homeostasis". In: *Trends in Endocrinology & Metabolism* 24.8, pp. 408–420. DOI: 10.1016/j.tem.2013.04.002.

Chen, Lin-Xing, Karthik Anantharaman, Alon Shaiber, A. Murat Eren, Jillian F. Banfield (Mar. 2020). "Accurate and complete genomes from metagenomes". In: *Genome Research* 30.3, pp. 315–333. DOI: 10.1101/gr.258640.119.

Chevalier, Claire, Silas Kieser, Melis Çolakoğlu, Noushin Hadadi, Julia Brun, Dorothée Rigo, Nicolas Suárez-Zamorano, Martina Spiljar, Salvatore Fabbiano, Björn Busse, Julijana Ivanišević, Andrew Macpherson, Nicolas Bonnet, Mirko Trajkovski (Oct. 2020). "Warmth Prevents Bone Loss Through the Gut Microbiota". In: *Cell Metabolism* 32.4, 575–590.e7. DOI: 10.1016/j.cmet.2020.08.012.

Chevalier, Claire, Ozren Stojanović, Didier J. Colin, Nicolas Suarez-Zamorano, Valentina Tarallo, Christelle Veyrat-Durebex, Dorothée Rigo, Salvatore Fabbiano, Ana Stevanović, Stefanie Hagemann, Xavier Montet, Yann Seimbille, Nicola Zamboni, Siegfried Hapfelmeier, Mirko Trajkovski, Ozren Stojanovi, Didier J. Colin, Nicola Zamboni, Siegfried Hapfelmeier, Mirko Trajkovski Correspondence (Dec. 2015). "Gut Microbiota Orchestrates Energy Homeostasis during Cold". In: *Cell* 163.6, pp. 1360–1374. DOI: 10.1016/j.cell.2015.11.004.

Clarke, Erik L., Louis J. Taylor, Chunyu Zhao, Andrew Connell, Jung-Jin Lee, Bryton Fett, Frederic D. Bushman, Kyle Bittinger (Dec. 2019). "Sunbeam: an extensible pipeline for analyzing metagenomic sequencing experiments". In: *Microbiome* 7.1, p. 46. DOI: 10.1186/s40168-019-0658-x.

Costea, Paul I, Luis Pedro Coelho, Shinichi Sunagawa, Robin Munch, Jaime Huerta-Cepas, Kristoffer Forslund, Falk Hildebrand, Almagul Kushugulova, Georg Zeller, Peer Bork (Dec. 2017). "Subspecies in the global human gut microbiome". In: *Molecular Systems Biology* 13.12, p. 960. DOI: 10.15252/msb.20177589.

Cypess, Aaron M., Lauren S. Weiner, Carla Roberts-Toler, Elisa Franquet Elía, Skyler H. Kessler, Peter A. Kahn, Jeffrey English, Kelly Chatman, Sunia A. Trauger, Alessandro Doria, Gerald M. Kolodny (Jan. 2015). "Activation of Human Brown Adipose Tissue by a β3-Adrenergic Receptor Agonist". In: *Cell Metabolism* 21.1, pp. 33–38. DOI: 10.1016/j.cmet.2014.12.009.

Dijk, Erwin L. van, Yan Jaszczyszyn, Delphine Naquin, Claude Thermes (Sept. 2018). "The Third Revolution in Sequencing Technology". In: *Trends in Genetics* 34.9, pp. 666–681. DOI: 10.1016/j.tig.2018.05.008.

Edgar, Robert C (July 2018). "Updating the 97% identity threshold for 16S ribosomal RNA OTUs". In: *Bioinformatics* 34.14. Ed. by Alfonso Valencia, pp. 2371–2375. DOI: 10.1093/bioinformatics/bty113.

Eren, A. Murat, Tom O. Delmont (Apr. 2017). *Predicting CPR genomes in metagenomic bins – Meren Lab*.

Eren, A. Murat, Özcan C. Esen, Christopher Quince, Joseph H. Vineis, Hilary G. Morrison, Mitchell L. Sogin, Tom O. Delmont (Oct. 2015). "Anvi'o: an advanced analysis and visualization platform for 'omics data". In: *PeerJ* 3, e1319. DOI: 10.7717/peerj.1319.

Fabbiano, Salvatore, Nicolas Suárez-Zamorano, Claire Chevalier, Vladimir Lazarević, Silas Kieser, Dorothée Rigo, Stefano Leo, Christelle Veyrat-Durebex, Nadia Gaïa, Marcello Maresca, Doron Merkler, Mercedes Gomez de Agüero, Andrew Macpherson, Jacques Schrenzel, Mirko Trajkovski (Aug. 2018). "Functional Gut Microbiota Remodeling Contributes to the Caloric Restriction-Induced Metabolic Improvements". In: *Cell Metabolism* 0.0. DOI: 10.1016/j.cmet.2018.08.005.

Fernandes, Andrew D, Jennifer Ns Reid, Jean M Macklaim, Thomas A McMurrough, David R Edgell, Gregory B Gloor (2014). "Unifying the analysis of high-throughput sequencing datasets: characterizing RNA-seq, 16S rRNA gene se-

quencing and selective growth experiments by compositional data analysis." In: *Microbiome* 2, p. 15. DOI: 10.1186/2049-2618-2-15.

Fernández, Lucía, Ana Rodríguez, Pilar García (May 2018). "Phage or foe: an insight into the impact of viral predation on microbial communities". In: *The ISME Journal* 12.5, pp. 1171–1179. DOI: 10.1038/s41396-018-0049-5.

Fleischmann, Robert D. et al. (July 1995). "Whole-genome random sequencing and assembly of Haemophilus influenzae Rd". In: *Science* 269.5223, pp. 496–512. DOI: 10.1126/science.7542800.

Franzosa, Eric A, Lauren J. McIver, Gholamali Rahnavard, Luke R Thompson, Melanie Schirmer, George Weingart, Karen Schwarzberg Lipson, Rob Knight, J Gregory Caporaso, Nicola Segata, Curtis Huttenhower (Nov. 2018). "Species-level functional profiling of metagenomes and metatranscriptomes". In: *Nature Methods* 15.11, pp. 962–968. DOI: 10.1038/s41592-018-0176-y.

Fritz, Adrian, Peter Hofmann, Stephan Majda, Eik Dahms, Johannes Dröge, Jessika Fiedler, Till R. Lesker, Peter Belmann, Matthew Z. Demaere, Aaron E. Darling, Alexander Sczyrba, Andreas Bremges, Alice C. McHardy (Feb. 2019). "CAMISIM: Simulating metagenomes and microbial communities". In: *Microbiome* 7.1, p. 17. DOI: 10.1186/s40168-019-0633-6.

Ghorbani, Masoud, Thomas H. Claus, Jean Himms-Hagen (July 1997). "Hypertrophy of brown adipocytes in brown and white adipose tissues and reversal of diet-induced obesity in rats treated with a β3-adrenoceptor agonist". In: *Biochemical Pharmacology* 54.1, pp. 121–131. DOI: 10.1016/S0006-2952(97)00162-7.

Glendinning, Laura, Robert D. Stewart, Mark J. Pallen, Kellie A. Watson, Mick Watson (Dec. 2020). "Assembly of hundreds of novel bacterial genomes from the chicken caecum". In: *Genome Biology* 21.1, p. 34. DOI: 10.1186/s13059-020-1947-1.

Gloor, Gregory B., Jean M. Macklaim, Vera Pawlowsky-Glahn, Juan J. Egozcue (Nov. 2017). "Microbiome Datasets Are Compositional: And This Is Not Optional". In: *Frontiers in Microbiology* 8, p. 2224. DOI: 10.3389/fmicb.2017.02224.

Goldenfeld, Nigel, Norman R. Pace (Feb. 2013). *Carl R. Woese (1928-2012)*. DOI: 10.1126/science.1235219.

Gordon-Rodriguez, Elliott, Thomas P Quinn, John P Cunningham (Feb. 2021). "Learning Sparse Log-Ratios for High-Throughput Sequencing Data". In: *bioRxiv*. DOI: 10.1101/2021.02.11.430695.

Gruber-Vodicka, Harald R., Brandon K. B. Seah, Elmar Pruesse (Oct. 2020). "phyloFlash: Rapid Small-Subunit rRNA Profiling and Targeted Assembly from Metagenomes". In: *mSystems* 5.5. Ed. by Mani Arumugam. DOI: 10.1128/mSystems.00920-20.

Guarner, Francisco, Juan-R Malagelada (Feb. 2003). "Gut flora in health and disease". In: *The Lancet* 361.9356, pp. 512–519. DOI: 10.1016/S0140-6736(03)12489-0.

Guerra, C, R A Koza, H Yamashita, K Walsh, L P Kozak (July 1998). "Emergence of brown adipocytes in white fat in mice is under genetic control. Effects on body weight and adiposity." In: *Journal of Clinical Investigation* 102.2, pp. 412–420. DOI: 10.1172/JCI3155.

Handelsman, Jo, Michelle R. Rondon, Sean F. Brady, Jon Clardy, Robert M. Goodman (Oct. 1998). "Molecular biological access to the chemistry of unknown soil microbes: a new frontier for natural products". In: *Chemistry & Biology* 5.10, R245–R249. DOI: 10.1016/S1074-5521(98)90108-9.

Heather, James M., Benjamin Chain (Jan. 2016). *The sequence of sequencers: The history of sequencing DNA*. DOI: 10.1016/j.ygeno.2015.11.003.

Hungate, R E (Nov. 1944). "Studies on Cellulose Fermentation: I. The Culture and Physiology of an Anaerobic Cellulose-digesting Bacterium." In: *Journal of bacteriology* 48.5, pp. 499–513. DOI: 10.1128/JB.48.5.499-513.1944.

Jain, Chirag, Luis M. Rodriguez-R, Adam M. Phillippy, Konstantinos T. Konstantinidis, Srinivas Aluru (Dec. 2018). "High throughput ANI analysis of 90K prokaryotic genomes reveals clear species boundaries". In: *Nature Communications* 9.1, p. 5114. DOI: 10.1038/s41467-018-07641-9.

Johnson, Jethro S., Daniel J. Spakowicz, Bo-Young Hong, Lauren M. Petersen, Patrick Demkowicz, Lei Chen, Shana R. Leopold, Blake M. Hanson, Hanako O. Agresta, Mark Gerstein, Erica Sodergren, George M. Weinstock (Dec. 2019). "Evaluation of 16S rRNA gene sequencing for species and strain-level microbiome analysis". In: *Nature Communications* 10.1, p. 5029. DOI: 10.1038/s41467-019-13036-1.

Josse, John, A D Kaiser, Arthur Kornberg (1961). *Enzymatic Synthesis of Deoxyribonucleic Acid VIII. FREQUENCIES OF NEAREST NEIGHBOR BASE SEQUENCES IN DEOXYRIBONUCLEIC ACID*. Tech. rep. 3, pp. 864–875. DOI: 10.1016/S0021-9258(18)64321-2.

Kanehisa, M, S Goto (Jan. 2000). "KEGG: kyoto encyclopedia of genes and genomes." In: *Nucleic acids research* 28.1, pp. 27–30.

Karst, Søren M, Morten S Dueholm, Simon J McIlroy, Rasmus H Kirkegaard, Per H Nielsen, Mads Albertsen (Feb. 2018). "Retrieval of a million high-quality, full-length microbial 16S and 18S rRNA gene sequences without primer bias". In: *Nature Biotechnology* 36.2, pp. 190–195. DOI: 10.1038/nbt.4045.

Kashtan, N., S. E. Roggensack, S. Rodrigue, J. W. Thompson, S. J. Biller, A. Coe, H. Ding, P. Marttinen, R. R. Malmstrom, R. Stocker, M. J. Follows, R. Stepanauskas, S. W. Chisholm (Apr. 2014). "Single-Cell Genomics Reveals Hundreds of Coexisting Subpopulations in Wild Prochlorococcus". In: *Science* 344.6182, pp. 416–420. DOI: 10.1126/science.1248575.

Kieser, Silas, Joseph Brown, Evgeny M. Zdobnov, Mirko Trajkovski, Lee Ann McCue (Dec. 2020). "ATLAS: a Snakemake workflow for assembly, annotation, and genomic binning of metagenome sequence data". In: *BMC Bioinformatics* 21.1, p. 257. DOI: 10.1186/s12859-020-03585-4.

Kieser, Silas, Shafiqul A. Sarker, Olga Sakwinska, Francis Foata, Shamima Sultana, Zeenat Khan, Shoheb Islam, Nadine Porta, Séverine Combremont, Bertrand Betrisey, Coralie Fournier, Aline Charpagne, Patrick Descombes, Annick Mercenier, Bernard Berger, Harald Brüssow (June 2018). "Bangladeshi children with acute diarrhoea show faecal microbiomes with increased Streptococcus abundance, irrespective of diarrhoea aetiology". In: *Environmental Microbiology* 20.6, pp. 2256–2269. DOI: 10.1111/1462-2920.14274.

Kieser, Silas, Evgeny M Zdobnov, Mirko Trajkovski (Mar. 2021). "Comprehensive mouse gut metagenome catalog reveals major difference to the human counterpart". In: *bioRxiv*, p. 2021.03.18.435958. DOI: 10.1101/2021.03.18.435958.

Kim, Kyoung-Han, Yun Hye Kim, Joe Eun Son, Ju Hee Lee, Sarah Kim, Min Seon Choe, Joon Ho Moon, Jian Zhong, Kiya Fu, Florine Lenglin, Jeong-Ah Yoo, Philip J Bilan, Amira Klip, Andras Nagy, Jae-Ryong Kim, Jin Gyoon Park, Samer MI Hussein, Kyung-Oh Doh, Chi-chung Hui, Hoon-Ki Sung (Nov. 2017). "Intermittent fasting promotes adipose thermogenesis and metabolic homeostasis via VEGF-mediated alternative activation of macrophage". In: *Cell Research* 27.11, pp. 1309–1326. DOI: 10.1038/cr.2017.126.

Konstantinidis, K. T., J. M. Tiedje (Feb. 2005). "Genomic insights that advance the species definition for prokaryotes". In: *Proceedings of the National Academy of Sciences* 102.7, pp. 2567–2572. DOI: 10.1073/pnas.0409727102.

Kopecky, J, G Clarke, S Enerbäck, B Spiegelman, L P Kozak (Dec. 1995). "Expression of the mitochondrial uncoupling protein gene from the aP2 gene promoter prevents genetic obesity." In: *Journal of Clinical Investigation* 96.6, pp. 2914–2923. DOI: 10.1172/JCI118363.

Kuczynski, Justin, Zongzhi Liu, Catherine Lozupone, Daniel McDonald, Noah Fierer, Rob Knight (Oct. 2010). "Microbial community resemblance methods differ in their ability to detect biologically relevant patterns". In: *Nature Methods* 7.10, pp. 813–819. DOI: 10.1038/nmeth.1499.

Lagkouvardos, Ilias et al. (Oct. 2016). "The Mouse Intestinal Bacterial Collection (miBC) provides host-specific insight into cultured diversity and functional potential of the gut microbiota". In: *Nature Microbiology* 1.10, p. 16131. DOI: 10.1038/nmicrobiol.2016.131.

Lane, D J, B Pace, G J Olsen, D A Stahl, M L Sogin, N R Pace (Oct. 1985). "Rapid determination of 16S ribosomal RNA sequences for phylogenetic analyses." In: *Proceedings of the National Academy of Sciences of the United States of America* 82.20, pp. 6955–9. DOI: 10.1073/pnas.82.20.6955.

Lesker, Till R., Abilash C. Durairaj, Eric J.C. Gálvez, Ilias Lagkouvardos, John F. Baines, Thomas Clavel, Alexander Sczyrba, Alice C. McHardy, Till Strowig (Mar. 2020). "An Integrated Metagenome Catalog Reveals New Insights into the Murine Gut Microbiome". In: *Cell Reports* 30.9, 2909–2922.e6. DOI: 10.1016/j.celrep.2020.02.036.

Li, Dinghua, Chi-Man Liu, Ruibang Luo, Kunihiko Sadakane, Tak-Wah Lam (May 2015). "MEGAHIT: an ultra-fast single-node solution for large and complex

metagenomics assembly via succinct de Bruijn graph". In: *Bioinformatics* 31.10, pp. 1674–1676. DOI: 10.1093/bioinformatics/btv033.

Li, Guolin, Cen Xie, Siyu Lu, Robert G. Nichols, Yuan Tian, Licen Li, Daxeshkumar Patel, Yinyan Ma, Chad N. Brocker, Tingting Yan, Kristopher W. Krausz, Rong Xiang, Oksana Gavrilova, Andrew D. Patterson, Frank J. Gonzalez (Oct. 2017). "Intermittent Fasting Promotes White Adipose Browning and Decreases Obesity by Shaping the Gut Microbiota". In: *Cell Metabolism* 26.4, 672–685.e4. DOI: 10.1016/j.cmet.2017.08.019.

Lucas Paoli et al. (Mar. 2021). "Uncharted biosynthetic potential of the ocean microbiome". In: *bioRxiv*. DOI: 10.1101/2021.03.24.436479.

Machado, Daniel, Sergej Andrejev, Melanie Tramontano, Kiran Raosaheb Patil (Sept. 2018). "Fast automated reconstruction of genome-scale metabolic models for microbial species and communities". In: *Nucleic Acids Research* 46.15, pp. 7542–7553. DOI: 10.1093/nar/gky537.

Machado, Daniel, Oleksandr M. Maistrenko, Sergej Andrejev, Yongkyu Kim, Peer Bork, Kaustubh R. Patil, Kiran R. Patil (Feb. 2021). "Polarization of microbial communities between competitive and cooperative metabolism". In: *Nature Ecology & Evolution* 5.2, pp. 195–203. DOI: 10.1038/s41559-020-01353-4.

Magne, Fabien, Martin Gotteland, Lea Gauthier, Alejandra Zazueta, Susana Pesoa, Paola Navarrete, Ramadass Balamurugan (May 2020). "The Firmicutes / Bacteroidetes Ratio: A Relevant Marker of Gut Dysbiosis in Obese Patients?" In: *Nutrients* 12.5. DOI: 10.3390/nu12051474.

Mallawaarachchi, Vijini, Anuradha Wickramarachchi, Yu Lin (June 2020). "GraphBin: refined binning of metagenomic contigs using assembly graphs". In: *Bioinformatics* 36.11. Ed. by Alfonso Valencia, pp. 3307–3313. DOI: 10.1093/bioinformatics/btaa180.

Manni, Mosè, Matthew R Berkeley, Mathieu Seppey, Felipe A Simao, Evgeny M Zdobnov (June 2021). "BUSCO update: novel and streamlined workflows along with broader and deeper phylogenetic coverage for scoring of eukaryotic, prokaryotic, and viral genomes". In: *ArXiv*.

Martín-Fernández, J. A., C. Barceló-Vidal, V. Pawlowsky-Glahn (Apr. 2003). "Dealing with Zeros and Missing Values in Compositional Data Sets Using Nonparametric Imputation". In: *Mathematical Geology* 35.3, pp. 253–278. DOI: 10.1023/A:1023866030544.

Martino, Cameron, James T. Morton, Clarisse A. Marotz, Luke R. Thompson, Anupriya Tripathi, Rob Knight, Karsten Zengler (Feb. 2019). "A Novel Sparse Compositional Technique Reveals Microbial Perturbations". In: *mSystems* 4.1. Ed. by Josh D. Neufeld, pp. 813–819. DOI: 10.1128/mSystems.00016-19.

Mason, Christopher (May 2021). *Could humans have contaminated Mars with life?*

McDonald, Daniel, Morgan N Price, Julia Goodrich, Eric P Nawrocki, Todd Z DeSantis, Alexander Probst, Gary L Andersen, Rob Knight, Philip Hugenholtz (Mar. 2012). "An improved Greengenes taxonomy with explicit ranks for eco-

logical and evolutionary analyses of bacteria and archaea". In: *The ISME Journal* 6.3, pp. 610–618. DOI: 10.1038/ismej.2011.139.

McMahon, Katherine (Feb. 2015). "'Metagenomics 2.0'". In: *Environmental Microbiology Reports* 7.1, pp. 38–39. DOI: 10.1111/1758-2229.12253.

Medema, Marnix H. et al. (Sept. 2015). "Minimum Information about a Biosynthetic Gene cluster". In: *Nature Chemical Biology* 11.9, pp. 625–631. DOI: 10.1038/nchembio.1890.

Mills, Evanna L., Kerry A. Pierce, Mark P. Jedrychowski, Ryan Garrity, Sally Winther, Sara Vidoni, Takeshi Yoneshiro, Jessica B. Spinelli, Gina Z. Lu, Lawrence Kazak, Alexander S. Banks, Marcia C. Haigis, Shingo Kajimura, Michael P. Murphy, Steven P. Gygi, Clary B. Clish, Edward T. Chouchani (Aug. 2018). "Accumulation of succinate controls activation of adipose tissue thermogenesis". In: *Nature* 560.7716, pp. 102–106. DOI: 10.1038/s41586-018-0353-2.

Morton, James T., Liam Toran, Anna Edlund, Jessica L. Metcalf, Christian Lauber, Rob Knight (Feb. 2017). "Uncovering the Horseshoe Effect in Microbial Analyses". In: *mSystems* 2.1, pp. 166–182. DOI: 10.1128/msystems.00166-16.

Myers, Eugene W. (Jan. 1995). "Toward Simplifying and Accurately Formulating Fragment Assembly". In: *Journal of Computational Biology* 2.2, pp. 275–290. DOI: 10.1089/cmb.1995.2.275.

Myers, Eugene W. et al. (Mar. 2000). "A Whole-Genome Assembly of Drosophila". In: *Science* 287.5461, pp. 2196–2204. DOI: 10.1126/science.287.5461.2196.

Nair, Prashant (Jan. 2012). "Woese and Fox: Life, rearranged." In: *Proceedings of the National Academy of Sciences of the United States of America* 109.4, pp. 1019–21. DOI: 10.1073/pnas.1120749109.

Nasko, Daniel J., Sergey Koren, Adam M. Phillippy, Todd J. Treangen (Oct. 2018). "RefSeq database growth influences the accuracy of k-mer-based lowest common ancestor species identification". In: *Genome Biology* 19.1, pp. 1–10. DOI: 10.1186/s13059-018-1554-6.

Nayfach, Stephen, Zhou Jason Shi, Rekha Seshadri, Katherine S. Pollard, Nikos C. Kyrpides (Apr. 2019). "New insights from uncultivated genomes of the global human gut microbiome". In: *Nature* 568.7753, pp. 505–510. DOI: 10.1038/s41586-019-1058-x.

Nielsen, Henrik Bjørn et al. (July 2014). "Identification and assembly of genomes and genetic elements in complex metagenomic samples without using reference genomes". In: *Nature Biotechnology* 32.8, pp. 822–828. DOI: 10.1038/nbt.2939.

Nissen, Jakob Nybo, Joachim Johansen, Rosa Lundbye Allesøe, Casper Kaae Sønderby, Jose Juan Almagro Armenteros, Christopher Heje Grønbech, Lars Juhl Jensen, Henrik Bjørn Nielsen, Thomas Nordahl Petersen, Ole Winther, Simon Rasmussen (Jan. 2021). "Improved metagenome binning and assembly using deep variational autoencoders". In: *Nature Biotechnology*. DOI: 10.1038/s41587-020-00777-4.

Nurk, Sergey, Sergey Koren, et al. (Jan. 2021). "The complete sequence of a human genome". In: *bioRxiv*, p. 2021.05.26.445798. DOI: 10.1101/2021.05.26.445798.

Nurk, Sergey, Dmitry Meleshko, Anton Korobeynikov, Pavel A. Pevzner (May 2017). "metaSPAdes: a new versatile metagenomic assembler". In: *Genome Research* 27.5, pp. 824–834. DOI: 10.1101/gr.213959.116.

Nussinov, Ruth (Oct. 1980). "Some rules in the ordering of nucleotides in the DNA". In: *Nucleic Acids Research* 8.19, pp. 4545–4562. DOI: 10.1093/nar/8.19.4545.

Okla, Meshail, Wei Wang, Inhae Kang, Anjeza Pashaj, Timothy Carr, Soonkyu Chung (Oct. 2015). "Activation of Toll-like Receptor 4 (TLR4) Attenuates Adaptive Thermogenesis via Endoplasmic Reticulum Stress". In: *Journal of Biological Chemistry* 290.44, pp. 26476–26490. DOI: 10.1074/jbc.M115.677724.

Ondov, Brian D., Todd J. Treangen, Páll Melsted, Adam B. Mallonee, Nicholas H. Bergman, Sergey Koren, Adam M. Phillippy (Dec. 2016). "Mash: fast genome and metagenome distance estimation using MinHash". In: *Genome Biology* 17.1, p. 132. DOI: 10.1186/s13059-016-0997-x.

Palarea-Albaladejo, Javier, Josep Antoni Martín-Fernández (Apr. 2015). "ZCompositions - R package for multivariate imputation of left-censored data under a compositional approach". In: *Chemometrics and Intelligent Laboratory Systems* 143, pp. 85–96. DOI: 10.1016/j.chemolab.2015.02.019.

Paoli, Lucas, Shinichi Sunagawa (Feb. 2021). "Space, time and microdiversity: towards a resolution revolution in microbiomics". In: *Environmental Microbiology Reports* 13.1, pp. 31–35. DOI: 10.1111/1758-2229.12897.

Parks, Donovan H, Maria Chuvochina, David W Waite, Christian Rinke, Adam Skarshewski, Pierre-Alain Chaumeil, Philip Hugenholtz (Nov. 2018). "A standardized bacterial taxonomy based on genome phylogeny substantially revises the tree of life". In: *Nature Biotechnology* 36.10, pp. 996–1004. DOI: 10.1038/nbt.4229.

Parks, Donovan H., Maria Chuvochina, Pierre-alain Chaumeil, Christian Rinke, Aaron J. Mussig, Philip Hugenholtz (Sept. 2020). "A complete domain-to-species taxonomy for Bacteria and Archaea". In: *Nature Biotechnology* 38.9, pp. 1079–1086. DOI: 10.1038/s41587-020-0501-8.

Parks, Donovan H., Christian Rinke, Maria Chuvochina, Pierre-Alain Chaumeil, Ben J. Woodcroft, Paul N. Evans, Philip Hugenholtz, Gene W. Tyson (Nov. 2017). "Recovery of nearly 8,000 metagenome-assembled genomes substantially expands the tree of life". In: *Nature Microbiology* 2.11, pp. 1533–1542. DOI: 10.1038/s41564-017-0012-7.

Pasolli, Edoardo, Francesco Asnicar, Serena Manara, Moreno Zolfo, Nicolai Karcher, Federica Armanini, Francesco Beghini, Paolo Manghi, Adrian Tett, Paolo Ghensi, Maria Carmen Collado, Benjamin L Rice, Casey DuLong, Xochitl C Morgan, Christopher D Golden, Christopher Quince, Curtis Huttenhower, Nicola Segata (Jan. 2019). "Extensive Unexplored Human Microbiome Diver-

sity Revealed by Over 150,000 Genomes from Metagenomes Spanning Age, Geography, and Lifestyle". In: *Cell* 176.3, 649–662.e20. DOI: 10.1016/j.cell.2019.01.001.

Pevzner, P. A., H. Tang, M. S. Waterman (Aug. 2001). "An Eulerian path approach to DNA fragment assembly". In: *Proceedings of the National Academy of Sciences* 98.17, pp. 9748–9753. DOI: 10.1073/pnas.171285098.

Qin, Junjie et al. (Mar. 2010). "A human gut microbial gene catalogue established by metagenomic sequencing". In: *Nature* 464.7285, pp. 59–65. DOI: 10.1038/nature08821.

Quast, Christian, Elmar Pruesse, Pelin Yilmaz, Jan Gerken, Timmy Schweer, Pablo Yarza, Jörg Peplies, Frank Oliver Glöckner (Nov. 2012). "The SILVA ribosomal RNA gene database project: improved data processing and web-based tools". In: *Nucleic Acids Research* 41.D1, pp. D590–D596. DOI: 10.1093/nar/gks1219.

Quinn, Thomas P, Ionas Erb, Mark F Richardson, Tamsyn M Crowley (Aug. 2018). "Understanding sequencing data as compositions: an outlook and review". In: *Bioinformatics* 34.16. Ed. by Jonathan Wren, pp. 2870–2878. DOI: 10.1093/bioinformatics/bty175.

Quinn, Thomas P, Elliott Gordon-Rodriguez, Ionas Erb (Apr. 2021). "A Critique of Differential Abundance Analysis, and Advocacy for an Alternative". In.

Richardson, Lorna J, Neil D Rawlings, Gustavo A Salazar, Alexandre Almeida, David R Haft, Gregory Ducq, Granger G Sutton, Robert D Finn (Jan. 2019). "Genome properties in 2019: a new companion database to InterPro for the inference of complete functional attributes". In: *Nucleic Acids Research* 47.D1, pp. D564–D572. DOI: 10.1093/nar/gky1013.

Sakoparnig, Thomas, Chris Field, Erik van Nimwegen (Jan. 2021). "Whole genome phylogenies reflect the distributions of recombination rates for many bacterial species". In: *eLife* 10, p. 601914. DOI: 10.7554/eLife.65366.

Sandberg, Rickard, Gösta Winberg, Carl Ivar Bränden, Alexander Kaske, Ingemar Ernberg, Joakim Cöster (Aug. 2001). "Capturing whole-genome characteristics in short sequences using a naïve Bayesian classifier". In: *Genome Research* 11.8, pp. 1404–1409. DOI: 10.1101/gr.186401.

Sanger, F., S. Nicklen, A. R. Coulson (Dec. 1977). "DNA sequencing with chain-terminating inhibitors". In: *Proceedings of the National Academy of Sciences* 74.12, pp. 5463–5467. DOI: 10.1073/pnas.74.12.5463.

Schloss, Patrick D (July 2021). "Amplicon Sequence Variants Artificially Split Bacterial Genomes into Separate Clusters". In: *mSphere*. Ed. by Katherine McMahon, p. 2021.02.26.433139. DOI: 10.1128/mSphere.00191-21.

Schloss, Patrick D., Jo Handelsman (Mar. 2005). "Introducing DOTUR, a Computer Program for Defining Operational Taxonomic Units and Estimating Species Richness". In: *Applied and Environmental Microbiology* 71.3, pp. 1501–1506. DOI: 10.1128/AEM.71.3.1501-1506.2005.

Segata, Nicola, Jacques Izard, Levi Waldron, Dirk Gevers, Larisa Miropolsky, Wendy S Garrett, Curtis Huttenhower (2011). "Metagenomic biomarker discovery and explanation". In: *Genome Biology* 12.6, R60. DOI: 10.1186/gb-2011-12-6-r60.

Segata, Nicola, Levi Waldron, Annalisa Ballarini, Vagheesh Narasimhan, Olivier Jousson, Curtis Huttenhower (Aug. 2012). "Metagenomic microbial community profiling using unique clade-specific marker genes". In: *Nature Methods* 9.8, pp. 811–814. DOI: 10.1038/nmeth.2066.

Shaffer, Michael, Mikayla A. Borton, Bridget B. McGivern, Ahmed A. Zayed, Sabina Leanti La Rosa, Lindsey M. Solden, Pengfei Liu, Adrienne B. Narrowe, Josué Rodríguez-Ramos, Benjamin Bolduc, M. Consuelo Gazitúa, Rebecca A. Daly, Garrett J. Smith, Dean R. Vik, Phil B. Pope, Matthew B. Sullivan, Simon Roux, Kelly C Wrighton (Sept. 2020). "DRAM for distilling microbial metabolism to automate the curation of microbiome function". In: *Nucleic Acids Research* 48.16, pp. 8883–8900. DOI: 10.1093/nar/gkaa621.

Shaiber, Alon, A. Murat Eren (June 2019). "Composite Metagenome-Assembled Genomes Reduce the Quality of Public Genome Repositories". In: *mBio* 10.3. Ed. by David A. Relman. DOI: 10.1128/mBio.00725-19.

Sieber, Christian M. K., Alexander J. Probst, Allison Sharrar, Brian C. Thomas, Matthias Hess, Susannah G. Tringe, Jillian F. Banfield (July 2018). "Recovery of genomes from metagenomes via a dereplication, aggregation and scoring strategy". In: *Nature Microbiology* 3.7, pp. 836–843. DOI: 10.1038/s41564-018-0171-1.

Silverman, Justin D., Kimberly Roche, Sayan Mukherjee, Lawrence A. David (Jan. 2020). "Naught all zeros in sequence count data are the same". In: *Computational and Structural Biotechnology Journal* 18, pp. 2789–2798. DOI: 10.1016/j.csbj.2020.09.014.

Sim, Kathleen, Michael J. Cox, Harm Wopereis, Rocio Martin, Jan Knol, Ming-Shi Li, William O. C. M. Cookson, Miriam F. Moffatt, J. Simon Kroll (Mar. 2012). "Improved Detection of Bifidobacteria with Optimised 16S rRNA-Gene Based Pyrosequencing". In: *PLoS ONE* 7.3. Ed. by Niyaz Ahmed, e32543. DOI: 10.1371/journal.pone.0032543.

Stackebrandt, E, Brett M. Goebel (Oct. 1994). "Taxonomic Note: A Place for DNA-DNA Reassociation and 16S rRNA Sequence Analysis in the Present Species Definition in Bacteriology". In: *International Journal of Systematic and Evolutionary Microbiology* 44.4, pp. 846–849. DOI: 10.1099/00207713-44-4-846.

Staden, R. (1979). "A strategy of DNA sequencing employing computer programs". In: *Nucleic Acids Research* 6.7, pp. 2601–2610. DOI: 10.1093/nar/6.7.2601.

Staley, J T, A Konopka (Oct. 1985). "Measurement of in Situ Activities of Nonphotosynthetic Microorganisms in Aquatic and Terrestrial Habitats". In: *Annual Review of Microbiology* 39.1, pp. 321–346. DOI: 10.1146/annurev.mi.39.100185.001541.

Stein, J L, T L Marsh, K Y Wu, H Shizuya, E F DeLong (1996). "Characterization of uncultivated prokaryotes: isolation and analysis of a 40-kilobase-pair genome fragment from a planktonic marine archaeon." In: *Journal of bacteriology* 178.3, pp. 591–599. DOI: 10.1128/JB.178.3.591-599.1996.

Steinegger, Martin, Steven L. Salzberg (May 2020). "Terminating contamination: Large-scale search identifies more than 2,000,000 contaminated entries in GenBank". In: *Genome Biology* 21.1, p. 115. DOI: 10.1186/s13059-020-02023-1.

Stewart, Robert D., Marc D. Auffret, Amanda Warr, Alan W. Walker, Rainer Roehe, Mick Watson (Aug. 2019). "Compendium of 4,941 rumen metagenome-assembled genomes for rumen microbiome biology and enzyme discovery". In: *Nature Biotechnology* 37.8, pp. 953–961. DOI: 10.1038/s41587-019-0202-3.

Stojanović, Ozren, Silas Kieser, Mirko Trajkovski (Dec. 2018). "Common traits between the beige fat-inducing stimuli". In: *Current Opinion in Cell Biology* 55, pp. 67–73. DOI: 10.1016/J.CEB.2018.05.011.

Strathern, Marilyn (July 1997). "'Improving ratings': audit in the British University system". In: *European Review* 5.03, p. 305. DOI: 10.1017/S1062798700002660.

Sunagawa, Shinichi et al. (Dec. 2013). "Metagenomic species profiling using universal phylogenetic marker genes". In: *Nature Methods* 10.12, pp. 1196–1199. DOI: 10.1038/nmeth.2693.

Tamames, Javier, Fernando Puente-Sánchez (Jan. 2019). "SqueezeMeta, A Highly Portable, Fully Automatic Metagenomic Analysis Pipeline". In: *Frontiers in Microbiology* 9. DOI: 10.3389/fmicb.2018.03349.

Tettamanti Boshier, Florencia A., Sujatha Srinivasan, Anthony Lopez, Noah G. Hoffman, Sean Proll, David N. Fredricks, Joshua T. Schiffer (Apr. 2020). "Complementing 16S rRNA Gene Amplicon Sequencing with Total Bacterial Load To Infer Absolute Species Concentrations in the Vaginal Microbiome". In: *mSystems* 5.2. Ed. by J. Gregory Caporaso. DOI: 10.1128/mSystems.00777-19.

Tringe, S. G. (Apr. 2005). "Comparative Metagenomics of Microbial Communities". In: *Science* 308.5721, pp. 554–557. DOI: 10.1126/science.1107851.

Turnbaugh, Peter J., Ruth E. Ley, Micah Hamady, Claire M. Fraser-Liggett, Rob Knight, Jeffrey I. Gordon (Oct. 2007). "The Human Microbiome Project". In: *Nature* 449.7164, pp. 804–810. DOI: 10.1038/nature06244.

Tyson, Gene W., Jarrod Chapman, Philip Hugenholtz, Eric E. Allen, Rachna J. Ram, Paul M. Richardson, Victor V. Solovyev, Edward M. Rubin, Daniel S. Rokhsar, Jillian F. Banfield (Mar. 2004). "Community structure and metabolism through reconstruction of microbial genomes from the environment". In: *Nature* 428.6978, pp. 37–43. DOI: 10.1038/nature02340.

Uritskiy, Gherman V., Jocelyne DiRuggiero, James Taylor (Dec. 2018). "MetaWRAP—a flexible pipeline for genome-resolved metagenomic data analysis". In: *Microbiome* 6.1, p. 158. DOI: 10.1186/s40168-018-0541-1.

Vallery-Radot, René (1902). *The life of Pasteur*. New York: Phillips McClure, p. 142.

Van Rossum, Thea, Pamela Ferretti, Oleksandr M Maistrenko, Peer Bork (Sept. 2020). "Diversity within species: interpreting strains in microbiomes". In: *Na-*

ture Reviews Microbiology 18.9, pp. 491–506. DOI: 10.1038/s41579-020-0368-1.

Vandeputte, Doris, Gunter Kathagen, Kevin D'hoe, Sara Vieira-Silva, Mireia Valles-Colomer, João Sabino, Jun Wang, Raul Y Tito, Lindsey De Commer, Youssef Darzi, Séverine Vermeire, Gwen Falony, Jeroen Raes (Nov. 2017). "Quantitative microbiome profiling links gut community variation to microbial load". In: *Nature* 551.7681, pp. 507–511. DOI: 10.1038/nature24460.

Venter, J Craig (Jan. 2006). "Shotgunning the Human Genome: A Personal View". In: *Encyclopedia of Life Sciences*. Chichester, UK: John Wiley & Sons, Ltd. DOI: 10.1038/npg.els.0005850.

Venter, J. Craig, Mark D. Adams, et al. (Feb. 2001). "The Sequence of the Human Genome". In: *Science* 291.5507, pp. 1304–1351. DOI: 10.1126/science.1058040.

Venter, J. Craig, Karin Remington, et al. (Apr. 2004). "Environmental Genome Shotgun Sequencing of the Sargasso Sea". In: *Science* 304.5667, pp. 66–74. DOI: 10.1126/science.1093857.

Venter, J. Craig, Hamilton O. Smith, Leroy Hood (May 1996). "A new strategy for genome sequencing". In: *Nature* 381.6581, pp. 364–366. DOI: 10 . 1038 / 381364a0.

Vijay-Kumar, Matam, Benoit Chassaing, Manish Kumar, MarkT Baker, Vishal Singh (2014). "Mammalian gut immunity". In: *Biomedical Journal* 37.5, p. 246. DOI: 10.4103/2319-4170.130922.

Vollmers, John, Sandra Wiegand, Anne-Kristin Kaster (2017). "Comparing and Evaluating Metagenome Assembly Tools from a Microbiologist's Perspective - Not Only Size Matters!" In: *PLOS ONE* 12.1, e0169662. DOI: 10.1371/journal.pone.0169662.

Washburne, Alex D., Justin D. Silverman, James T. Morton, Daniel J. Becker, Daniel Crowley, Sayan Mukherjee, Lawrence A. David, Raina K. Plowright (May 2019). "Phylofactorization: a graph partitioning algorithm to identify phylogenetic scales of ecological data". In: *Ecological Monographs* 89.2, e01353. DOI: 10.1002/ecm.1353.

Whitman, W. B., D. C. Coleman, W. J. Wiebe (June 1998). "Prokaryotes: The unseen majority". In: *Proceedings of the National Academy of Sciences* 95.12, pp. 6578–6583. DOI: 10.1073/pnas.95.12.6578.

Wilson, K H, R B Blitchington (July 1996). "Human colonic biota studied by ribosomal DNA sequence analysis." In: *Applied and environmental microbiology* 62.7, pp. 2273–8. DOI: 10.1128/AEM.62.7.2273-2278.1996.

Woese, Carl. R., George. E. Fox (Nov. 1977). "Phylogenetic structure of the prokaryotic domain: The primary kingdoms". In: *Proceedings of the National Academy of Sciences* 74.11, pp. 5088–5090. DOI: 10.1073/pnas.74.11.5088.

Wong, Ruth G., Jia R. Wu, Gregory B. Gloor (Sept. 2016). "Expanding the UniFrac Toolbox". In: *PLOS ONE* 11.9. Ed. by Gabriel Moreno-Hagelsieb, e0161196. DOI: 10.1371/journal.pone.0161196.

Wood, Derrick E, Steven L Salzberg (Mar. 2014). "Kraken: ultrafast metagenomic sequence classification using exact alignments". In: *Genome Biology* 15.3, R46. DOI: 10.1186/gb-2014-15-3-r46.

Wood, Derrick E., Jennifer Lu, Ben Langmead (Dec. 2019). "Improved metagenomic analysis with Kraken 2". In: *Genome Biology* 20.1, p. 257. DOI: 10.1186/s13059-019-1891-0.

Wu, Jia R., Jean M. Macklaim, Briana L. Genge, Gregory B. Gloor (Apr. 2017). "Finding the centre: corrections for asymmetry in high-throughput sequencing datasets". In.

Xiao, Liang et al. (Oct. 2015). "A catalog of the mouse gut metagenome". In: *Nature Biotechnology* 33.10, pp. 1103–1108. DOI: 10.1038/nbt.3353.

Yooseph, Shibu et al. (Mar. 2007). "The Sorcerer II Global Ocean Sampling Expedition: Expanding the Universe of Protein Families". In: *PLoS Biology* 5.3. Ed. by Sean Eddy, e16. DOI: 10.1371/journal.pbio.0050016.

Young, Ed (2017). *Norm Pace Blew The Door Off The Microbial World*.

Zdobnov, Evgeny M, Dmitry Kuznetsov, Fredrik Tegenfeldt, Mosè Manni, Matthew Berkeley, Evgenia V Kriventseva (Jan. 2021). "OrthoDB in 2020: evolutionary and functional annotations of orthologs". In: *Nucleic Acids Research* 49.D1, pp. D389–D393. DOI: 10.1093/nar/gkaa1009.

Zhu, Qiyun, Christopher L. Dupont, Marcus B. Jones, Kevin M. Pham, Zhi-Dong Jiang, Herbert L. DuPont, Sarah K. Highlander (Dec. 2018). "Visualization-assisted binning of metagenome assemblies reveals potential new pathogenic profiles in idiopathic travelers' diarrhea". In: *Microbiome* 6.1, p. 201. DOI: 10.1186/s40168-018-0579-0.

Zhu, Qiyun, Shi Huang, et al. (Apr. 2021). "OGUs enable effective, phylogeny-aware analysis of even shallow 1 metagenome community structures". In: *bioRxiv*. DOI: 10.1101/2021.04.04.438427.

Ziętak, Marika, Petia Kovatcheva-Datchary, Lidia H Markiewicz, Marcus Ståhlman, Leslie P Kozak, Fredrik Bäckhed (June 2016). "Altered Microbiota Contributes to Reduced Diet-Induced Obesity upon Cold Exposure". In: *Cell Metabolism* 23.6, pp. 1216–1223. DOI: 10.1016/j.cmet.2016.05.001.

Acknowledgments

I would like to thank **Prof. Sunagawa** and **Prof. Schmolke** for serving as my thesis advisory committee. Your insightful feedbacks have brought my work to a higher level.

I would like to thank my supervisor, **Prof. Mirko Trajkovski**, for his enthusiasm for all the new ideas I brought up. Thank you for letting me try out new things, and at the same time, guiding me to focus on what is essential.

I would also like to thank my co-supervisor, **Prof. Evgeny Zdobnov**, whose expertise was invaluable to my work. Thank you for always having an open ear for me.

I would like to thank **Dr. Joseph Brown** for welcoming me as a developer for the atlas pipeline and his foundation. I would like to thank the community of atlas-users, especially **Dr. Jackson M. Tsuji**, **Dr. Sofie Thijs**, **Dr. Lee Bergstrand**, and **Dr. Taylor Reiter**. Thanks to your feedbacks and contributions, the pipeline is what it is today.

I could not have done this Ph.D. without my colleagues, who were always there to answer my questions and to have fun in the lab or virtually:

Specifically, I would like to thank **Dr. Salvatore Fabbiano**, **Dr. Ozren Stojanović**, and **Dr. Nicolas Suarez** for showing me how things are done in the lab, for teaching me how to handle mice, and for all the good discussions at lunch, for instance about the inventor of the Big Bang.

A great thank you to **Dr. Claire Chevalier** for the great collaboration about warm exposure. I liked working together with you in the lab very much, even if this implied making the same error simultaneously. Thank you for the lively discus-

sions about microbiome analysis and just for creating such a good atmosphere in the team.

How could I thank **Dorothée Rigo** enough? Thank you for all you have done to help me, from bacteria gram stainings to qPCRs, not forgetting mice dissection and all the discussions and advice on work, life, and children.

I would like to thank **Dr. Martina Špiljar** for all the effort in promoting a team spirit in the lab. Your journal clubs helped me to learn quite a lot about immunology. Thank you for being around, encouraging me, or simply "um Trübsal zu blasen".

Thank you, **Melis Colakoglu**, for the teamwork with the mice, even when they didn't lose weight as expected. Thank you for all the good time we had in the laboratory and the interest you showed in my family and me.

I would like to thank **Dr. Noushin Hadadi** for the inspiring discussions about bioinformatics, academia, and life in general. It was fun to compare the mental development of our children with the training of artificial neuronal networks. Not to forget the excellent food and the invitation to your home, which was definitely one of the best lab excursions.

I would like to thank **Dr. Jing Xue** for making spatial-transcriptomics a reality and for helping to rob a bank in the Geneva escape room. Thank you, **Aleksandar Arsović**, for looking after everybody and helping us not to miss a birthday. Thank you, **Vincent Berweiler**, for creating so much laughter in the lab. Thank you, **Dr. Haiping Wang**, for always having the right paper at hand.

I would also like to thank my colleagues from the Zdobnov lab. You helped me to not forget my geeky side. In particular, I would like to thank **Dr. Felipe A Simão** for spending many long hours teaching me the library preparation for shotgun-metagenomics; **Dr. Mosè Manni** for the constructive discussions about genomic distance and species delineation. Thank you, **Dr. Mathieu Seppey** and **Dr. Christopher Rands**, for being around and for all the discussions about metagenomics and programming.

Thank you, **Dr. Pierre Fabre**, for initiating me, and consequently our lab to spatial transcriptomics. Thank you for the stimulating discussions and the valuable career advice.

I would like to thank **Dr. Olga Komarynets** for giving me hope that it is possible to plan one's research, despite the unforeseen outcomes.

I think it is appropriate to thank the team from the High-Performance Computing facility at the University of Geneva, without whom I couldn't have done much of my work.

And it is also more than appropriate to thank my Master thesis supervisors: **Dr. Bernard Berger**, **Dr. Olga Sakwinska**, and **Dr. Harald Brüssow**, who initiated me to the world of microbiomics; who made my think critically about the sometimes overhyped microbiome literature and who fostered in me a desire to do research that has a real-world impact.

I would like to thank **Milena Kieser** for being my Ph.D. mate. Thank you for all the encouragements and for your efforts to understand my day-to-day work. I would like to thank my son, **Timon**, for insisting that I play with him and for reminding me that there is so much more to life than work. I would also like to thank my daughter **Sophonie** for having set a clear due date to finish writing my thesis. I would like to thank my parents-in-law, **Anne-Lise** and **Bernhard** for their support through the ups and downs during my Ph.D.

Last but not least, I would like to thank my parents **Tabea** and **Daniel** as well as **Torsten** for fostering curiosity in me.

Review article

This is a review to which I contributed.

Available online at www.sciencedirect.com

ScienceDirect

Current Opinion in Cell Biology

Common traits between the beige fat-inducing stimuli

Ozren Stojanović[1,2], Silas Kieser[1,2] and Mirko Trajkovski[1,2,3]

Adipose tissues play an essential role in regulating the metabolic homeostasis and can be found in almost all parts of the body. Excessive adiposity leads to obesity and can contribute to metabolic and other disorders. Adipocytes show remarkable plasticity in their function, which can be pushed toward energy storage, or energy expenditure — a 'browning' of fat. Browning is controlled by the cellular *milieu* of the adipose tissue, with sympathetic innervation and by immune responses as key integrators of the signals that promote browning. Here, we describe the latest contributions to our understanding of how different metabolic stimuli can shape the adipocyte function. We especially focus on the role of the gut microbiota and the negative energy balance in regulating the browning.

Addresses
[1] University of Geneva, Faculty of Medicine, Department of Cell Physiology and Metabolism, Centre Médical Universitaire, 1211 Geneva, Switzerland
[2] University of Geneva, Diabetes Centre, Faculty of Medicine, 1211 Geneva, Switzerland
[3] Institute for Genetics and Genomics in Geneva, University of Geneva, 1211 Geneva, Switzerland

Corresponding author: Trajkovski, Mirko (Mirko.Trajkovski@unige.ch)

Current Opinion in Cell Biology 2018, **55**:67–73

This review comes from a themed issue on **Differentiation and disease**

Edited by **Katja Röper** and **Xosé R Bustelo**

For a complete overview see the Issue and the Editorial

Available online 11th July 2018

https://doi.org/10.1016/j.ceb.2018.05.011

Introduction

Adipose tissue is traditionally classified into white and brown fat, with opposite functions. White adipose tissue (WAT) stores energy mainly in form of triglycerides, packed as a large, single lipid droplet that occupies most of the volume in the mature white adipocyte. It secretes hormones and cytokines ('adipokines'), which mediate, both locally and systemically, many aspects of physiology [1]. WAT is found in many parts of the body, but the main locations are the subcutaneous and abdominal visceral depots; the latter being associated with more adverse metabolic effects [2,3]. Brown adipose tissue (BAT) is of different origin and shares similar developmental progenitors with skeletal muscle cells [1,4]. BAT oxidizes triglycerides (and to lesser extent, glucose) in its mitochondria, with energy dissipated as heat, a function conferred by the BAT-specific Uncoupling protein 1 (UCP1). Brown cells are rich in UCP1+ mitochondria, they are typically smaller than the white adipocytes, and have multilocular appearance with several lipid droplets. BAT first developed in placental mammals as a mechanism to maintain body warmth in cold temperatures. It is now firmly established that functional BAT exists in adult humans [5]. BAT depots are located in interscapular region (by far the most important location in rodents), perirenal and axillary depots; in humans, the main depot is between anterior neck and thorax [1,5]. BAT activity is induced by ***cold exposure*** and the sensation is transmitted to the BAT through sympathetic innervation. Norepinephrine released from the nerve endings stimulate the β_3-adrenergic receptor (β-AR). Agonists of β-AR are frequently used to mimic cold exposure and experimentally induce thermogenesis. Beta-adrenergic signaling raises intracellular cyclic AMP levels [6], activates protein kinase A, which induces expression of key browning transcriptional regulators, Peroxisome proliferator-activated receptor gamma (PPARγ) coactivator 1-alpha (PGC1-α) and PR domain containing 16 (PRDM16). Exact downstream steps that drive longer-term recruitment of brown cells and thermogenic program are currently investigated and converge on PPARγ as a key transcriptional driver.

In response to cold brown fat cells also emerge within the subcutaneous WAT, called 'beige' or 'brite' cells (brown-in-white) in a process referred to as fat browning. With the brown cells they share UCP1+ mitochondria, multilocular appearance and thermogenic capacity, but they also seem to express unique markers, such as Cd137 or Tmem26 [4]. The thermogenic activity of the beige fat is also dependent on the sympathetic nervous system via norepinephrine signaling [6,7]. Lineage tracing studies suggest that in the subcutaneous WAT, the beige adipocytes emerge by *de novo* differentiation [8], but also that mature beige adipocytes may interconvert into white and vice versa [9,10]. The available evidence does not exclude that both might be the case, in particular during different cold exposure periods, or after re-exposure to cold.

Many ways to induce browning

While it is easy to see how induction of thermogenesis in cold conditions is a beneficial evolutionary adaptation of warm-blooded animals, browning can be activated in numerous other conditions in which the benefit of thermogenesis is less obvious. Interestingly, we recently noted that many browning stimuli have in common an

overarching leitmotif — a negative energy balance [11••] (Figure 1).

In skeletal muscle, the response to increased energy demand in ***endurance exercise*** is mediated by the transcription factor PGC-1α, which promotes oxidative over glycolytic metabolism [12]. Exercise also decreases adiposity and promotes an anti-inflammatory phenotype in WAT. Several groups observed in mice models that physical exercise or PGC-1α overexpression reduces adipocyte size and lipid content in WAT, but also stimulates browning, primarily in subcutaneous WAT [13–16]. However, there is no solid evidence yet that exercise induces browning in humans [17]. In addition, even the browning in mice might depend on particular exercise regime (reviewed in [18]): for example, small effect of exercise on browning of WAT is greatly enhanced by environmental enrichment (physically and socially more complex housing) in mice's cages [16]. A molecular link between exercise and browning has been sought in secreted myokines in trained mice [19,20]. Among them, meteorin-like-1 (Metrnl) [21] is a target of Pgc1α4, and is secreted from exercised muscles likely to induce browning through a type 2 immune signaling cascade [22].

Adipose depots are an evolutionary answer to conditions of decreased energy availability, a situation frequently encountered by nearly all animals. In these cases, previously stored triglycerides are released from adipocytes in form of free fatty acids and glycerol, as an energy source for most of the body. Surprisingly, ***caloric restriction*** (CR) in mice by 40% without malnutrition or lean mass loss, markedly induces beige adipocyte appearance in WAT, with functional thermogenic capacity and increased oxygen consumption rates [11••]. Genetic inhibition of the type 2 immune signaling (described below) suppresses the CR-induced browning and subcutaneous WAT loss. Interestingly, CR reduces the total energy expenditure [23] and this is further lowered by blocking the type 2 immunity and browning during CR, suggesting opposing roles of different organs to the energy balance during CR [11••]. On the other hand, mice that grow obese due to genetically increased appetite (*ob*/*ob*), have lower core body temperature and insufficient browning and cold resistance [24], though data for humans are less conclusive [25–27]. Interestingly, very low caloric restriction (VLCR) in obese humans (~800 kcal/day) does not provoke browning [28•]. This could go in line with the

Figure 1

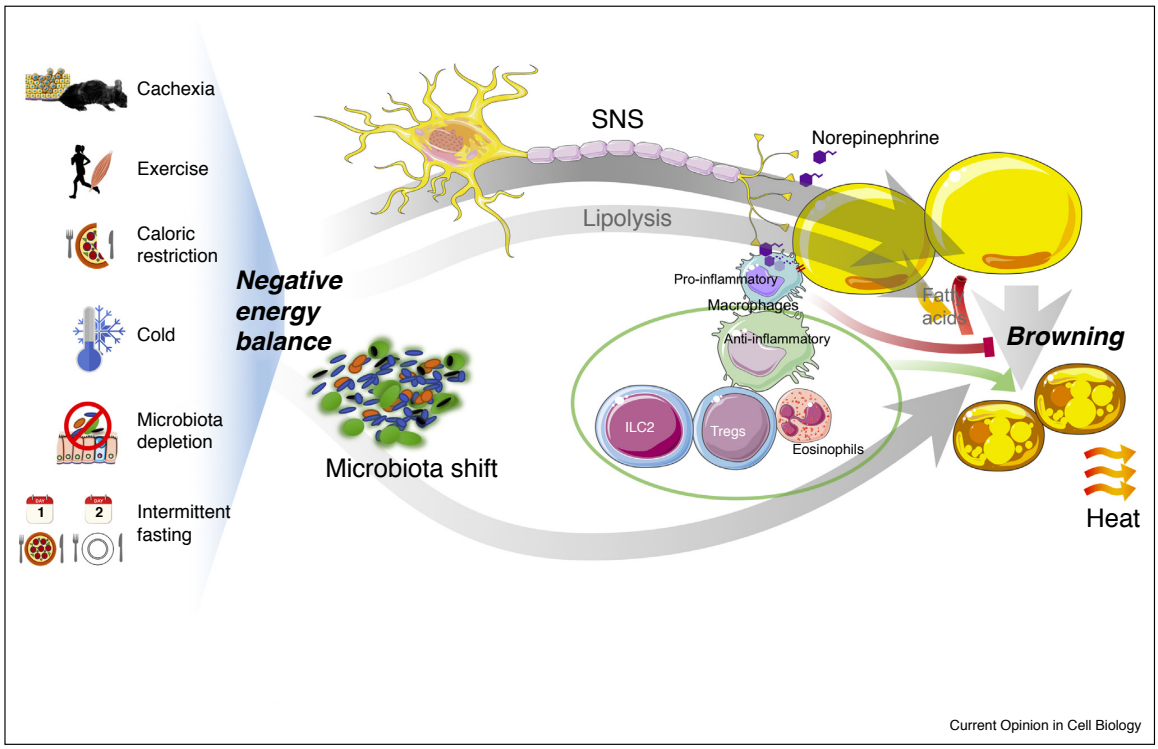

Schematic representation of the browning stimuli. Common feature between many conditions that induce browning is the energy stress to the organism, or the negative energy balance. These stimuli may trigger and/or potentiate the browning by an orchestrated interplay between the sympathetic nervous system (SNS), the innate immunity and the induction of lipolysis. Abbreviations: ILC2 — type 2 innate lymphoid cells; Tregs — regulatory T cells.

studies in mice, where CR coupled to malnutrition also limits the browning. That might indicate that other signals are able to overwrite the browning effects, and would agree with the hypothesis that after VLCD or lean mass decrease, the signals of the lean mass loss (e.g., muscle cell death and/or inflammation) could contribute to the overall metabolic slowdown and weight gain overshoot in patients after VLCD. Accordingly, it is likely that the balance of fat versus lean mass loss, as well as the rates and magnitude of the fat loss during different diets and the obesity status, play a critical role in shifting the adipocytes toward beige or white. Thus, an alternative explanation for the lack of browning during the VLCD in the obese humans could be that the fat loss (14.0% in males, 8.5% in females) is not sufficient to induce the browning. Additional work is needed to uncover which of these scenarios could explain this phenomenon.

Intermittent fasting consists of alternating days of *ad libitum* feeding with days of fasting. Increased food intake on the feeding day compensates for previous fasting and the bodyweight remains constant. It is therefore different from CR, but still induces a fasting stress. Intermittent fasting increases the expression of beige markers at room temperature and thermoneutrality, and protects against weight gain during high-fat diet [29•,30•]. Interestingly, just as it happens in cold exposure and exercise [14,31], there is increased vascularisation of the subcutaneous WAT through induction of vascular endothelial growth factor (VEGF). This periodic expression of VEGF in WAT was sufficient to induce browning [30•]. In human WAT, VEGF expression correlates with the expression of browning-markers as well as alternatively activated, M2 polarized macrophages.

The list of conditions [32] that may not necessarily require heat production, but cause browning goes further: ***cancer cachexia*** [33] (a pathology associated with increased resting energy expenditure), elevated FGF21 circulatory levels [34,35] (a hormone secreted by liver that mediates starvation response), FXR agonism [36] (bile acid regulation), and upon ***gastric bypass surgery*** in mice [37]. Another recently-discovered potent stimulus that drives fat browning linked with energy loss is the ***microbiota depletion*** [38].

Gut microbiota is linked with browning of fat

Intestines are colonized by trillions of symbiotic bacteria called the intestinal microbiota. These bacteria break down undigested fibers and can produce vitamins and secondary metabolites. Often overlooked is the role of microbiota biomass in the heat production [39]. Mice and rats treated with antibiotics have initial drop of ~1 °C in the core body temperature [40]. To raise body temperature back for 1 °C, the metabolic rate of the animal must increase 10% [41]. Microbiota depletion by means of antibiotics treatment improves insulin sensitivity [38,42]. Despite the preferential increase in the glucose uptake to the WAT during the microbiota depletion, these fat stores have decreased volume and weight, and their adipocytes show multilocular appearance and increased oxygen consumption rates [38,43]. They do this by developing functional beige cells in the inguinal subcutaneous adipose tissue and to a lesser extent in the perigonadal visceral adipose tissue. This phenomenon is also evident when microbiota-depleted mice are maintained at thermoneutrality. Similar increase in browning is found in germ-free mice that are born and raised aseptically. Microbiota depletion improves metabolic health in lean mice, obese leptin-deficient (*ob/ob*) mice and high-fat diet (HFD)-fed mice [38].

Cold exposure leads to a major reshaping of the gut microbiome [43,44], marked by increase in *Firmicutes* and *Deferiobacteres* phila, and decrease of *Verrucomicrobia*. Transplanting the cold-adapted microbiota to germ-free recipients is sufficient to increase the browning of WAT [43], and it also induces the BAT activity [43,44] when compared to controls transplanted with microbiota from room temperature-housed mice. This contributes to a better cold tolerance and an improved glycaemic status of the cold-microbiota transplanted mice. Similarly, the intermittent fasting regime [29•] induces increase in *Firmicutes*, a phylum that has been associated with increased browning markers and insulin sensitivity in obese patients [45]. Transplantation of this intermittent fasting-altered microbiota also leads to enhanced browning [29•].

Microbiota produce and transform metabolites, which can act as signaling molecules throughout the body. Bile acids (BA) induce energy expenditure in muscles and BAT, and could induce browning of WAT through binding to BA receptor TGR5 [46]. The microbiota of cold-exposed mice has less deconjugation activity, and the BA profile is richer in conjugated BAs similarly to the germ-free mice. Short chain fatty acids (SCFA) are fermentation products which can signal to the host and provide preferred energy source for particular cell types. SCFAs, especially acetate, have been shown to induce browning [44,47,48]. Short (6 days) and long term intermittent fasting (IF) increase acetate as well as lactate in the blood. This shift could not be induced in germ-free mice on IF but was when they received gut microbiota from fasted mice. Lactate produced during IF or exercise could increase VEGF, which contributes to the browning. Heat, and acidification due to acetate and lactate can be sensed directly by vagus afferents through transient receptor potential cation channel subfamily V member 1 (TRPV-1) [41]. In obese patients, *Firmicutes* family *Ruminococcaceae*, which is also increased in cold [44], was associated with elevated plasma acetate levels, which are turn positively linked with the expression of PRDM16 in subcutaneous WAT and insulin sensitivity [45]. In lean subjects, exercise for 6 weeks is associated with an increase of genera producing

SCFAs [49]. All these signaling cascades could be potential ways by which microbiota exerts its effects of browning, and they remain to be experimentally tested.

Browning and mobilization of fuel

It is not clear why would the browning program be activated during CR or microbiota depletion in mice, as this can lead to further increase in the energy expenditure. One possibility is that during decreased caloric intake, the lower thermal isolation due to the diminished adiposity would need to be compensated by increased thermogenesis. The interesting finding however, is that these effects also occur at thermoneutrality and are orchestrated by immune-derived signals. Thus, identifying the signals upstream of this immune-fat axis would be an exciting area for further research.

As mentioned above, a feature that is common to many diverse and seemingly unrelated physiological, or interventional stimuli of browning is the energy stress: the energy available to the cells is lower than energy expenditure (or so is signaled to the fat). To respond to this negative energy balance, the organism must respond by correcting one or both sides of the energy balance seesaw. Energy scarcity occurs due to different reasons. During cold exposure, extra energy is needed to produce heat. Loss of intestinal microbiota deprives organism of calories that become accessible to organism through bacterially-assisted degradation of food, while exercise increases caloric demand due to muscular work. Activators of browning, the sympathetic nervous system and the thyroid hormones, are stimuli associated with increased metabolic rate and energy consumption. So, could browning of white fat, at least in part, serve as a means for energy mobilization or control, and how? Two groups in 2017 knocked-out lipolysis specifically in BAT [50••,51••]. Shin *et al.* [51••] generated UCP1-Cre-driven, BAT-specific knock-out of CGI-58, a protein that co-activates adipose triglyceride lipase (ATGL) and, through association with lipid droplets, participates in cytosolic lipolysis. Using similar approach, Schreiber *et al.* [50••] knocked-out ATGL in BAT. These mice, which could not oxidize BAT's own fat as they would do normally [52], were not cold sensitive and had normal heat generation and UCP1 content in BAT, even while fasting. As a compensation, the sympathetic nervous signaling induced lipolysis and browning in subcutaneous WAT, and released fatty acids that fueled the BAT thermogenesis. In contrast, blocking lipolysis in all (adiponectin-expressing) adipocytes suppressed the brown fat induction and rendered mice [50••,51••] and (by pharmacological inhibition) men [53] more cold-sensitive. Although the beige adipocytes express UCP1, and as such should have the deletion of the ATGL or CGI-58 also in the beige cells, it was not tested whether indeed there is a strong enough induction of the Cre expression to drive the KOs in these adipocytes without cold exposure-induced UCP1 expression. The lipolysis rates are higher in the browned adipose tissues compared to the white [11••,33], which might lead to increased release of glycerol [11••] and fatty acids [33] into the blood. Thus, it would be interesting to know if the fatty acids during cold or CR are released primarily from the beige or the white adipocytes, or equally from both; and whether the local increase in the fatty acids ultimately induces the browning of the white adipocytes. Distinction between beige, brown and white fat has been recently blurred by the discovery that not all beige adipocytes express UCP1, and those that do not are still capable of thermogenicity [54–56].

A recurrent pattern that is associated with beige adipogenesis is the recruitment of anti-inflammatory signals in fat [11••,22,38,57]. Low-grade inflammation of white fat is a hallmark of obesity and is linked to macrophage infiltration in the WAT, their activation into inflammatory M1 cells, and diminished capacity for browning. Chawla and colleagues showed [57] that after cold exposure, the WAT is infiltrated by an increased number of eosinophils that could drive macrophage polarization from pro-inflammatory towards anti-inflammatory state, leading to fat browning. The exact mechanisms by which WAT-resident macrophages could exert their browning role are debated: it was originally proposed that macrophages locally produce norepinephrine, which would lead to sympathetic-independent induction of browning [58•]. To test this, tyrosine hydroxylase, the rate limiting enzyme in the catecholamine biosynthesis, was knocked-out in hematopoietic cells. This did not diminish the browning upon cold exposure, and the bone marrow-derived macrophages did not release norepinephrine upon IL-4 stimulation [59•]. In a possible solution to the apparent paradox, it was recently revealed that M1 cells stay attached to adipocytes by binding of integrin α4 to VCAM-1 [60], thus sustaining the inhibition of the beiging program. An additional model that could explain the ways by which macrophages can regulate the browning is the recent discovery of sympathetic neuron-associated macrophages (SAMs), a subpopulation of macrophages that take up and degrade norepinephrine [61•,62•] released from the network of sympathetic nerve endings in the WAT [63]. SAMs are increased in obesity and ablation of norepinephrine uptake increases browning. The increased sympathetic innervation in BAT can be influenced by the macrophages [58•], but the potential importance of the immune cells in influencing the sympathetic innervation in subcutaneous WAT has not yet been addressed. CR [11••] and the microbiota depletion [38] lead to anti-inflammatory macrophage polarization, and irrespective of the exact downstream mode of action, blocking the type 2 immunity suppresses the fat browning. During aging, the inflammasome-driven norepinephrine degradation in macrophages blunts lipolysis [61•]. With respect to the increased lipolysis during CR and microbiota depletion, it would be interesting to study if the lipolysis contributes to the CR-induced and

microbiota depletion-induced browning, and is there an interplay between the lipolysis rates and type 2 immunity. Finally, other immune cells can also interact with sympathetic β-AR signaling, where a Stat6/Pten axis could link the regulatory T cells with the fat function and browning: CD8+ T-cells inhibit the beiging process [64] and regulatory T-cells [65] promote it.

Conclusion

It is estimated that activated brown fat in adult human would burn an energy equivalent of 4.1 kg of adipose tissue in one year [5]. We are just starting to understand the various physiological conditions that lead to beige fat development. These diverse environmental and physiological cues cause energy stress and activate common set of mediators of browning: sympathetic, anti-inflammatory, and bile acid signaling, which promote catabolism in adipose tissue through shared transcriptional cascade. Thus, uncovering the mechanisms that lay upstream of the type 2 immune cascade, but also the link between the microbiota changes and the fat browning necessary to understand the core triggers that promote beiging, could lead to novel therapeutics to improve metabolic health.

Acknowledgements

We thank all members of the Trajkovski lab for discussions and reading the manuscript. Figure 1 was generated using images available from Servier Medical Art, licensed under a Creative Common Attribution 3.0 Generic License http://smart.servier.com/. This work was supported by the European Research Council under the European Union's Seventh Framework Programme (FP/2007-2013)/ERC Grant Agreement n. 336607 [ERC-2013-StG-336607]; the Clayton foundation, and the Swiss National Science Foundation (SNSF) Professorship to M.T.

References and recommended reading

Papers of particular interest, published within the period of review, have been highlighted as:

- • of special interest
- •• of outstanding interest

1. Rosen ED, Spiegelman BM: **What we talk about when we talk about fat**. *Cell* 2014, **156**:20-44.

2. Wajchenberg BL: **Subcutaneous and visceral adipose tissue: their relation to the metabolic syndrome**. *Endocr Rev* 2000, **21**:697-738.

3. Porter SA, Massaro JM, Hoffmann U, Vasan RS, O'Donnel CJ, Fox CS: **Abdominal subcutaneous adipose tissue: a protective fat depot?** *Diabetes Care* 2009, **32**:1068-1075.

4. Hepler C, Vishvanath L, Gupta RK: **Sorting out adipocyte precursors and their role in physiology and disease**. *Genes Dev* 2017, **31**:127-140.

5. Virtanen KA, Lidell ME, Orava J, Heglind M, Westergren R, Niemi T, Taittonen M, Laine J, Savisto NJ, Enerback S *et al.*: **Functional brown adipose tissue in healthy adults**. *N Engl J Med* 2009, **360**:1518-1525.

6. Cannon B, Nedergaard J: **Brown adipose tissue: function and physiological significance**. *Physiol Rev* 2004, **84**:277-359.

7. Oelkrug R, Polymeropoulos ET, Jastroch M: **Brown adipose tissue: physiological function and evolutionary significance**. *J Comp Physiol B* 2015, **185**:587-606.

8. Wang QA, Tao C, Gupta RK, Scherer PE: **Tracking adipogenesis during white adipose tissue development, expansion and regeneration**. *Nat Med* 2013, **19**:1338-1344.

9. Rosenwald M, Perdikari A, Rulicke T, Wolfrum C: **Bi-directional interconversion of brite and white adipocytes**. *Nat Cell Biol* 2013, **15**:659-667.

10. Lee YH, Kim SN, Kwon HJ, Granneman JG: **Metabolic heterogeneity of activated beige/brite adipocytes in inguinal adipose tissue**. *Sci Rep* 2017, **7**:39794.

11. •• Fabbiano S, Suárez-Zamorano N, Rigo DE, Veyrat-Durebex C, Stevanovic Dokic A, Colin DJJ, Trajkovski M, Suárez-Zamorano N, Rigo DE, Veyrat-Durebex C *et al.*: **Caloric restriction leads to browning of white adipose tissue through type 2 immune signaling**. *Cell Metab* 2016, **24**:434-446.
Caloric restriction in rodents on two different genetic backgrounds leads to development of functional beige fat. Suppression of the type 2 immunity in the hematopoetic cells suppresses the browning and limits the subcutaneous fat loss during caloric restriction.

12. Handschin C, Spiegelman BM: **The role of exercise and PGC1alpha in inflammation and chronic disease**. *Nature* 2008, **454**:463-469.

13. Stanford KI, Middelbeek RJ, Goodyear LJ: **Exercise effects on white adipose tissue: beiging and metabolic adaptations**. *Diabetes* 2015, **64**:2361-2368.

14. Stanford KI, Middelbeek RJ, Townsend KL, Lee MY, Takahashi H, So K, Hitchcox KM, Markan KR, Hellbach K, Hirshman MF *et al.*: **A novel role for subcutaneous adipose tissue in exercise-induced improvements in glucose homeostasis**. *Diabetes* 2015, **64**:2002-2014.

15. Peppler WT, Townsend LK, Knuth CM, Foster MT, Wright DC: **Subcutaneous inguinal white adipose tissue is responsive to, but dispensable for, the metabolic health benefits of exercise**. *Am J Physiol Endocrinol Metab* 2018, **314**:E66-E77.

16. Cao L, Choi EY, Liu X, Martin A, Wang C, Xu X, During MJ: **White to brown fat phenotypic switch induced by genetic and environmental activation of a hypothalamic-adipocyte axis**. *Cell Metab* 2011, **14**:324-338.

17. Vosselman MJ, Hoeks J, Brans B, Pallubinsky H, Nascimento EB, van der Lans AA, Broeders EP, Mottaghy FM, Schrauwen P, van Marken Lichtenbelt WD: **Low brown adipose tissue activity in endurance-trained compared with lean sedentary men**. *Int J Obes (Lond)* 2015, **39**:1696-1702.

18. Aldiss P, Betts J, Sale C, Pope M, Budge H, Symonds ME: **Exercise-induced' browning' of adipose tissues**. *Metabolism* 2018, **81**:63-70.

19. Bostrom P, Wu J, Jedrychowski MP, Korde A, Ye L, Lo JC, Rasbach KA, Bostrom EA, Choi JH, Long JZ *et al.*: **A PGC1-alpha-dependent myokine that drives brown-fat-like development of white fat and thermogenesis**. *Nature* 2012, **481**:463-468.

20. Jedrychowski MP, Wrann CD, Paulo JA, Gerber KK, Szpyt J, Robinson MM, Nair KS, Gygi SP, Spiegelman BM: **Detection and quantitation of circulating human irisin by tandem mass spectrometry**. *Cell Metab* 2015, **22**:734-740.

21. Rao RR, Long JZ, White JP, Svensson KJ, Lou J, Lokurkar I, Jedrychowski MP, Ruas JL, Wrann CD, Lo JC *et al.*: **Meteorin-like is a hormone that regulates immune-adipose interactions to increase beige fat thermogenesis**. *Cell* 2014, **157**:1279-1291.

22. Nguyen KD, Qiu Y, Cui X, Goh YP, Mwangi J, David T, Mukundan L, Brombacher F, Locksley RM, Chawla A: **Alternatively activated macrophages produce catecholamines to sustain adaptive thermogenesis**. *Nature* 2011, **480**:104-108.

23. University of Minnesota: **Laboratory of physiological hygiene**. In *The Biology of Human Starvation*. Edited by AB y. Minneapolis: University of Minnesota Press; 1950.

24. Davis TR, Mayer J: **Imperfect homeothermia in the hereditary obese-hyperglycemic syndrome of mice**. *Am J Physiol* 1954, **177**:222-226.

25. Heikens MJ, Gorbach AM, Eden HS, Savastano DM, Chen KY, Skarulis MC, Yanovski JA: **Core body temperature in obesity**. *Am J Clin Nutr* 2011, **93**:963-967.

26. Landsberg L, Young JB, Leonard WR, Linsenmeier RA, Turek FW: **Is obesity associated with lower body temperatures? Core**

temperature: a forgotten variable in energy balance. *Metabolism* 2009, **58**:871-876.

27. Grimaldi D, Provini F, Pierangeli G, Mazzella N, Zamboni G, Marchesini G, Cortelli P: **Evidence of a diurnal thermogenic handicap in obesity**. *Chronobiol Int* 2015, **32**:299-302.

28. • Barquissau V, Leger B, Beuzelin D, Martins F, Amri EZ, Pisani DF, Saris WHM, Astrup A, Maoret JJ, Iacovoni J *et al.*: **Caloric restriction and diet-induced weight loss do not induce browning of human subcutaneous white adipose tissue in women and men with obesity**. *Cell Rep* 2018, **22**:1079-1089.
Very low caloric diet intervention in obese humans does not lead to browning, but decreases the fat mass for 14% in men, and 8.5% in women.

29. • Li G, Xie C, Lu S, Nichols RG, Tian Y, Li L, Patel D, Ma Y, Brocker CN, Yan T *et al.*: **Intermittent fasting promotes white adipose browning and decreases obesity by shaping the gut microbiota**. *Cell Metab* 2017, **26** 672−685.e674.
These two reports [29•,30•] demonstrate that the intermittent (every second day) fasting stimulates beige fat development and reduces obesity, insulin resistance, and hepatic steatosis. In part, this is mediated by the type 2 immunity, and/or altered microbiota composition.

30. • Kim K-H, Kim YH, Son JE, Lee JH, Kim S, Choe MS, Moon JH, Zhong J, Fu K, Lenglin F *et al.*: **Intermittent fasting promotes adipose thermogenesis and metabolic homeostasis via VEGF-mediated alternative activation of macrophage**. *Cell Res* 2017, **27**:1309-1326.
See annotation to Ref.[29•].

31. Xue Y, Petrovic N, Cao R, Larsson O, Lim S, Chen S, Feldmann HM, Liang Z, Zhu Z, Nedergaard J *et al.*: **Hypoxia-independent angiogenesis in adipose tissues during cold acclimation**. *Cell Metab* 2009, **9**:99-109.

32. Kajimura S, Spiegelman BM, Seale P: **Brown and beige fat: physiological roles beyond heat generation**. *Cell Metab* 2015, **22**:546-559.

33. Petruzzelli M, Schweiger M, Schreiber R, Campos-Olivas R, Tsoli M, Allen J, Swarbrick M, Rose-John S, Rincon M, Robertson G *et al.*: **A switch from white to brown fat increases energy expenditure in cancer-associated cachexia**. *Cell Metab* 2014, **20**:433-447.

34. Emanuelli B, Vienberg SG, Smyth G, Cheng C, Stanford KI, Arumugam M, Michael MD, Adams AC, Kharitonenkov A, Kahn CR: **Interplay between FGF21 and insulin action in the liver regulates metabolism**. *J Clin Investig* 2014, **124**:515-527.

35. Hanssen MJ, Broeders E, Samms RJ, Vosselman MJ, van der Lans AA, Cheng CC, Adams AC, van Marken Lichtenbelt WD, Schrauwen P: **Serum FGF21 levels are associated with brown adipose tissue activity in humans**. *Sci Rep* 2015, **5**:10275.

36. Fang S, Suh JM, Reilly SM, Yu E, Osborn O, Lackey D, Yoshihara E, Perino A, Jacinto S, Lukasheva Y *et al.*: **Intestinal FXR agonism promotes adipose tissue browning and reduces obesity and insulin resistance**. *Nat Med* 2015, **21**:71-77.

37. Neinast MD, Frank AP, Zechner JF, Li QL, Vishvanath L, Palmer BF, Aguirre V, Gupta RK, Clegg DJ: **Activation of natriuretic peptides and the sympathetic nervous system following Roux-en-Y gastric bypass is associated with gonadal adipose tissues browning**. *Mol Metab* 2015, **4**:427-436.

38. Suárez-Zamorano N, Fabbiano S, Chevalier C, Stojanović O, Colin DJ, Stevanović A, Veyrat-Durebex C, Tarallo V, Rigo D, Germain S *et al.*: **Microbiota depletion promotes browning of white adipose tissue and reduces obesity**. *Nat Med* 2015, **21**:1497-1501.

39. Rosenberg E, Zilber-Rosenberg I: **Do microbiotas warm their hosts?** *Gut Microbes* 2016, **7**:283-285.

40. Kluger MJ, Conn CA, Franklin B, Freter R, Abrams GD: **Effect of gastrointestinal flora on body temperature of rats and mice**. *Am J Physiol-Regul Integr Comp Physiol* 1990, **258**:R552-R557.

41. Liao W-H, Henneberg M, Langhans W: **Immunity-based evolutionary interpretation of diet-induced thermogenesis**. *Cell Metab* 2016, **23**:971-979.

42. Backhed F, Manchester JK, Semenkovich CF, Gordon JI: **Mechanisms underlying the resistance to diet-induced obesity in germ-free mice**. *Proc Natl Acad Sci U S A* 2007, **104**:979-984.

43. Chevalier C, Stojanović O, Colin DJJ, Zamboni N, Hapfelmeier S, Correspondence MT, Stojanović O, Colin DJJ, Suarez-Zamorano N, Tarallo V *et al.*: **Gut Microbiota orchestrates energy homeostasis during cold**. *Cell* 2015, **163**:1360-1374.

44. Zie?tak M, Kovatcheva-Datchary P, Markiewicz LH, Ståhlman M, Kozak LP, Bäckhed F: **Altered microbiota contributes to reduced diet-induced obesity upon cold exposure**. *Cell Metab* 2016, **23**:1216-1223.

45. Moreno-Navarrete JM, Serino M, Blasco-Baque V, Azalbert V, Barton RH, Cardellini M, Latorre J, Ortega F, Sabater-Masdeu M, Burcelin R *et al.*: **Gut microbiota interacts with markers of adipose tissue browning, insulin action and plasma acetate in morbid obesity**. *Mol Nutr Food Res* 2018:62.

46. Velazquez-Villegas LA, Perino A, Lemos V, Zietak M, Nomura M, Pols TWH, Schoonjans K: **TGR5 signalling promotes mitochondrial fission and beige remodelling of white adipose tissue**. *Nat Commun* 2018, **9**:245.

47. Lu Y, Fan C, Li P, Lu Y, Chang X, Qi K: **Short chain fatty acids prevent high-fat-diet-induced obesity in mice by regulating G protein-coupled receptors and gut microbiota**. *Sci Rep* 2016, **6**:37589.

48. Sahuri-Arisoylu M, Brody LP, Parkinson JR, Parkes H, Navaratnam N, Miller AD, Thomas EL, Frost G, Bell JD: **Reprogramming of hepatic fat accumulation and 'browning' of adipose tissue by the short-chain fatty acid acetate**. *Int J Obes* 2016, **40**:955-963.

49. Allen JM, Mailing LJ, Niemiro GM, Moore R, Cook MD, White BA, Holscher HD, Woods JA: **Exercise alters gut microbiota composition and function in lean and obese humans**. *Med Sci Sports Exerc* 2018, **50**:747-757.

50. •• Schreiber R, Diwoky C, Schoiswohl G, Feiler U, Wongsiriroj N, Abdellatif M, Kolb D, Hoeks J, Kershaw EE, Sedej S *et al.*: **Cold-induced thermogenesis depends on atgl-mediated lipolysis in cardiac muscle, but not brown adipose tissue**. *Cell Metab* 2017, **26** 753-+.
These two reports [50••,51••] demonstrate that genetic inhibition of lipolysis in the UCP1-expressing brown adipocytes is not affecting the BAT activity. In contrast, genetic abation of the lipolysis in all the adipocytes suppresses the brown fat function.

51. •• Shin HS, Ma YY, Chanturiya T, Cao Q, Wang YL, Kadegowda AKG, Jackson R, Rumore D, Xue BZ, Shi H *et al.*: **Lipolysis in brown adipocytes is not essential for cold-induced thermogenesis in mice**. *Cell Metab* 2017, **26** 764-+.
See annotation to Ref.[50••].

52. Ouellet V, Labbe SM, Blondin DP, Phoenix S, Guerin B, Haman F, Turcotte EE, Richard D, Carpentier AC: **Brown adipose tissue oxidative metabolism contributes to energy expenditure during acute cold exposure in humans**. *J Clin Investig* 2012, **122**:545-552.

53. Blondin DP, Frisch F, Phoenix S, Guerin B, Turcotte EE, Haman F, Richard D, Carpentier AC: **Inhibition of intracellular triglyceride lipolysis suppresses cold-induced brown adipose tissue metabolism and increases shivering in humans**. *Cell Metab* 2017, **25**:438-447.

54. Kazak L, Chouchani ET, Lu GZ, Jedrychowski MP, Bare CJ, Mina AI, Kumari M, Zhang S, Vuckovic I, Laznik-Bogoslavski D *et al.*: **Genetic depletion of adipocyte creatine metabolism inhibits diet-induced thermogenesis and drives obesity**. *Cell Metab* 2017, **26**:693.

55. Ikeda K, Kang Q, Yoneshiro T, Camporez JP, Maki H, Homma M, Shinoda K, Chen Y, Lu X, Maretich P *et al.*: **UCP1-independent signaling involving SERCA2b-mediated calcium cycling regulates beige fat thermogenesis and systemic glucose homeostasis**. *Nat Med* 2017, **23**:1454-1465.

56. Bertholet AM, Kazak L, Chouchani ET, Bogaczynska MG, Paranjpe I, Wainwright GL, Betourne A, Kajimura S, Spiegelman BM, Kirichok Y: **Mitochondrial patch clamp of beige adipocytes reveals UCP1-positive and UCP1-negative cells**

both exhibiting futile creatine cycling. *Cell Metab* 2017, **25** 811-+.

57. Lee MW, Odegaard JI, Mukundan L, Qiu Y, Molofsky AB, Nussbaum JC, Yun K, Locksley RM, Chawla A: **Activated type 2 innate lymphoid cells regulate beige fat biogenesis**. *Cell* 2015, **160**:74-87.

58. • Wolf Y, Boura-Halfon S, Cortese N, Haimon Z, Sar Shalom H, Kuperman Y, Kalchenko V, Brandis A, David E, Segal-Hayoun Y *et al.*: **Brown-adipose-tissue macrophages control tissue innervation and homeostatic energy expenditure**. *Nat Immunol* 2017, **18**:665-674.

Mice lacking Mecp2 in macrophages develop spontaneous obesity linked to impaired BAT function. Mice with the mutant macrophages show diminished sympathetic innervation and lower local titers of norepinephrine, leading to lower expression of thermogenic factors by the brown adipocytes.

59. • Fischer K, Ruiz HH, Jhun K, Finan B, Oberlin DJ, van der Heide V, Kalinovich AV, Petrovic N, Wolf Y, Clemmensen C *et al.*: **Alternatively activated macrophages do not synthesize catecholamines or contribute to adipose tissue adaptive thermogenesis**. *Nat Med* 2017, **23**:623-630.

Myeloid specific tyrosine hydroxylase deletion does not affect the norephinephrine levels and fat browning.

60. Chung KJ, Chatzigeorgiou A, Economopoulou M, Garcia-Martin R, Alexaki VI, Mitroulis I, Nati M, Gebler J, Ziemssen T, Goelz SE *et al.*: **A self-sustained loop of inflammation-driven inhibition of beige adipogenesis in obesity**. *Nat Immunol* 2017, **18**:654-664.

61. • Camell CD, Sander J, Spadaro O, Lee A, Nguyen KY, Wing A, Goldberg EL, Youm YH, Brown CW, Elsworth J *et al.*: **Inflammasome-driven catecholamine catabolism in macrophages blunts lipolysis during ageing**. *Nature* 2017, **550**:119-123.

These two reports [61•,62•] demonstrate that macrophages can regulate the local white fat norepinephrine levels by catabolising it.

62. • Pirzgalska RM, Seixas E, Seidman JS, Link VM, Sanchez NM, Mahu I, Mendes R, Gres V, Kubasova N, Morris I *et al.*: **Sympathetic neuron-associated macrophages contribute to obesity by importing and metabolizing norepinephrine**. *Nat Med* 2017, **23**:1309-1318.

See annotation to Ref.[61•].

63. Jiang H, Ding X, Cao Y, Wang H, Zeng W: **Dense intra-adipose sympathetic arborizations are essential for cold-induced beiging of mouse white adipose tissue**. *Cell metabolism* 2017, **26** 686–692.e683.

64. Moysidou M, Karaliota S, Kodela E, Salagianni M, Koutmani Y, Katsouda A, Kodella K, Tsakanikas P, Ourailidou S, Andreakos E *et al.*: **CD8+ T cells in beige adipogenesis and energy homeostasis**. *JCI Insight* 2018:3.

65. Kalin S, Becker M, Ott VB, Serr I, Hosp F, Mollah MMH, Keipert S, Lamp D, Rohner-Jeanrenaud F, Flynn VK *et al.*: **A Stat6/Pten axis links regulatory T cells with adipose tissue function**. *Cell Metab* 2017, **26** 475-+.